Heinrich Stadials recorded in Northeast Brazilian Stalagmites

A Thesis
SUBMITTED TO THE FACULTY OF
UNIVERSITY OF MINNESOTA
BY

Kathleen Ann Wendt

IN PARTIAL FULFILLMENT OF THE REQUIREMENTS
FOR THE DEGREE OF
MASTER OF SCIENCE

Advisor: Dr. R. Lawrence Edwards

May 2015

Acknowledgements

I would like to thank my advisor, Dr. Larry Edwards, for his guidance and inspiration over the past two years. Thanks to Dr. Katsumi Matsumoto and Dr. Brandy Toner for their mentorship and participation in my committee. Thanks to Dr. Augusto Auler, Dr. Xianfeng Wang, and Dr. Calvin Alexander for their patient answers to my many questions. Thanks to Dr. Dominik Fleitmann, Anamaria Häuselmann, and Maniko Solheid for their important contributions to this research. Thanks to Dr. Mark Bourne and Dr. Ian Orland for their valuable advice and editing assistance. Thanks to Dr. Julie Retrum for her unending patience when training me in the lab. Finally, thanks to Dr. Yanbin Lu and Mathieu Pythoud for the many mid-afternoon conversations over coffee and toast.

This thesis is dedicated to my family and Mike for all their support and love.

Abstract

During the last glaciation, periods of extreme cooling triggered massive freshwater and iceberg discharges into the North Atlantic. These periods of cooling, referred to as Heinrich Stadials, are believed to have caused an abrupt reorganization of atmospheric and oceanic circulation. Studying the behavior of tropical precipitation systems during Heinrich Stadials is important to understanding the response of tropical hydroclimate change to North Atlantic climate anomalies. In addition, tropical precipitation records may provide insight into the detailed timing and structure of Heinrich Stadials. Doing so is critical to understanding the underlying causes of Heinrich Stadials and their associated discharge events.

The position of the Inter-Tropical Convergence Zone (ITCZ) plays a key role in the locality and amount of tropical precipitation worldwide. Paleo-records suggest that Heinrich Stadials triggered a southward migration of the ITCZ. The semiarid region of Northeast (NE) Brazil is located immediately south of the modern-day Atlantic ITCZ position. Short-lived speleothems that decorate the dry caves of NE Brazil suggest past periods of intense rainfall due to southerly migrations of the ITCZ. Previous studies have linked NE Brazil speleothem growth phases to Heinrich Stadials (Wang et al. 2004). Thus, reconstructing NE Brazilian pluvial periods will provide important insight into the chronology and structure of Atlantic ITCZ migrations associated with Heinrich Stadials.

Here, we present a high-resolution, absolute dated, multi-stalagmite record of Heinrich Stadial (HS) 1, 4, 5 and 6 as recorded in NE Brazilian stalagmites. This thesis will focus on HS4 and HS1 time periods. Results show a detailed anti-correlation between NE Brazil and Northern Hemisphere subtropical records during HS4 and HS1, such as the Hulu Cave record from China (Wang et al. 2001). The synchronicity of these two distant records suggests a rapid transmission of atmospheric signals, likely through the global migration of the ITCZ. In addition, the 2-phased precipitation structure of HS1 and HS4 recorded in NE Brazil may reflect 2-stepped cooling observed in North and mid-Atlantic sea surface temperatures (Bond et al. 1992; Martrat et al. 2007). This supports the hypothesis that climate-ocean forcings were the underlying cause of Heinrich Events and highlights the relationship between mid-Atlantic sea surface temperatures and the position of the Atlantic ITCZ during the last glaciation.

Arid NE Brazil is situated between the Amazon and the Atlantic rainforests. Evidence suggests that the pluvial periods associated with Heinrich Stadials promoted an ecological “bridge” between both rainforests. This bridge may have permitted the transfer of species between rainforests. In this thesis, we compare NE Brazil speleothem precipitation records to NE Brazil palynological marine records to suggest the precise timing of rainforest expansion during HS1. Characterizing these NE Brazil pluvial anomalies are critical in understanding the link between climate change and the response of environmental systems.

Table of contents

List of Tables

Supplementary Tables

List of Figures

Supplementary Figures

Chapter 1: Introduction

1.1 Heinrich Events: a historical review

In 1977, a pioneer study by W.F. Ruddiman demonstrated that the concentrations of ice rafted debris (IRD) in North Atlantic sediments are correlated to Milankovitch-forced growth and decay of Northern Hemisphere ice sheets (Ruddiman 1977). A decade later, German scientist Hartmut Heinrich discovered a series of IRD-rich sediment layers embedded in multiple North Atlantic marine cores. Curiously, the millennial-scale timing of these layers (7-10 kyr) did not fit the Milankovitch-scale forcings. Instead, Heinrich hypothesized that the large lithic fragment deposits originated from an armada of icebergs that were periodically discharged from the Laurentide Ice Sheet during the last glaciation (Heinrich, 1988). Heinrich's hypothesis went largely unnoticed until 1992, when Wallace Broecker and his colleagues at Columbia University confirmed the presence of IRD layers embedded within additional western North Atlantic sediment cores (Broecker et al. 1992). Within 10 years of their discovery, over 200 papers have been published regarding the so-called Heinrich Events and their associated stadials (Hemming, 2004). The interest surrounding Heinrich Events continues today.

Several subsequent studies have found correlative horizons of IRD layers throughout the North Atlantic. Geochemical analysis of IRD layers suggest that icebergs largely originate from the Laurentide Ice Sheet (Heinrich, 1998; Broecker et al. 1992), although later studies also suggest minor contribution from the Fennoscandian, Greenland, and British Ice Sheets (Grousset et al. 1993; Scourse et al. 2009). A total of six Heinrich events are generally considered to have occurred during the last glaciation, identified as H1-H6 (Heinrich 1998; Broecker et al. 1992; Bond et al. 1999). The thickness of the IRD layers associated with Heinrich Events varies amongst the cores, with thicker layers (tens of centimeters) of sediment near the Labrador Sea and thinner layer (few centimeters) on the eastern side of the Atlantic basin bear the Iberian Peninsula (Hemming et al. 1998). In order to deposit this vast

fan of ice-rafted sediment, model simulations suggest that a total of $6x10^5$ km^3 of ice was released (Robert et al. 2014).

The underlying causes of Heinrich Events remain largely unknown. Milankovitch parameters are not detected within millennial time scales, thus exempting the possibility of orbital forcing (Heinrich 1998; Bond et al. 1992). Heinrich Events, which occur on a cycle of 7-10 thousand years, are therefore most likely linked to processes within the Earth's system. In 1992, Bond et al. were the first to propose a possible mechanism. Analyzing a series of North Atlantic marine cores, they noted that Heinrich deposits were a composite of two processes (figure 1). The first was an increase in concentrations of cold-water thriving *N. pachyderma* foraminifera (Bond et al. 1992). The second phase was a brief but massive discharge of Laurentide icebergs indicated by rapid deposition of carbonate-rich IRD. Bond et al. (1992) suggested that shortly after sea surface temperatures (SSTs) began to decline, ice streams in eastern Canada advanced rapidly. As ice fronts reached maximum seaward positions, massive calving occurred, resulting in a release of glacier ice into the North Atlantic. They concluded that abrupt atmospheric cooling, accompanied by falling North Atlantic SSTs, triggered the observed Heinrich Events. At the time, however, they did not have direct evidence for atmospheric cooling, nor could they explain what caused it.

In 1993, MacAyeal proposed an opposing mechanism referred to as the "binge/purge" mechanism. Using a mathematical model, he argued that factors internal to the ice sheet caused ice sheets to periodically discharge large ice volumes (MacAyeal 1993). An accumulation of ice on the Laurentide ice sheet led to a gradual increase in mass (the "binge" phase). Simultaneously, geothermal heat promoted basal melting. Once an ice sheet reaches critical mass and enough basal melt is present, the ice sheet may effectively slide into the adjacent ocean (the "purge" phase). After an ice sheet purge, accumulation of ice resumed and the cycle continued. MacAyeal's opposing

hypothesis sparked a debate of internal (ice sheet) versus external (climate) mechanisms that drove Heinrich Events.

During the same year of 1993, publications from the Greenland Ice Core Project (GRIP) and Greenland Ice Sheet Project 2 (GISP2) revealed that the North Atlantic region experienced large millennial-scale climate shifts between cold (stadial) and warmer (interstadial) conditions during the last glaciation (Dansgaard et al. 1993; Grootos et al. 1993). This pattern, now commonly referred to as Dansgaard-Oeschger (D/O) Oscillations, is characterized by remarkably abrupt transitions between climate states. Bond et al. (1993) were quick to notice that the discharge events recorded in North Atlantic sediments occurred in striking alignment with the D/O cycles documented in ice cores (Bond et al. 1993). They built upon the hypothesis that Heinrich Events were caused by abrupt North Atlantic cooling during periods of optimal sea ice coverage (Bond et al. 1992; Alley et al. 2006). This hypothesis has since been supported by numerous North Atlantic paleo-records (Bond and Lotti 1995; Hulbe 1997, 2004; McCabe and Clark 1998; Bond et al. 1999, Bard et al. 2000; Hemming 2004 *and references therein*).

The term "Heinrich Stadial" represents a period of cool conditions, during which a relatively brief Heinrich Event occurred. A number of paleoclimate archives have shown that century-scale variability within stadials (Bond et al. 2002, 1999; Martrat et al. 2007; Naughton et al. 2007). Bond et al. (1992) were the first to propose a two-phased structure to Heinrich Stadials: (1) an initial decrease in SSTs (the "precursor-cooling" phase), followed by (2) a rapid deposition of IRD (the Heinrich Event) accompanied by subsequently cooler SSTs evoked by freshwater discharge (figure 1). Evidence for this "cool to cooler" Heinrich Stadial structure has since been identified in marine cores across the North and mid-Atlantic (Bond and Lotti 1995; Bond et al. 1999; Bard et al. 2000; Peck et al. 2007; Jullien et al. 2006; Naughton et al. 2007; Martrat et al. 2007). What caused the precursor-cooling phases are largely unknown, although some studies point to changes in ocean circulation (Martrat et al. 2007; Bard

et al. 2000) while others suggest that small-scale non-Laurentide discharge events from neighboring ice sheets have caused cooling prior to the proper Heinrich Event (Grousset et al. 2001; Jullien et al. 2006).

It is important to note, however, that the 2-phased cooling signals are absent from Greenland temperature records during Heinrich Stadials 2-6 (Dansgaard et al. 1993; Grootos et al. 1993). Within a single Heinrich Stadial, Greenland ice cores suggest little to no temperature variation. This view was reinforced in 2004 with the first publication of the Northern Greenland Ice Core Project (NGRIP) high-resolution temperature record (NGRIP, 2004). However some argue that as sea ice progression reaches certain latitudes, Greenland $\delta^{18}O$ values saturate—resulting in a seemingly constant climate conditions during stadials (Deplazes et al. 2013). This may explain the discrepancy between recorded Greenland temperatures and North Atlantic SSTs, which suggest a more complex stadial dynamic (Martart et al. 2007). Inconsistencies between Greenland air temperature and North Atlantic SST records during Heinrich Stadials remain an ongoing debate.

In 1993, Grimm et al. published the first evidence of climate anomalies associated with Heinrich Events beyond the North Atlantic. Using pollen records preserved in Florida lake cores, Grimm (1993) observed anomalous wet periods occurred in correlation with Heinrich Stadials. Soon after, Lowell et al. (1995) observed evidence for alpine glacier advances in the Chilean Andes in response to Heinrich Stadials. Due to these early paleo-record studies, Heinrich Stadials were quickly realized to be a global-wide climate phenomenon.

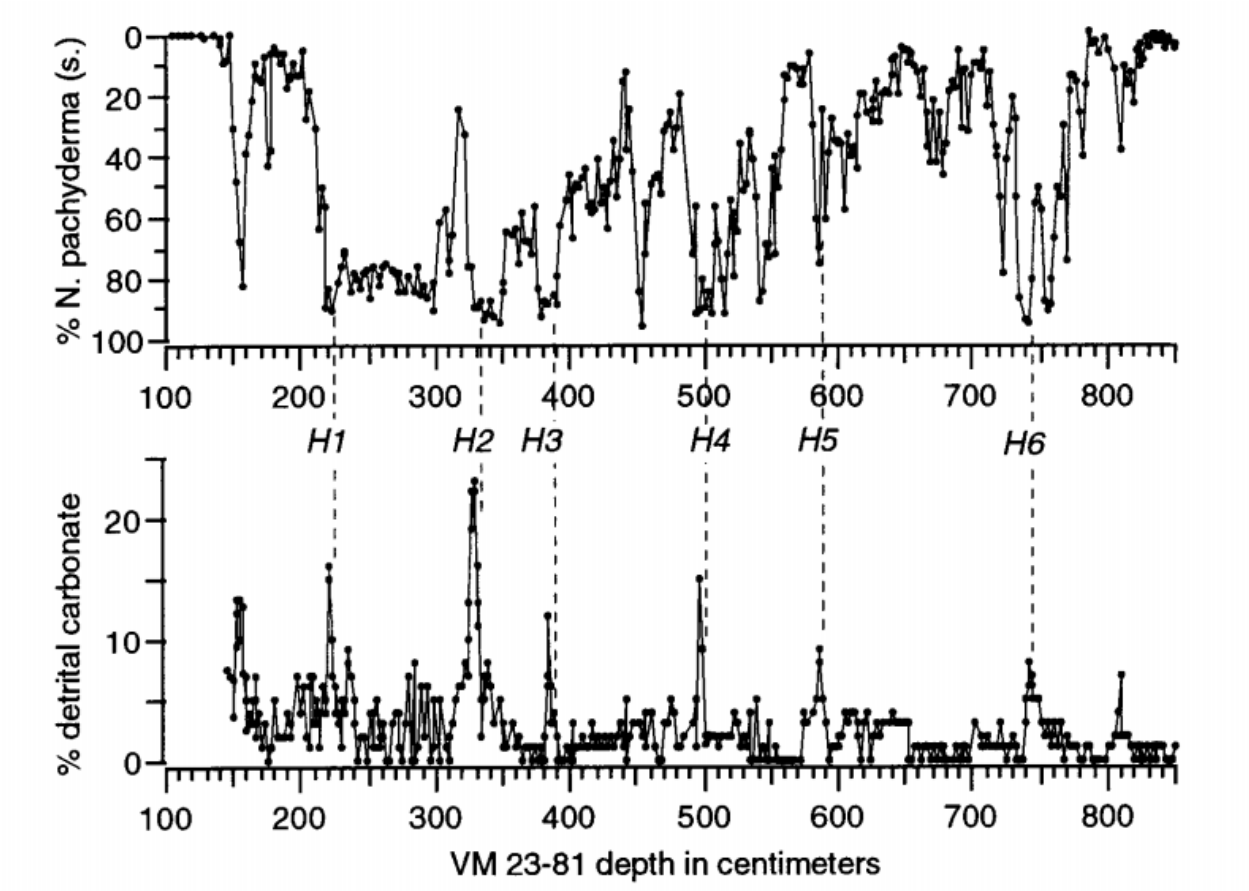

Figure 1: Results from core VM 23-81 presented by Bond et al. (1999). Results shows a comparison of *N. Pachyderma (s.)* percent concentration and Heinrich Events as defined by increase in percentage of detrital carbonate. Dashed lines demonstrated that cooling, as indicated by an increase in percentage of *N. Pachyderma (s.)*, leads each increase in percentage of detrital carbonate about ambient values (Bond et al. 1999).

Proxy evidence of Heinrich Stadial climate anomalies have since been identified worldwide, including Venezuela (Deplazes et al. 2013; Peterson et al. 2000), China (Wang et al. 2001), the French Alps (Heiri et al. 2014), Papua New Guinea (Yokoyama et al. 2001; Chappell 2002), the Iberian Peninsula (Bard et al. 2000; Salgueiro et al. 2014), Bolivia (Baker et al. 2001), Israel (Barr-Mathews et al. 1999; 2000), the Amazon (Cheng et al. 2013; Mosblech et al. 2012), Turkey (Fleitman et al. 2009), Australia (Muller et al. 2008), and the Andes (Kanner et al. 2012), to name a few. Collectively, these distant paleo-records demonstrate that Heinrich Stadials triggered a rapid reorganization of the global climate-ocean system.

How does a cold anomaly in the North Atlantic become a worldwide phenomenon? Heinrich stadials are believed to have triggered an overall cooling of the Northern Hemisphere (Kageyama 2009 *and references therein)*. This is achieved by two contributing factors: first by an abrupt decrease in Northern Hemisphere high-latitude temperatures at the onset of Heinrich Stadials (NGRIP, 2004). Second, paleo-records and climate simulations suggest that Heinrich Events forced the Atlantic Meridional Ocean Circulation (AMOC) system to slow, if not shutdown (Kageyama 2009 *and references therein*). AMOC is the Earth's largest transporter of heat to the northern hemisphere (Houghton et al. 1996, Trerberth and Solomon 1994). The massive volumes of freshwater released to the North Atlantic during Heinrich Events are believed to have created a freshwater cap that prevented the flow of deep-water convection. Halting the formation of North Atlantic Deep Water would effectively slow, if not stop, AMOC's conveyor belt-like circulation system. Recent data from Antarctic ice cores may also prove evidence for an AMOC slowdown in response to a Heinrich Event (Ahn and Brook 2014). Results show that atmospheric CO_2 progressively increase during each Heinrich stadial, but remained constant or slightly decreased during D/O stadials (Ahn and Brook 2014). In addition, opal flux reconstructions in the Southern Ocean presented by Denton et al. (2010) suggest that increase ocean upwelling and CO_2 release occurred during Heinrich Stadials, whereas minimal variation occurred during D/O stadials. These two lines of evidence point to

the existence of additional feedbacks involving the carbon cycle during Heinrich Stadials that does not operate during D/O stadials. This suggests that significant changes in Atlantic Ocean circulation, such as a slowdown of AMOC, occurred after a Heinrich Event (Ahn and Brook 2014). So-called "freshwater hosing" climate simulations, in which fully coupled ocean-atmospheric models are forced with a freshwater flux in the North Atlantic, also support the slowdown of AMOC in response to a Heinrich Event (Dahl and Broccoli 2006; Roche et al. 2014). A slowdown of AMOC, and the heat its transports, therefore contributed to Northern Hemisphere cooling during a Heinrich Stadial.

Northern Hemisphere-wide cooling during a Heinrich Stadial resulted in a disturbance the interhemispheric thermal gradient (Bischoff and Schneider 2014). This thesis will focus on the response of a particular tropical precipitation system whose position is largely sensitive to variations in the interhemispheric thermal gradient. Before continuing on, we digress in section 1.2 to introduce and discuss the climate dynamics influencing the position of the Intertropical Convergence Zone (ITCZ).

1.2 Climate dynamics of the ITCZ

Global precipitation is most intense along the Intertropical Convergence Zone (ITCZ), a tropical belt of deep convective rainclouds. The ITCZ is fed by the convergence of warm, moist trade winds near the surface. The ITCZ is characterized as the ascending branch of a larger meridional overturning system referred to as the Hadley cell.

The location of the ITCZ is not static. On seasonal timescales, the ITCZ fluctuates north-south following the insolation maxima (Bischoff and Schneider, 2014; Figure 2). On longer timescales, paleo-records indicate that the annual mean position of the ITCZ has undergone significant migrations that appear largely unrelated to solar

forcings (Schneider et al.., 2014 *and references therein*). The precise mechanisms that control the long-term annual average position of the ITCZ remain largely unknown.

In order to examine the behavior of the ITCZ, one can begin by building a simple energy balance model (Figure 3). As an air mass rises, it gains moist static energy—a thermodynamic term used to describe the efficiency of lateral transport (Neelin and Held, 1987). By vertically integrating over atmospheric columns, we observe that the moist static energy flux (F) increases going poleward from Earth's tropics. In other words, energy is exported away from the ITCZ in the direction of its ascending branch. By considering F we can examine F_{eq}, or the total amount of moist static energy crossing the geographical equator. The divergence of F_{eq} is related to the net equatorial energy input to the atmosphere, which consists of the net downward shortwave radiation (S_0) at the top of the atmosphere, minus the outgaining longwave radiation (L_0), and any ocean energy uptake (O_0). By expanding the meridional energy flux to the first order and considering Earth's radius (a), we obtain:

$$\delta = -\frac{1}{a}\frac{F_{eq}}{S_0 - L_0 - O_0} \qquad (1)$$

Equation 1, proposed by Bischoff and Schneider (2014), estimates the mean annual position of the ITCZ (δ) in an idealized ocean-atmosphere system. It argues that the ITCZ position depends, to the first order, on the cross-equatorial atmospheric flux of moist static energy (F_{eq}) and on the net energy input to the atmosphere at the equator (S_0-L_0-O_0). Thus, the position of the ITCZ is sensitive to both incoming shifts of insolation and disturbances in energy transport, such as a change in the interhemispheric temperature gradient.

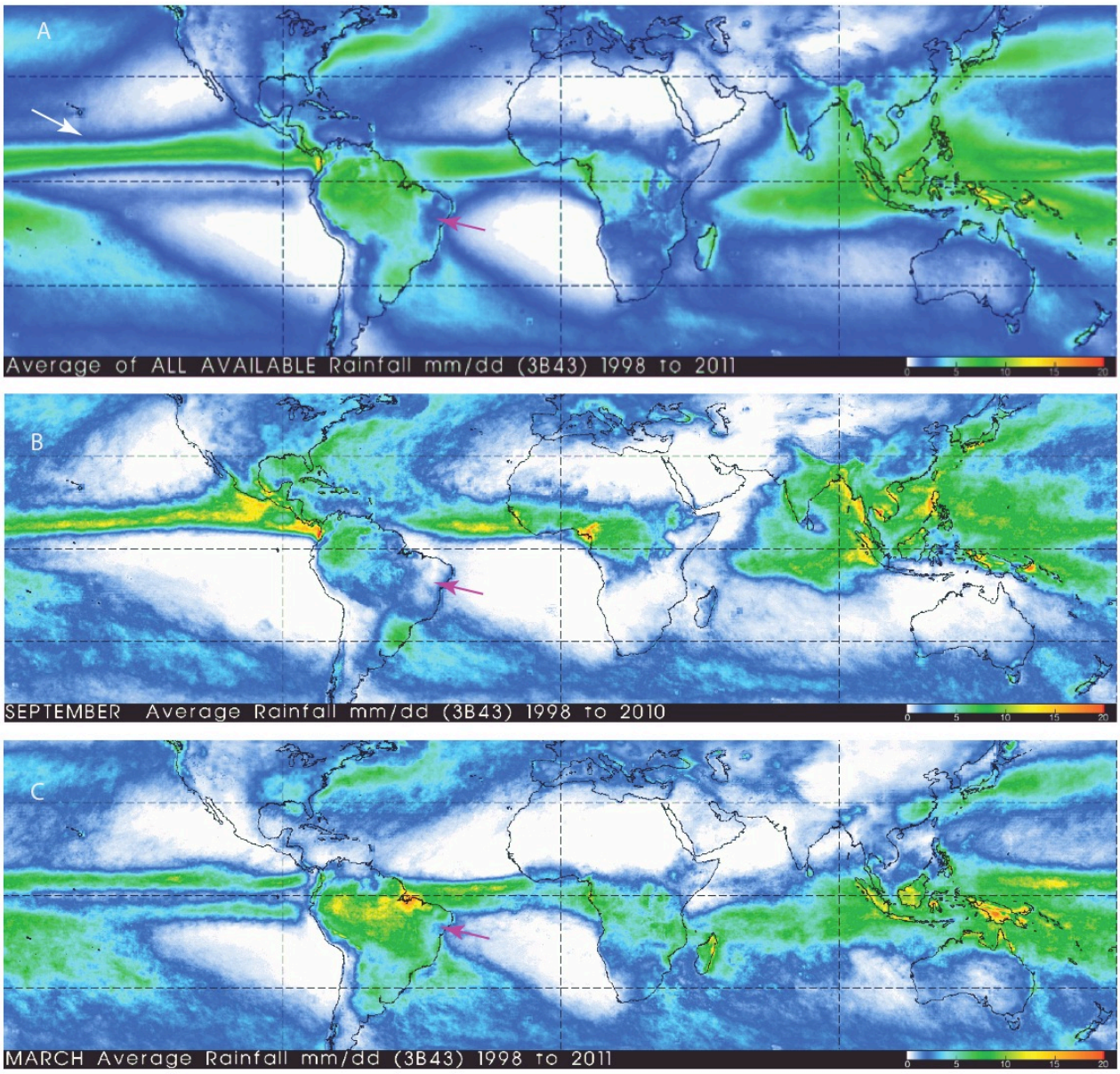

Figure 2: Average global precipitation (mm/day) as measured by NASA's Tropical Rainfall Measuring Mission (TRMM) satellite (Huffman et al. 2007). Maps are calculated to a 0.25° to 0.2°5 resolution grid by combining TRMM's 3-hourly merged IR estimates with the monthly accumulated Global Precipitation Climatology Centre (GPCC) rain gauge analysis (Adler et al. 1979-2013). A) Average global precipitation rate from 1998 to 2011. White arrow indicates the global belt of rain clouds known as the Inter-Tropical Convergence Zone (ITCZ). Purple arrow represents study site. B) Average global precipitation rate during the month of September from 1998-2010, during which the ITCZ is at its northern-most position. C) Average global precipitation rate during the month of March from 1998-2011, during which the ITCZ is at its southern-most position. Between the months of February and April, our study site (indicated by purple arrow) receives 65% of its annual rainfall due to a southerly position of the ITCZ (Hastenrath 2011).

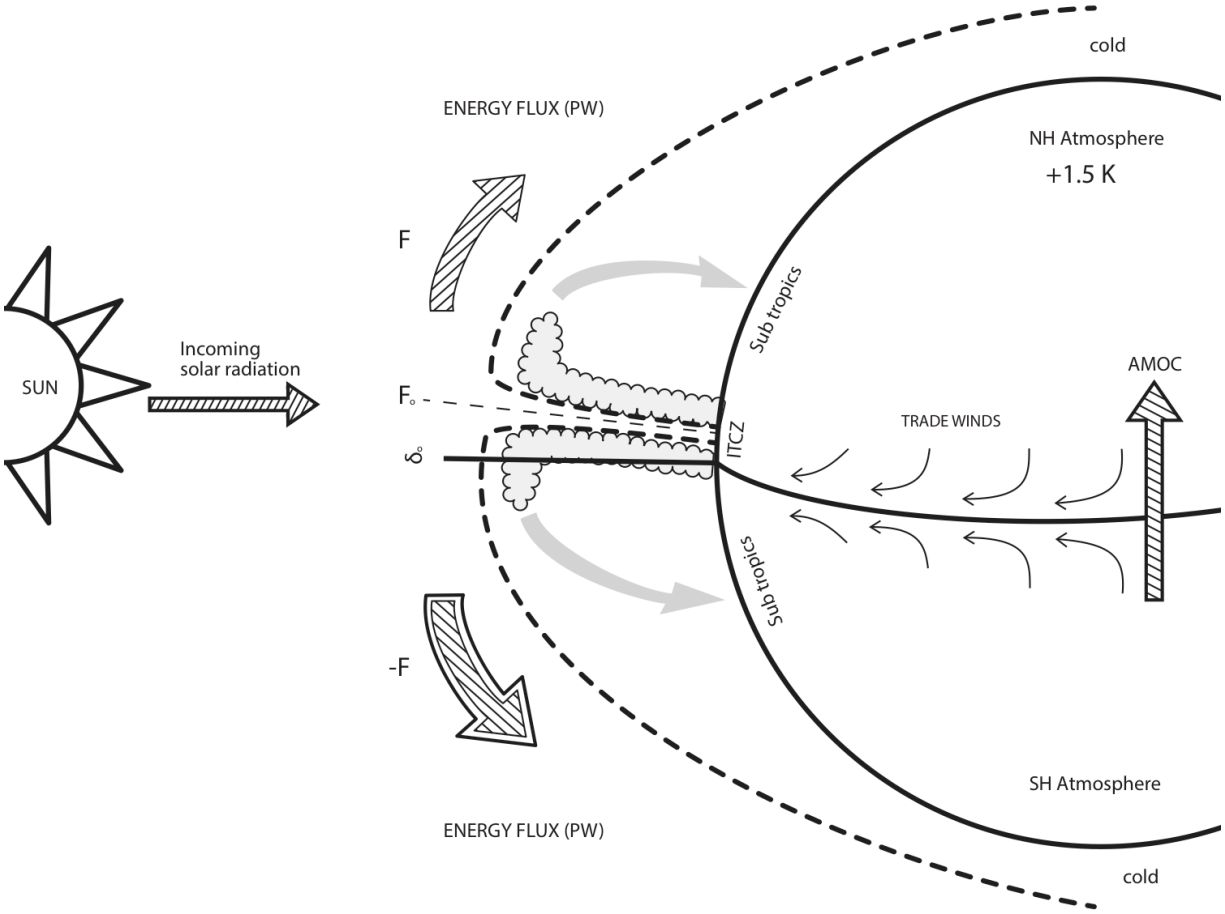

Figure 3: an idealized ITCZ diagram modeled after Schneider et al. (2014). Under modern conditions, the Northern Hemisphere averages 1.2-1.5 K warmer than the Southern Hemisphere due, in part, to the northern transport of heat due to the Atlantic Meridional Ocean Circulation (AMOC). The difference in temperatures creates an inter-hemisphere temperature gradient that is compensated by an intensification of the southern branch of the Hadley Cell, allowing a stronger moist static energy flux (F) towards the Southern Hemisphere. This meridionally asymmetrical Hadley Cell "pushes" the ITCZ northward. As demonstrated in equation 1, the position of the ITCZ is influenced, to first order, by the interhemispheric temperature gradient (represented by F) and the incoming solar radiation at the equator. Under modern climate conditions, the atmosphere transports roughly 0.3 PW of energy southward across the equator and the net equatorial energy input to the atmosphere is 18 Wm^{-2}, resulting in a mean annual ITCZ position of $3^{\circ}N$ (Fasullo and Trenberth, 2008; Bischoff and Schneider, 2014). One can begin to imagine that a disturbance in the inter-hemispheric temperature gradient may trigger a migration of the ITCZ—as suggested by proxy data.

A modern-day interhemispheric thermal gradient exists due to a slightly warmer (1.2-1.5 K) Northern Hemisphere due to, in part, a northward heat transport from AMOC (Houghton et al. 1996). A warmer Northern Hemisphere triggers an intensification of the southern branch of the Hadley Cell, providing a stronger energy flux to the Southern Hemisphere—represented in equation 1 by cross-equatorial energy flux (F_{eq}). Expanding the southern branch of the Hadley Cell results in a meridional asymmetry, such that its ascending branch (the ITCZ) lies farther north (Figure 3). Under modern climate conditions, the atmosphere transports roughly 0.3 PW of energy southward across the equator and the net equatorial energy input to the atmosphere is 18 Wm^{-2} (Fasullo and Trenberth, 2008). Utilizing equation 1, this accurately approximates the mean annual ITCZ position at 4°N (Bischoff and Schneider, 2014; Figure 2).

It must be emphasized that Equation 1 is a highly simplified energy balance that cannot imply causality. A mechanistic understanding how extratropical temperature shifts lead to ITCZ migrations remains to be developed. Equation 1 does, however, provide a starting point for the paleoclimate community when considering possible triggering mechanisms. In order to establish links, it is important to discuss how a particular mechanism may have induced energetic shifts necessary for an ITCZ migration.

1.3 Past ITCZ migrations

Climate simulations suggest that past changes in the thermal contrast between hemispheres can trigger ITCZ migrations (Chiang and Friedman, 2012). This contrast between hemispheres is referred to as the interhemispheric thermal gradient. Past variation in the interhemispheric thermal gradient is often identified through averaged air temperature records or SST reconstructions. Returning to the idealized ITCZ governed by equation 1, one can visualize how a disturbance in the interhemispheric thermal gradient directly influences the flux of exported energy (F) to each

hemisphere. Past shifts in the thermal contrast between hemispheres have been recorded in in Antarctica and Greenland ice cores: correlations between the high latitude records demonstrate that Greenland and Antarctica were asynchronous during the last glaciation—referred to as the interhemispheric (or bipolar) seesaw (Blunier and Brook 2001). The warming and cooling hemispheres is thought to be influenced by millennial-scale extratropical temperature disturbances, although variations in insolation due to the Earth's precessional (21 kyr) cycle also played a role (Zhang et al. 2014).

Heinrich Stadials represent a fascinating example of extreme extratropical cooling that likely disturbed the global interhemispheric thermal gradient. Numerous proxies suggest a southern migration of the ITCZ during a Heinrich Stadial (Figure 4). Broadly, a southward displacement of the ITCZ would results in direr conditions in northern low latitudes and wetter condition in the southern low latitude wetter.

In 2000, Peterson et al. were among the first to publish a high-resolution, long-term record of Atlantic ITCZ migrations throughout the last ice age, as recorded in Cariaco Basin sediments. Located off the coast of Venezuela, the modern Atlantic ITCZ is positioned directly overhead the Cariaco Basin during boreal summer. Under these conditions, Cariaco sediments accumulate dark, organic-rich terrestrial detritus from river runoff. Variations in the reflectance of basin sediments therefore reflect variation in precipitation amount, such that dark, unreflective sediments represent increased precipitation. Throughout the last glaciation, pronounced drying intervals recorded in Cariaco sediments correspond with Heinrich Stadials. Thus, cooling of North Atlantic temperatures during Heinrich Stadials are associated with dry conditions over Northern Venezuela, as supported by a southern migration of the Atlantic ITCZ (Peterson et al. 2000, Deplazes et al. 2014). During the same year, DeMenocal et al. (2000) introduced a marine core record collected off the coast of West Africa. Like the Cariaco Basin, rainfall over the Northern Hemisphere West Africa region is sensitive to the ITCZ position. Increased dust concentrations within

the collected sediment core represent periods of increased aridity (DeMenocal et al. 2000). Their results suggest that during Heinrich Stadials, West Africa experienced drought—an observation coherent with a southern migrations of the ITCZ (DeMenocal et al. 2000; Tjallingi et al. 2008; Stager et al. 2011). One year later, Wang et al. (2001) introduced a high-resolution speleothem record from Eastern China extending through the late Pleistocene. Eastern Chinese speleothems $\delta^{18}O$ profiles represent variation in the East Asian Monsoon (Wang et al. 2001). A northerly position of the ITCZ feeds the intensity of rainfall during the East Asian Monsoon system. Throughout the last glaciation, periods of abrupt weakening of the East Asian Monsoon correspond to Heinrich Stadials—providing evidence of a southern migration of the Pacific ITCZ (Wang et al. 2001).

In anti-phase with the Northern Hemisphere subtropics, paleo-records suggest an increase in precipitation in the Southern Hemisphere subtropics due to a southward migration of the ITCZ (Figure 4). Arz et al. (1998) analyzed a marine core collected from the Northeast (NE) Brazil margine that, much like the Cariaco Basin, records periods of increased river runoff associated with increased precipitation. Their record, first published in 1998, suggest an increase in precipitation over NE Brazil during Heinrich Stadials, indicating a southern migration of the ITCZ. The chronology of the original record, however, has undergone multiple revisions (Dupont et al. 2010, Burckel et al. 2014).

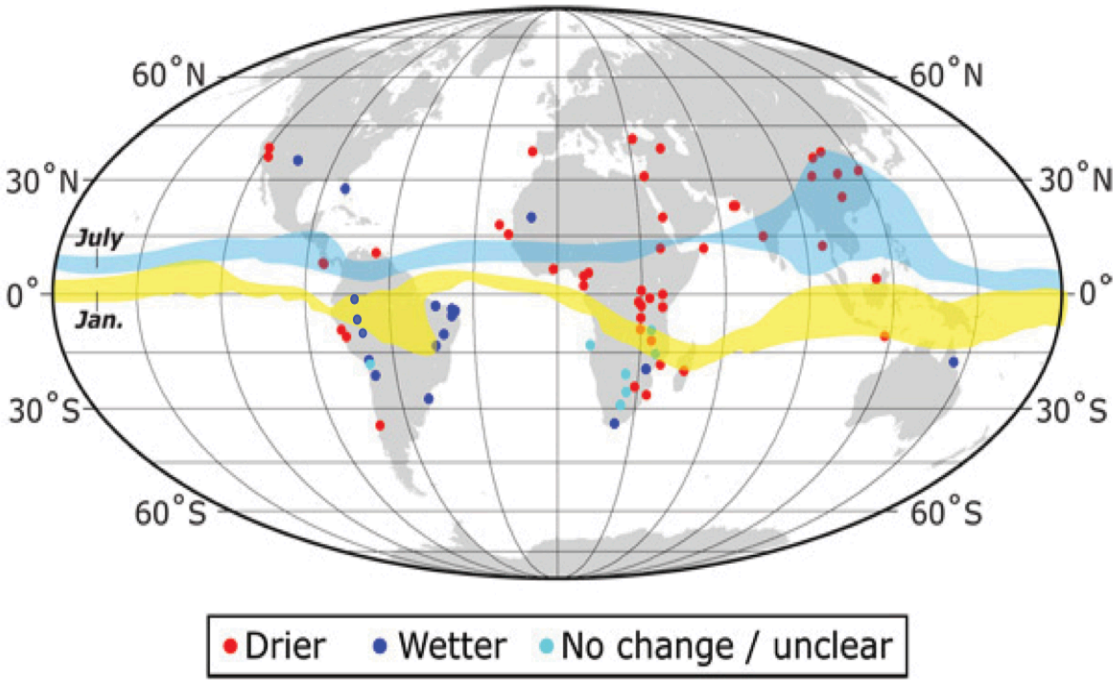

Figure 4: Global distribution of paleo-precipitation records that became drier (red) or wetter (blue) during Heinrich Stadial 1. Modern precipitation associated with seasonal migration of the ITCZ and tropical monsoons are also shown in blue (northern extent) and yellow (southern extent) color ribbons. Figure adapted from Oppo and Curry (2012). Recently published records added to image include Cheng et al. (2013), Mosblech et al. (2012), and Kanner et al. (2012).

In 2004, Wang et al. published a unique record that dated the growth phases of NE Brazil speleothems. Speleothems found in the caves of modern-day arid NE Brazil suggest that the region experienced enhanced precipitation and groundwater recharge (Auler and Smart, 2001; Wang et al. 2004). Using Uranium-series dating techniques, Wang et al. (2004) discovered that speleothem growth phases aligned with Heinrich Stadials. By comparing Cariaco Basin (Northern Hemisphere) sediment record to NE Brazil (Southern Hemisphere) speleothem growth phases, Wang et al. (2004) confirmed the following observation: periods of extreme North Atlantic cooling correspond to a dry interval is observed in the Cariaco basin and a wet interval in NE Brazil, suggesting a southward Atlantic ITCZ migration. Since 2004, additional paleo-records worldwide continue to support a global southern migration of the ITCZ in response to North Atlantic cooling during Heinrich Stadials (Figure 4).

Paleo-records provide valuable insight into the tropical hydroclimate response to abrupt North Atlantic cooling. Additional high-resolution paleo-records are needed to accurately examine the exact timing and extent of ITCZ migration during a Heinrich Stadial. We turn now to discuss a specific proxy that has the potential to provide absolute dated, high-resolution precipitation reconstructions: the speleothem.

1.4 Speleothems as a paleo-precipitation proxy

Speleothems are powerful paleoclimate and paleohydrology proxies. They can be found in many terrestrial locations worldwide, sampled at high-resolution, and precisely dated. The word "speleothem" is an umbrella term to describe secondary carbonate deposits, including stalagmites, stalactites, and flowstones. Speleothems are formed through the following process: as water percolates through a soil column, CO_2 is dissolved. The dissolved CO_2 interacts with water to form carbonic acid.

$$CO_{2(g)} \rightarrow CO_{2(aq)} \quad (2.1)$$

$$H_2O + CO_{2(aq)} \rightarrow H_2CO_3 \quad (2.2)$$

Carbonic acid dissociates rapidly to produce a bicarbonate ion, which in turn dissociates to form a carbonate ion.

$$H_2CO_3 \rightarrow H^+ + HCO_3^- \quad (2.3)$$

$$HCO_3^- \rightarrow H^+ + CO_3^{2-} \quad (2.4)$$

Due to the free protons (H^+) released in this reaction, percolating waters become weakly acidic. Bedrock composed of alkaline limestone ($CaCO_3$) is readily dissolved by the acidic waters, leading to the hydration of a carbonate ion.

$$CaCO_3 + H^+ \rightarrow Ca^{2+} + {}^+HCO_3^- \quad (2.5)$$

The net result depicting limestone dissolution is summarized as:

$$CaCO_3 + CO_2 + H_2O \rightarrow Ca^{2+} + 2HCO_3^- \quad (2.6)$$

Dissolution continues until the solution becomes saturated with respect to Ca_2^+ and HCO_3^-. The atmospheric pCO_2 of a cave is often much lower than the supersaturated waters. Once reaching the cave system, a CO_2 molecule degasses from the solution leaving a $CaCO_3$ mineral deposit.

$$Ca^{2+} + 2HCO_3^- \rightarrow CaCO_3 + CO_2 + H_2O \quad (2.7)$$

Over time a speleothem may develop multiple, if not thousands, of $CaCO_3$ layers. Carbonate layers may, under appropriate conditions, preserve the isotopic signature of the drip water from which it precipitated. Analyzing these layers may therefore provide a paleohydrological record.

1.4.1 Aragonite in speleothems

Aragonite is the high-pressure polymorph of $CaCO_3$ (Helgeson et al. 1978), yet is formed at atmospheric pressures and temperatures. Aragonite has been observed in speleothems over a wide range of cave temperatures, although massive aragonite is usually found in relatively warm and dry caves (Cabrol 1978). The formation of

speleothem aragonite has been attributed to an increase in magnesium (Mg) concentration within drip water, probably related to evaporation that, in turn, may be due to seasonal dryness (Railsback et al. 1994). The presence of cave aragonite, therefore, could be used as an indicator of paleo-aridity (Frisia et al. 2002). Under equilibrium conditions, aragonite $\delta\ ^{18}O$ can be ~0.6‰ higher than calcite $d^{18}O$ (Tarutani et al.., 1969). Speleothem carbonate must be carefully characterized to prevent misinterpretations of the $\delta\ ^{18}O$ signal, as shifts in $\delta\ ^{18}O$ between mineral boundaries could be the result of changing carbonate mineralogy rather than climate forcing.

1.4.2 U/Th dating

Radiometric techniques provide independent time constraints on long-term speleothem deposition. The most widely accepted radiometric technique is ^{230}Th-^{234}U-^{238}U disequilibrium dating (Barns et al. 1956; Broecker and Thurber 1965; Edwards et al. 1987). This technique can be used between a few hundred years to 600,000 years before present (Edwards et al. 1987; Dorale et al. 2004; Cheng et al. 2013). Uranium is soluble, and can therefore be transported from the surface and bedrock into the cave system by percolating waters. Uranium is ultimately incorporated into $CaCO_3$ as the uranyl ion (UO_2^{2+}). Thorium, however, is practically insoluble and will not be incorporated into the precipitated carbonate unless transported by separate processes.

^{238}U decays through a series of intermediate daughters to ^{206}Pb. ^{238}U has a half-life that is much longer than the half-lives of its intermediate daughters. In a closed-system scenario, the nuclides will approach a state of secular equilibrium such that their activities (a product of decay rate and number of nuclides) are equal. Suppose that this system undergoes chemical fractionation, thus disturbing its state of secular equilibrium. For example, imagine that a number of uranium and thorium atoms coexist in a layer of bedrock. Ground water that infiltrates this bedrock will induce a

chemical fractionation by dissolving only soluble uranium. We may then imagine that the dissolved uranium is transported to a cave system, where it is co-precipitated on a speleothem. As layers accumulate, our layer of focus becomes a closed system. The moment at which the system closes is referred to as time-zero. With the passage of time, uranium will decay and slowly approach secular equilibrium once again. The approach to unity is a function of time, which can be calculated by solving the equations of radioactive production and decay. In other words, if the initial activity ratio at time-zero is known and the current activity ratio can be measured, then the interval of time since time-zero to can be calculated using the following equation:

$$[^{230}Th/^{238}U]_{act}-1 = -\exp(-\lambda_{230}T) + [\delta^{234}U(0)/1000][\lambda_{230}/(\lambda_{230}-\lambda_{234})][1-\exp(-(\lambda_{230}-\lambda_{234})T)$$

and

$$\delta^{234}U(T) = [\delta^{234}U(0)][\exp(\lambda_{234}T)]. \quad (3)$$

Where λ is the respective decay rate, and T is time. Accurate ages are possible if samples contain ppb-ppm levels of uranium, have well constrained initial ^{230}Th values, and if the system has remained closed to post-depositional exchange of uranium and thorium (Broecker and Thurber 1965).

1.4.3 Confocal Microscopy

In a manner analogous to tree-ring analysis, the annual layers of speleothems can be utilized to establish well-constrained lamina chronology. Confocal laser fluorescent microscopy (CLFM) is a powerful, non-destructive tool in identifying and imaging individual speleothem layers. Confocal microscopes reflect the light of a high-powered laser off the surface of a sample, thus eliminating the need for thin sections that are necessary for transmission light microscopes. A confocal microscope creates sharp images of a fluorescent specimen that would otherwise appear blurred when viewed with a conventional microscope. To achieve this, confocal microscopes passes

light emitted from the fluorescent specimen through a pinhole aperture that effectively rejects rays that do not directly originate from the focal point.

As speleothem grow, they often incorporate light organic molecules, such as fulvic and humic acids, into their layered structure. The combination of excitation wavelengths (488nm) and emission wavelengths (500nm) required to generate speleothem fluorescence indicate the presence of organic acids (McGarry and Baker 2000). Therefore, detecting fluorescence within a speleothem suggests that organic acids were present in dripwater during calcite precipitation. Multiple studies suggest that cave systems located in wet/dry climate regimes receive an annual flush of organic-rich dripwater from the overlying soil profile (Orland 2009, 2012; Tan et al. 2014 and references therein). The saturated drip water may then be recorded as a bright (or light) fluorescent band. Conversely, calcite that precipitated during a dry season produces a relatively organic-poor, dark band. The result is a series of bright-to-dark fluorescent band couplets along the growth axis. Under the correct climate and environmental condition, banding couplets may represent annual layers (Tan et al.. 2006; Orland et al.. 2012; Orland et al.. 2009; van Beynen et al.., 2001). Observational studies of actively growing speleothem in China and England confirm clear bright-to-dark annual growth layers (Tan et al. 2006).

By counting annual layers revealed by CLFM, one can independently constrain the limits and test the accuracy of an U/Th derived age model. In addition to band counting, studies have used CLFM to identify “sub-annual” banding that may provide further insight about variations in seasonality (Tan et al. 2006; Baker et al. 2002; Linge et al. 2001). Finally, the thickness of annual layers can be measured to infer speleothem growth-rate per year. These high-resolution growth rates may provide evidence of annual-scale variation in temperature (Tan et al. 2003) and precipitation (Proctor et al. 2000).

1.4.4 Oxygen isotope variations

The spatial and seasonal variations in oxygen isotope ratios of modern-day precipitation are well studied. Latitude, altitude, distance from source, precipitation amount, and surface air temperatures all serve as climatic "effects" that influence oxygen isotope ratios of precipitation. Oxygen isotope ratios are commonly written in delta notation:

$$\delta\,^{18}O = [[(^{18}O/^{16}O) / (^{18}O/^{16}O)_{std}] - 1] \times 1000 \quad (4)$$

Where std represents an international standard for $^{18}O/^{16}O$ ratios.

In low-latitude regions (such as the focus of this thesis) decreasing $\delta\,^{18}O$ in meteoric precipitation is largely related to increased rainfall amount, commonly referred to as the "amount-effect" (Dansgaard 1964). Based on the Rayleigh fractionation model (Dansgaard 1964), the amount-effect can be viewed as a measure of the percentage of water vapor removed from original air masses. Increasing rainfall would therefore result in continuous depletion of $\delta\,^{18}O$ precipitation source.

Under equilibrium conditions, the isotopic composition of speleothem calcite reflects the isotopic composition of the water from which is precipitated (Hendy 1971). However, kinetic fractionation may disrupt the isotopic equilibrium between the cave drip water and the subsequent calcite deposited. Kinetic fractionation often occurs due to excess evaporation, such as in a well-ventilated and low-humidity cave system. It is difficult to evaluate if past calcite precipitation met equilibrium conditions, although a number of techniques have been proposed (Dorale and Liu 2009; Hendy 1971). Hendy (1971) proposed a test, commonly referred to as the "Hendy Test," in which multiple stable isotope subsamples are drilled along a single growth layer. If speleothem calcite was deposited in isotopic equilibrium with dripwater, then (1) $\delta^{18}O$ values should remain constant with distance along the growth layer and (2)

measured $\delta^{18}O$ and $\delta^{13}C$ values should not co-vary along the growth axis of a speleothem (Hendy 1971).

Assuming isotopic equilibrium, oxygen isotope ratios of cave drip water therefore reflect those of surface precipitation. Variations in oxygen isotope ratios across the growth axis of speleothems have been widely used as a paleoclimate proxy (McDermott 2004). $\delta^{18}O$ values in speleothem calcite have been shown to vary with the $\delta^{18}O$ of above-surface precipitation (Cobb et al. 2007). $\delta^{18}O$ values have also been used to infer changes in past precipitation patterns or total amount (Bard et al. 2002; Bar-Matthews et al. 1999, 2000)

Examples of cave records that are subject to the amount-effect include Oman speleothems that record Indian monsoon (Fleitman et al. 2003), Chinese speleothems that record Chinese monsoon (Wang et al. 2001), and Brazilian speleothem that record the South American monsoon (Wang et al. 2006).

1.5 Conclusion

Heinrich Stadials have been used to explain unusual high frequency climatic anomalies at low latitudes during the last glaciation. Evidence suggests that during the last glaciation, Heinrich Events caused a slowdown of AMOC—therefore disrupting the interhemispheric thermal gradient (Kageyama 2009). The position of the ITCZ plays a key role in the locality and amount of tropical precipitation worldwide. Its position is largely dependent on the interhemispheric thermal gradient and the equatorial incoming solar radiation. Paleo-records suggest that Heinrich Stadials triggered Northern Hemispheric cooling. This induced an asymmetric expansion of the Hadley cell to the North, ultimately forcing the mean annual position of the ITCZ south.

Low latitude paleo-precipitation records are a key factor in understanding (1) how North Atlantic climate anomalies may have affected tropical hydroclimate change and (2) how to assess the processes that influence the mean position and variability of ITCZ migrations. Speleothems are an ideal proxy for paleo-precipitation and may provide valuable insight into the timing and duration of pluvial anomalies due to a southern position of the ITCZ.

Chapter 2: Heinrich Stadials recorded in NE Brazilian stalagmites, a case study of Heinrich Stadial 4

2.1 Introduction

Constraining the chronology of Heinrich Stadials is critical to understanding their role in global climate change. Reconstructing the migration of the ITCZ, specifically, will advance current knowledge on the timing and response of tropical climate systems to North Atlantic anomalies. In addition, tropical precipitation records may provide insight into the detailed structure of Heinrich Stadials. Doing so is critical to understanding the underlying causes of Heinrich Events.

Speleothems are powerful paleoclimate and paleohydrology proxies because they can be found in many terrestrial locations worldwide, sampled at high-resolution, and absolute dated. NE Brazilian speleothems will allow us to identify the exact onset, duration, and recovery of Brazilian pluvial anomalies associated with Heinrich Stadials. By comparing the NE Brazil speleothems to additional low-latitude precipitation records, one can track the timing and extent of ITCZ migration during Heinrich Stadials.

Here, we provide high-resolution, multi-stalagmite record of Heinrich Stadial (HS) 1, 4, 5 and 6 as recorded in NE Brazilian stalagmites. Our immediate focus is on HS 4. Using two independent dating techniques, we have constrained the onset, duration, and structure of NE pluvial period associated with HS4.

2.2 Background

2.2.1. Previous work on Heinrich Stadial 4

Heinrich Event 4 is arguably the largest of six events by volume during the last glacial period (Roche et al. 2004). The volume of detritus discharged across the North Atlantic during Heinrich Event 4 has been estimated to be 350 km^3 (Hemming 2004).

Roche et al. (2004) estimated an ice release equivalent to a 2±1 m sea-level rise during HS4. Opal flux reconstructions presented by Anderson et al. (2009) demonstrate that ocean upwelling and CO_2 rises in the Southern Ocean were largest during Heinrich Stadial (HS) 4, as compared to subsequent Heinrich events. North Atlantic sediment cores can be correlated with a particular confidence near Heinrich layer 4 because the event occurred shortly after the Laschamp geomagnetic excursion (Hemming 2004). The duration of Heinrich Event 4, however, remains largely unknown. Duration estimates range from 210 years (Thomson et al. 1995) to 2280 years (Cortijo et al. 1997).

Global climate anomalies associated with HS4 have been identified in paleo-proxies worldwide (Peterson et al. 2000; Wang et al. 2001; Cheng et al. 2013; Deplazes et al. 2013). The end of HS4 is associated with the abrupt warming identified as D/O 8 beginning at approximately 38.33 ± 0.1 ka B.P. (Edwards et al. *in prep*). Greenland ice core records and subtropical proxies agree on this age determination with an uncertainty of less than 200 years (NGRIP 2004; Deplazes et al. 2013; Wang et al. 2001). The start of HS4, however, is largely unclear. Age estimates range from 38.78 (Arabian Sea) to 38.75 (Peruvian speleothems), and from 40.01 (Chinese speleothems) to 40.25 (Greenland ice cores)—resulting in a 1500 year uncertainty (Deplazes et al. 2013; Kanner et al. 2012; Edwards et al. *in prep*; NGRIP 2004).

2.2.2. Modern oxygen isotope variation along the Atlantic ITCZ

The distribution of modern day $\delta\,^{18}O$ precipitation values across central and northeastern South America is largely influenced by the mean annual position of the ITCZ (Hastenrath, 1990; Hastenrath 2011). Since 1969, modern $\delta\,^{18}O$ precipitation values have been measured at numerous stations and are open for public access using the International Atomic Energy Agency's (IAEA) Global Network of Isotopes in Precipitation (GNIP) database (IAEA/WMO 2015). Figure 5 indicates the location and averaged $\delta\,^{18}O$ precipitation values of IAEA stations across NE Brazil, collected

from 1969 to 1990. Stations were selected based on the proximity to the study site. Figure 6 shows the long-term average (1965-1990) of monthly accumulated precipitation and $\delta^{18}O$ values at the GNIP station Belem, Brazil.

The resulting pattern indicates a gradient of increasing $\delta^{18}O$ values from the mean annual position of the ITCZ to its southern-most branch. This suggests an anti-correlation between precipitation $\delta^{18}O$ values and precipitation amount—a common characteristic of the amount effect (as seen in figure 6). One can hypothesize that a southern migration of the ITCZ would be recorded as a decrease in $\delta^{18}O$ values within the NE Brazil speleothem record.

2.2.3 Study Site

The interior of NE Brazil is a semiarid region located immediately south of the modern ITCZ. Annual temperatures average 28°C and accumulated precipitation averages 500mm per year (figure 6). The position of the ITCZ determines the seasonality of rainfall over NE Brazil: over 65% of annual rainfall is restricted to the months of February-April, when the ITCZ reaches its southernmost position (Hastenrath, 1990; Hastenrath 2011). In addition to low precipitation, the aridity of NE Brazil is attributed to high evapotranspiration rates (>1,400 mm annually). Modern-day NE Brazil experiences frequent and extreme droughts (Garreaud 2009; Moura and Shukla, 1988; Hastenrath and Heller, 1977). Observed droughts have been linked to an anomalously northern position of the ITCZ (Hastenrath, 1990). Northern migrations of the ITCZ are attributed to anomalously warm Northern Hemisphere subtropical sea surface temperatures (SST) relative to Southern Hemisphere (Hastenrath 2000). Conversely, sea surface temperatures anomalies in the opposite sense (cooler Northern Hemisphere SSTs) would suggest a southward shift of the ITCZ, as observed in this study.

The region has a well-developed underground karst system, with shallow cave passages developing in selected bedding horizons of dolomite. Surface streams in the area are dry, with ephemeral flow only after high precipitation events (Auler 1999). Short-lived speleothems that decorate the modern day dry caves of NE Brazil are relics of past wet period. Stalagmite growth phases likely correspond to high rainfall, as precipitation levels must exceed soil and bedrock thresholds to allow for speleothem growth. Previous work on NE Brazil stalagmites reveal that pluvial phases are synchronous with North Atlantic Heinrich Events, as well as cold periods in Greenland, periods of decreased river runoff to the Cariaco Basin, and periods of weak East Asian summer monsoons (Wang et al. 2004). The synchronicity of these events is in agreement with the hypothesis of a southward migrating ITCZ during Heinrich Stadials. To date, NE Brazil pluvial phases have been identified to occur during HS-1, HS-4, HS-5, and HS-6 (Wang et al. 2004).

Our study site is located in the Salitre river valley, 500 km west of the Atlantic. Samples were collected from Toca da Boa Vista (TBV) and Toca da Barracuda (TBR) caves (40^{o}51'39"W 10^{o}09'36"S, 600m above sea level). The two caves are separated by a 1 km gap and are therefore unaffected by one another's internal temperature, humidity, and ventilation changes. Both caves share the same Precambrian dolomite bedrock of the Una Group (Auler 1999).

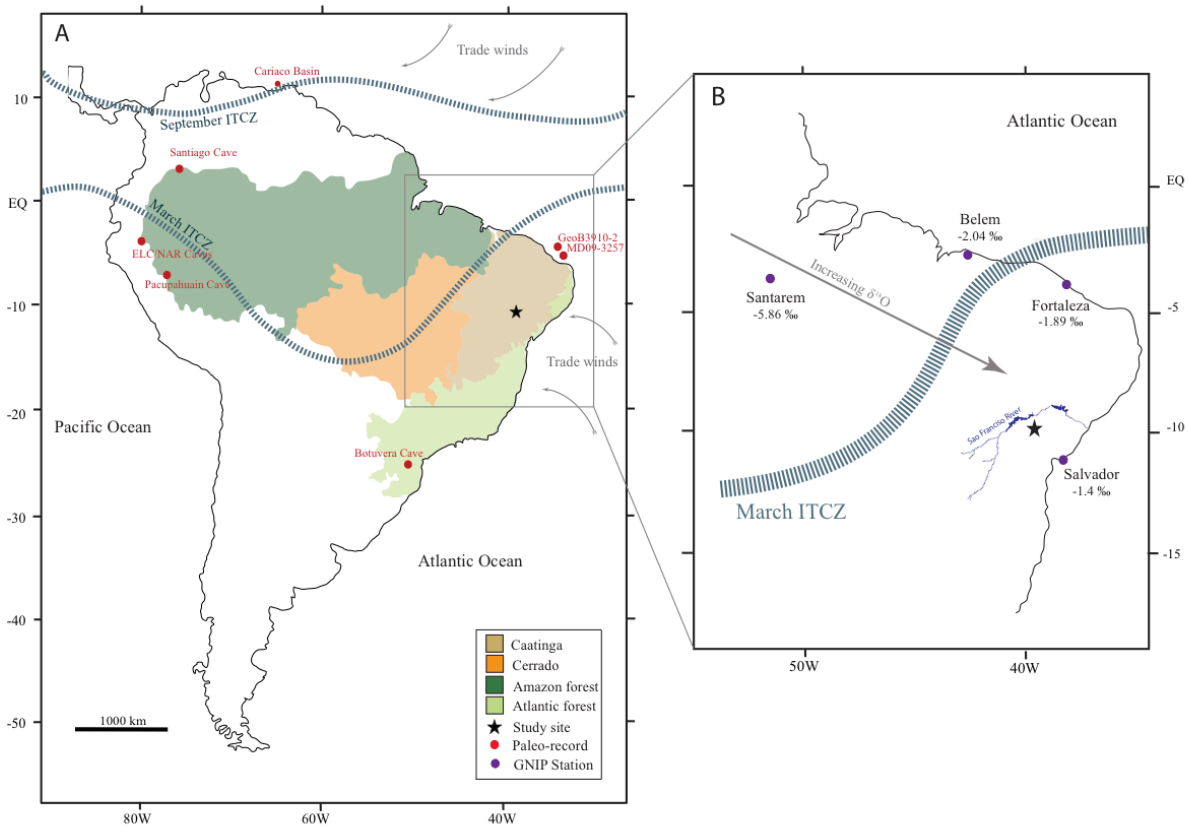

Figure 5: Map of study area. A) Red circles indicate the location of paleo-records. Dashed blues lines show the northern-most (September) and southern-most (March) extent of the ITCZ. B) map indicating the indicates the location and average $\delta^{18}O$ values (1969-1990) of Global Network of Isotopes in Precipitation (GNIP) stations across NE Brazil (IAEA/WMO 2015). A spatial gradient in precipitation $\delta^{18}O$ values is observed from the modern mean annual position of the ITCZ towards its southern-most extent and beyond. Black star indicates study site.

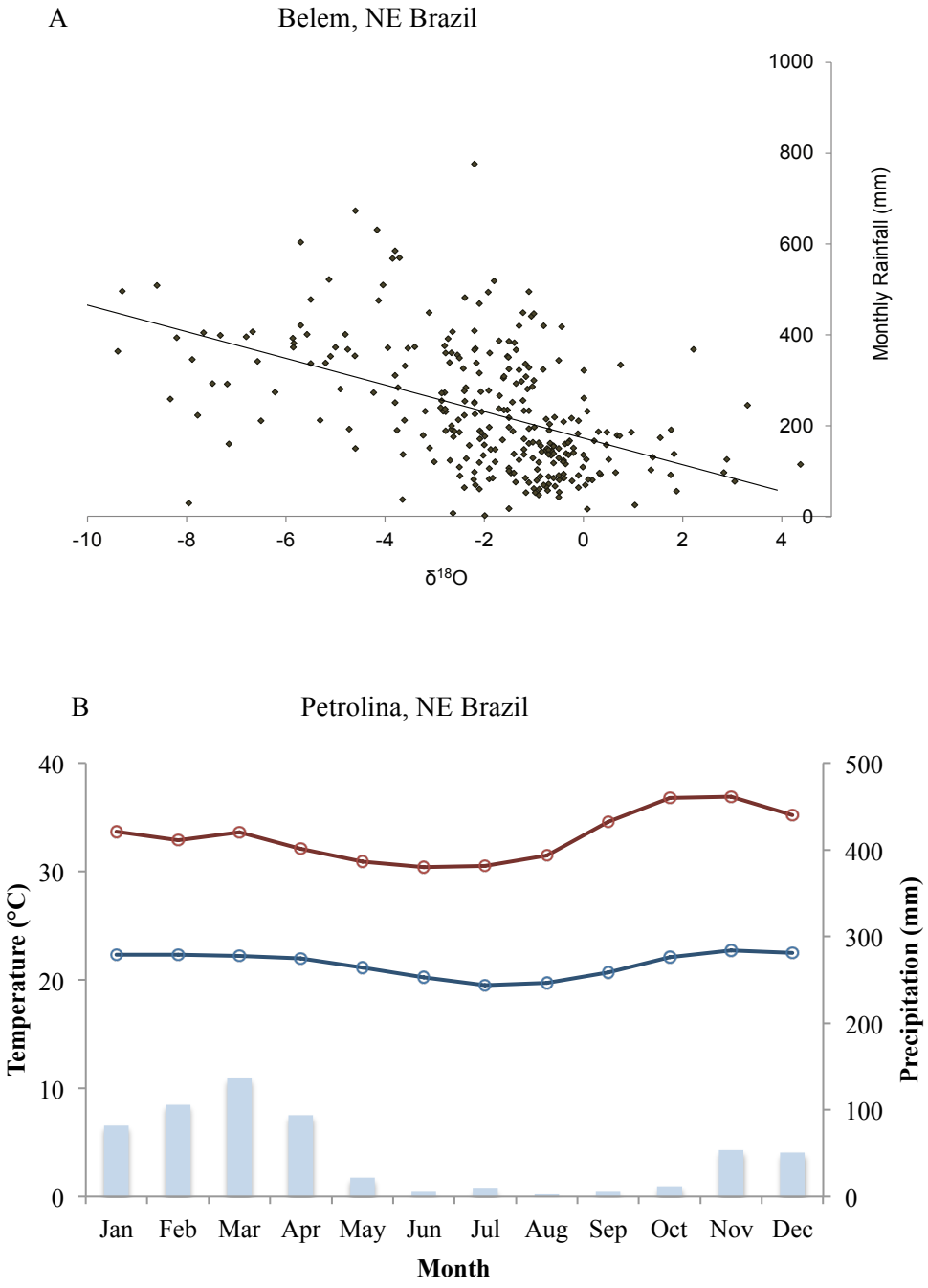

Figure 6: A) Modern rainfall amount and $\delta^{18}O$ values measured monthly from 1965-1990 at the GNIP station in Belem, Brazil (IAEA/WMO 2015). R^2 = 0.3, although scatter is expected due to variations in precipitation source and season. General long-term trends indicate an increase of $\delta^{18}O$ values with decreasing precipitation amount, commonly referred to as the "amount effect". B) Modern average temperatures (red=temperature highs, blue=temperature lows) and accumulated monthly precipitation from the nearby city of Petrolia, Brazil—approximately 120 km from study site. Data collected from 1961-1990 by the Instituto Nacional de Meteorologia (INMET) of Brazil (http://www.inmet.gov.br/portal/).

2.3 Methods

Stalagmites TBV40, TBV63, and TBR14 were selected for analysis. Samples were halved along the growth axis and polished. A total of 34 subsamples were drilled for U/Th dating techniques, with an additional 6 replicate subsamples were drilled adjacent to their U/Th original date. The purpose of replicates is to determine the consistency and reproducibility of sample analysis. Due to the anomalously low uranium concentration, calcite powder sample sizes were calculated as follows:

$$Sample\ size\ (g) = \left(\frac{Desired\ counts}{Ion\ eff.} * \frac{1}{Av}\right) * \left(\frac{\lambda 230}{\lambda 238} * \frac{1}{\left(\frac{230}{238}\right)Act}\right) * \left(\frac{238\ g/mol}{238U\ conc}\right) \qquad (3)$$

Where the average ionization efficiency (ion eff) of samples 0.01, λ represents respective decay rate of ^{230}Th and ^{238}U, Av represents Avogadro's number, and the desired counts—determined by counting statistics—is 4 million ions. The respective activity ratios (Act) of ^{230}Th and ^{238}U used were previously measured by Wang et al. (2004),

Samples were dissolved in 14N HNO_3 acid and spiked with a ^{235}U-^{233}U-^{229}Th double spike described in Edwards et al. (1987). Spike amounts were calculated such that the ^{235}U to ^{233}U (sample to spike) ratio was 13. Spiked samples were fumed with concentrated $HClO_4$ and dried. Samples were re-dissolved with 2N HCl and 0.1 mg of Fe was added (see supplementary figure 5). Uranium and thorium ions were co-precipitated with Fe by titrating with ammonium hydroxide until neutral (pH 7). The resulting precipitant was centrifuged 3 times, rinsing with super-clean H_2O and disposing of supernatant between centrifuge runs. Samples were re-dissolved in 0.5 ml 7N HNO_3 and loaded into an anion exchange column. Using this column, thorium and uranium fractions can be extracted and collected separately. First, the Fe was eluted from the column using 7N HNO_3. The thorium fraction was then extracted with 6N HCl into one beaker and the uranium with super-clean H_2O into a separate

beaker. Extracted solutions were fumed with $HClO_4$, dried, dissolved with HNO_3, dried again, and finally dissolved with a mixture of 99% super-clean H_2O and 1% HNO_3 and HF.

Separate uranium and thorium liquid extracts were measured using induction-coupled mass spectrometry (ICP-MS) on the Thermo Neptune ICP-MS. Sample solution is ionized and measured automatically. Isotopes ^{235}U, ^{234}U, and ^{233}U were measured for approximately 1000 cycles. Isotopes ^{232}Th, ^{230Th}, and ^{229}Th were measured for 500-700 cycles, depending on sample concentration. Acquisition times for ^{234}U and ^{230}Th were both 1 second per cycle. Background values and chemistry blanks were measured and carefully subtracted (see supplementary table 2). Resulting ages were calculated following Edwards et al. (1987).

Separate age models were developed for each HS growth phase using the Bayesian statistical software OxCal version 4.2 (Ramsey 2009a; Ramsey and Lee 2013). The age models were calculated using P-sequence with a variable k value of 0.1. For details on the process of running OxCal age models, see examples in supplementary figures 2 and 3.

Subsamples were drilled along the growth axis of each sample for micro X-Ray diffraction (XRD) powder analysis, totaling 15 measurements. For each subsample, 1-2 mg of powder was hand drilled and adhered to an Eulerian Cradle sample holder. Samples were analyzed using a Bruker-AXS Microdiffractometer with a 2.2 kW sealed Cu X-ray source. Results were analyzed using Jade v7.0 Advanced Powder Data Processing Software (Materials Data, Inc). Diffractograms were identified using the Whole Pattern Fit function.

A total of 1004 stable isotope samples were micro-drilled and analyzed for oxygen and carbon isotope ratios. Samples were measured using a Finnigan Delta V Advantage mass spectrometer equipped with an automated carbonate preparation

system (Gas Bench II) at the Institute of Geological Sciences of the University of Bern. An additional 200 stable isotope samples were hand-drilled due to the difficultly in micro-drilling positioning (top 5 cm of sample TBV 40 and bottom 4 cm of sample TBR14). The additional 200 samples were measured on a Finnigan MAT252 Mass Spectrometer at the University of Minnesota. Results are reported relative to the Vienna Peedee Belemnite (VPDB) standard. Analytical errors for $\delta^{18}O$ are 0.07 ‰ VPDB (1σ) (Fleitmann et al.., 2009). Resulting data show no discrepancy between the two mass spectrometers. Finally, three Hendy tests were analyzed by drilling five subsamples along a single layer of each stalagmite.

Confocal laser fluorescent microscopy (CLFM) techniques were conducted to identify banding in the HS4 calcitic portion of each sample. CLFM was completed at the University Imaging Center at the University of Minnesota using a Nikon A1R Multi-Photon operating with a 488nm argon-sourced laser line. Digital images of speleothem fluorescence were collected using an emission filter for wavelengths between 505 and 539 nm. A series of overlapping images, totaling approximately 60 x 1.2 mm, were collected with a 10x objective lends (1.23 μm/pixel) along the growth axis of each stalagmite. Linear image adjustment was applied in order to improve contrast of published images.

Individual bands widths were measured and counted using the *Nikon Elements Viewer* software. Each clearly visible light band was given a count of one. When banding was not clear and/or two bands were not clearly distinguishable, each band was given a count of 1.5 and assigned an error of 0.5. This method was adopted after the ice core layer-counting procedure described by Alley et al.. (1997). The individual widths of growth bands were measured using the *Nikon Elements Viewer* measurement tool. While counting, bands were categorized as a single or multi-event band. Single bands consist of a dark-to-light couplet within a single growth band. Multi-event bands are characterized as one or more light band within a single growth band.

2.4 Results

XRD techniques revealed sections of both calcite and aragonite in samples TBV40 and TBV63 (figure 7). TBV40 exhibited aragonite growth during HS6 and the first portion (490 years, as determined by U/Th dating) of HS4 growth phases, followed by a calcite growth phase corresponding to the final portion of HS4. TBV63 exhibited aragonite growth during the beginning of HS5 followed by a layer of mixed aragonite and calcite, suggesting alteration. As a result, HS5 recorded in TBV63 was not included in this study. TBV63 exhibited aragonite growth at the beginning of HS4 (83 years, as determined by U/Th dating) followed by calcite growth for the reminder of HS4. Results for TBR14 suggested pure calcite. XRD results are summarized below in Table 1.

TBV-40	Location (from top)	
	53 mm	calcite
	133 mm	aragonite
	194mm	aragonite
TBV-14		
	38 mm	calcite
	115 mm	calcite
	145 mm	calcite
TBV-63		
	19 mm	aragonite
	62 mm	aragonite
	64 mm	calcite
	68 mm	aragonite-calcite mix
	74 mm	aragonite-calcite mix
	110 mm	aragonite
	140 mm	aragonite

Table 1: summary of powder micro- XRD results, as determined by Jade mineral identification software.

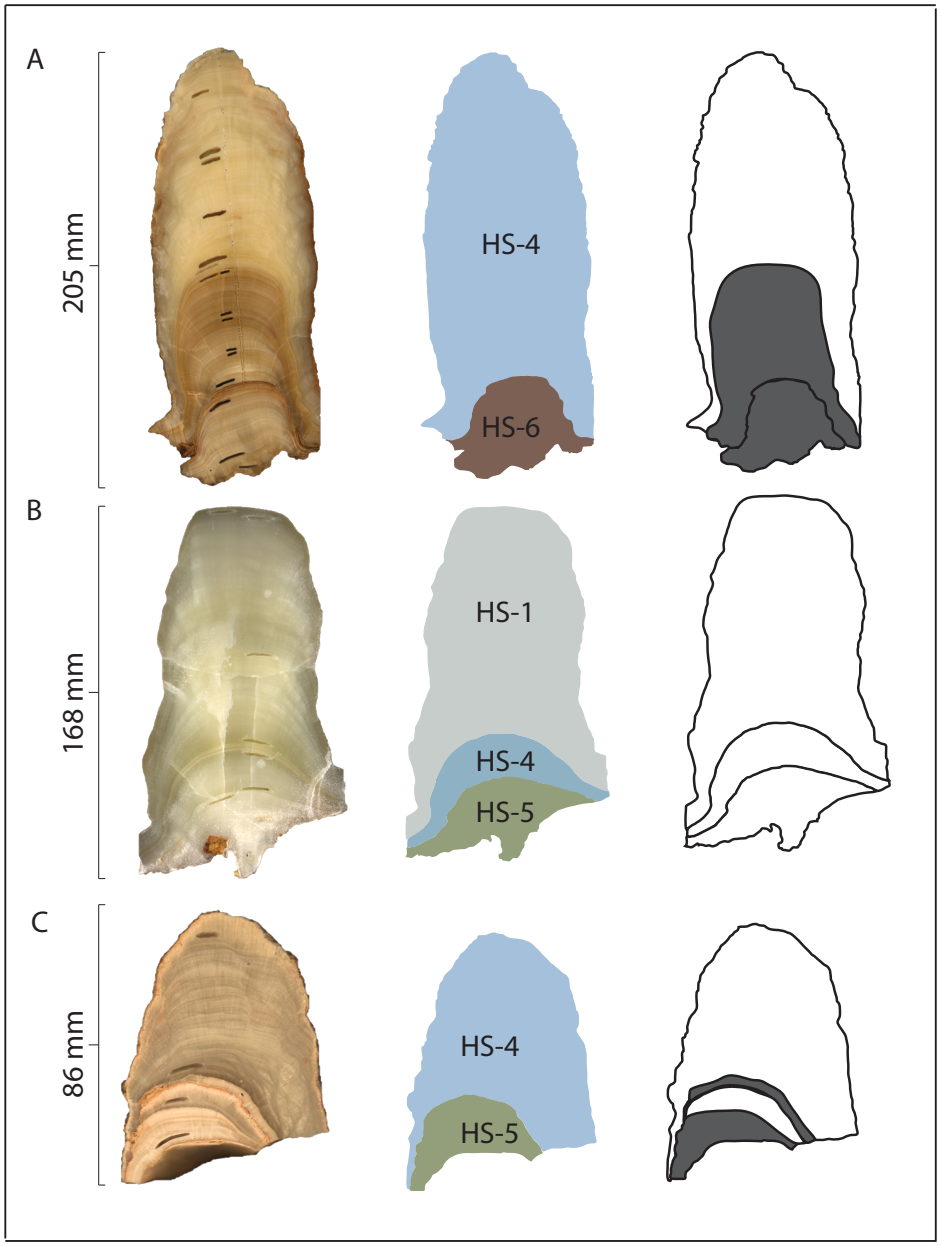

Figure 7: Samples of focus from TBV and TBR caves. First column: real-color images of (A) TBV40 (B) TBR14 and (C) TBV63. Second column: stalagmites can be divided into separate growth phases that correspond with Heinrich Stadial (HS) Events, as shown in colored contours. Third column: grey sections within sample outlines indicate areas of XRD-confirmed aragonite.

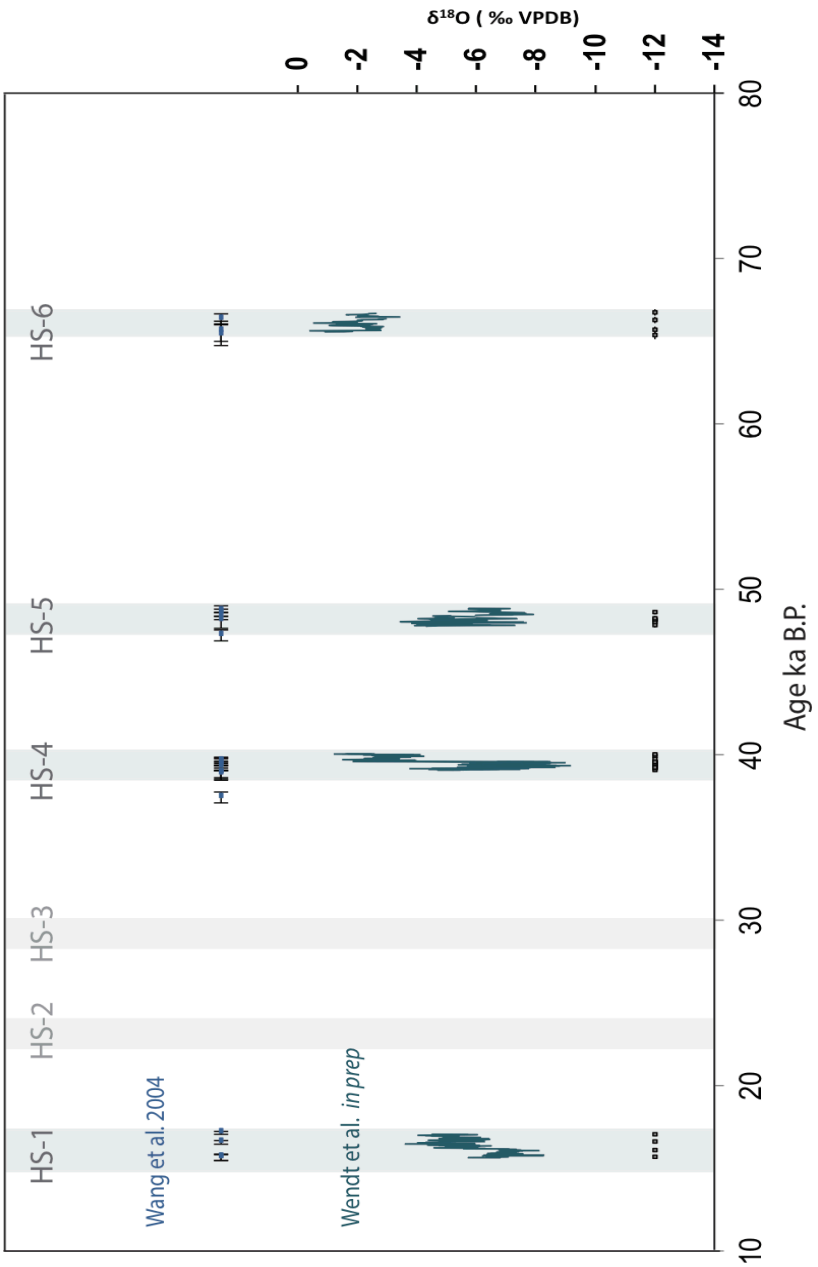

Figure 8: NE Brazil pluvial periods corresponding to HS1, HS4, HS5, and HS6, as recorded in NE Brazilian stalagmites. Gaps in record indicate periods of no speleothem growth. Plotted above: Wang et al. (2004) U/Th dates with error for stalagmites TBV40, TBV63, TBR14. Plotted below: Wendt et al. (*in prep*) U/Th dates with error for stalagmites TBV40, TBV63, TBR14. Also included in the Wendt et al. (*in* prep) oxygen isotope record. We interpret that a decrease in $\delta^{18}O$ values indicates an increase in precipitation.

A total of 32 U/Th dates are in stratigraphic order within measured uncertainties. All replicates were within error of their respective dates. Two dates in HS-4 growth phases (39.1 and 38.3 ka B.P.) were eliminated from the age model because the two subsamples were drilled too closely to the rind (edge) of the speleothem and are therefore unreliable. The edges of NE Brazilian speleothems have likely undergone condensation corrosion, as described by Auler and Smart (2004). For a full list of U/Th dates, see supplementary table 1.

Recorded pluvial periods in stalagmites range from -2‰ to -9‰. This unusually large range in values is also attributed to, in part, change in speleothem mineralogy from aragonite to calcite (Tarutani et al.., 1969). Results of Hendy tests show that along a single growth layer, $\delta^{18}O$ varies no more than -0.5‰, without any overarching trends of increasing or decreasing values. TBR14 exhibited relatively low correlations (R^2 of 0.3) between $\delta^{18}O$ and $\delta^{13}C$ suggests that kinetic fractionation has little effect (see supplementary figure 4). TBV40 and TBV63, however, exhibit a larger correlation (R^2 of 0.6 to 0.7), suggesting that kinetic processes—such as excess evaporation—may have an effect. Excess evaporation would like result in a less depleted isotopic signature, as lighter isotopes are kinetically favorable to evaporate. Despite this correlation, we argue that additional evidence supports that speleothems from TBV cave do, indeed, reflect climatic processes above the cave system (see section 2.5).

2.4.1 Results specific to HS-4 growth phases

XRD techniques reveal an aragonitic growth phase in the HS4 growth phase of TBV40 and TBV63 (figure 11). Aragonite sections were identified by Jade software as pure aragonite, suggesting that they did not undergo alteration. The aragonite phase identified in TBV40 and TBV63 is U/Th dated from 40.06 to 39.60 ka B.P within errors of 0.1 ka. Both aragonite phases are followed by a calcite growth phase, U/Th dated from 39.60 to 39.06 ka B.P. (±0.1 ka). XRD confirmed the HS-4 growth phase of TBR14 to be entirely calcite, U/Th dated from 39.59 to 39.07 ka B.P. (±0.1 ka).

The HS-4 growth phase of TBR14 therefore corresponds to the calcitic growth phases of TBV40 and TBV63, within error. U/Th determined ages of aragonite and calcite phases are summarized in Table 2.

	Calcite (years)	**Aragonite (years)**	**Total**
TBR14	520 ± 280	*x*	520 ± 280
TBV63	510 ± 170	80 ± 140	590 ± 200
TBV40	470 ± 120	500 ± 110	970 ± 140

Table 2: Total number of years, as determined by the OxCal age model, in each calcite and aragonite section of each sample.

Fluorescent bands were discovered in the HS-4 calcitic portion of all three stalagmites, suggesting that organic acids were present in dripwater during calcite precipitation (Figure 9). Banding counting results are summarized in Table 3. U/Th years were calculated by subtracting the derived OxCal age model date at the top (z=0) of each HS-4 section. Band counts for calcitic portion of each stalagmite are within error of U/Th dates, and therefore are in high agreement (Figure 10).

	Total Confocal bands	**U/Th years of calcitic portion**
TBV40	373 ± 60	470 ± 120
TBV63	457 ± 228	500 ± 160
TBR14	423 ± 139	520 ± 280

Table 3: Fluorescent bands vs U/Th years in the calcitic section of each sample

In addition to bands, multiple small hiatuses were identified in each sample. Hiatuses are characterized as a single bright band that is exceptionally distinct in structure and brightness from surrounding growth bands (see supplementary figure 5 for example). The presence of hiatuses can cause discrepancies between band-counts and U-series geochronology.

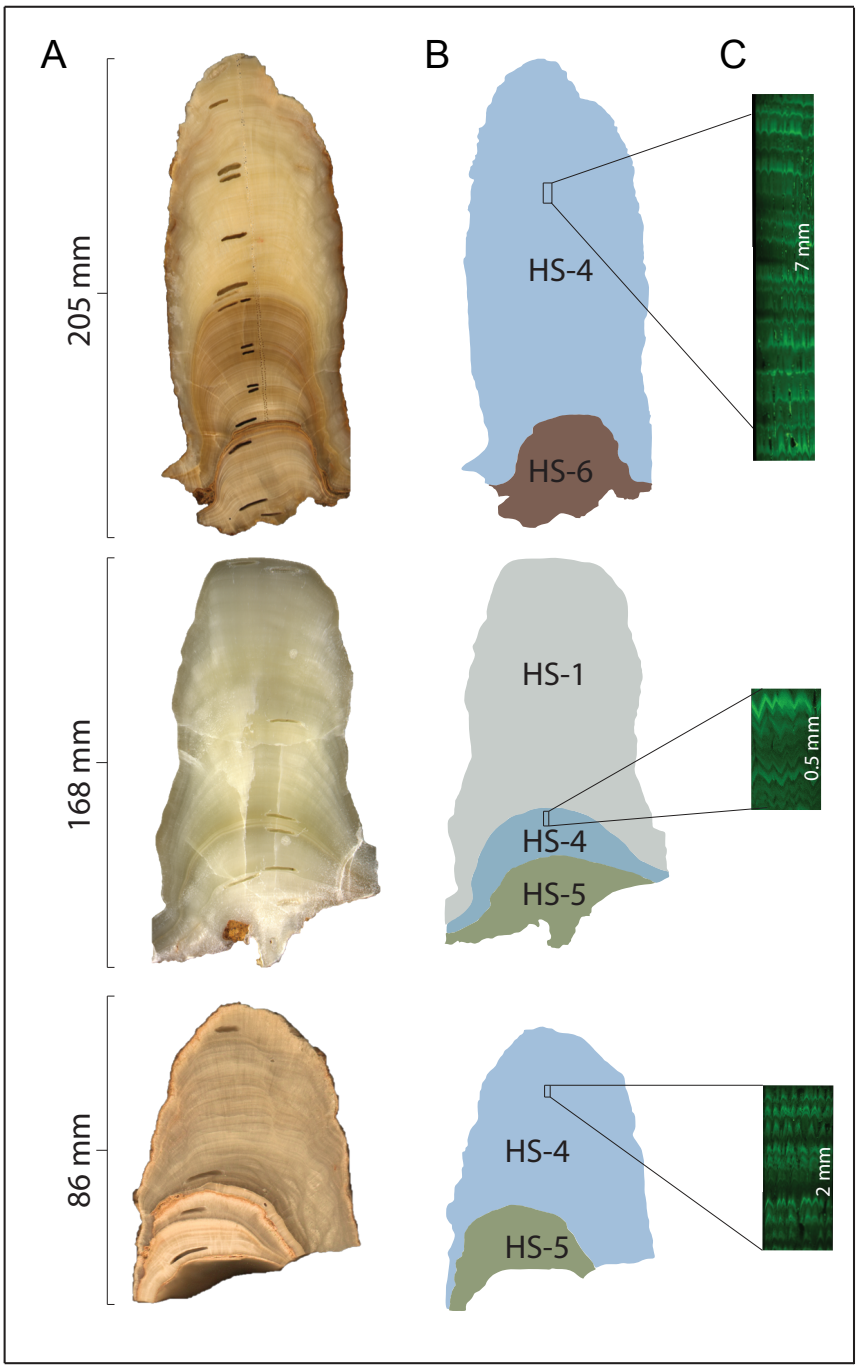

Figure 9: TBV and TBR samples. (A) Real-color images from top: TBV40, TBR14, TBV63. (B) Stalagmites can be divided into separate growth phases that correspond with Heinrich Stadial (HS) Events. The focus of this study is on HS- 4, as all three samples include a Heinrich Stadial 4 growth phase. (C) Confocal fluorescent banding has been identified in the Heinrich Stadial 4 portion of all three samples.

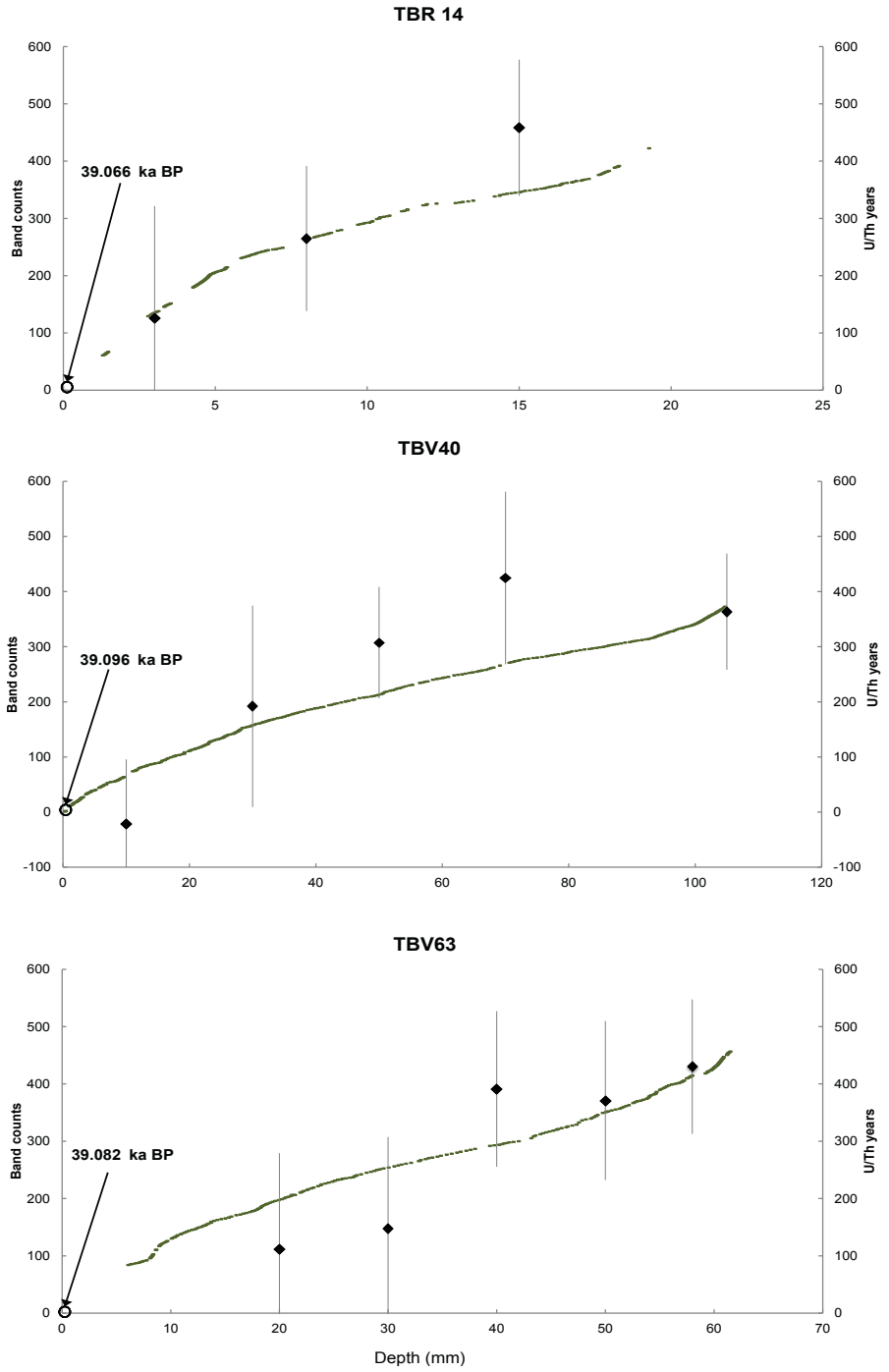

Figure 10: Comparison of fluorescent-band counting methods and U-series dating for the calcitic portion of each three samples, plotted across depth. Total number of fluorescent band counts (green points) plotted against total number of U-series (U/Th) years, with error. Gaps in confocal chronology represent areas of unclear banding. Within these areas, bands were interpolated (see text for details). U/Th years were calculated by subtracting the OxCal age model date at the top (z=0) of each HS-4 section. Band counting and U/Th age chronologies are in high agreement, within error.

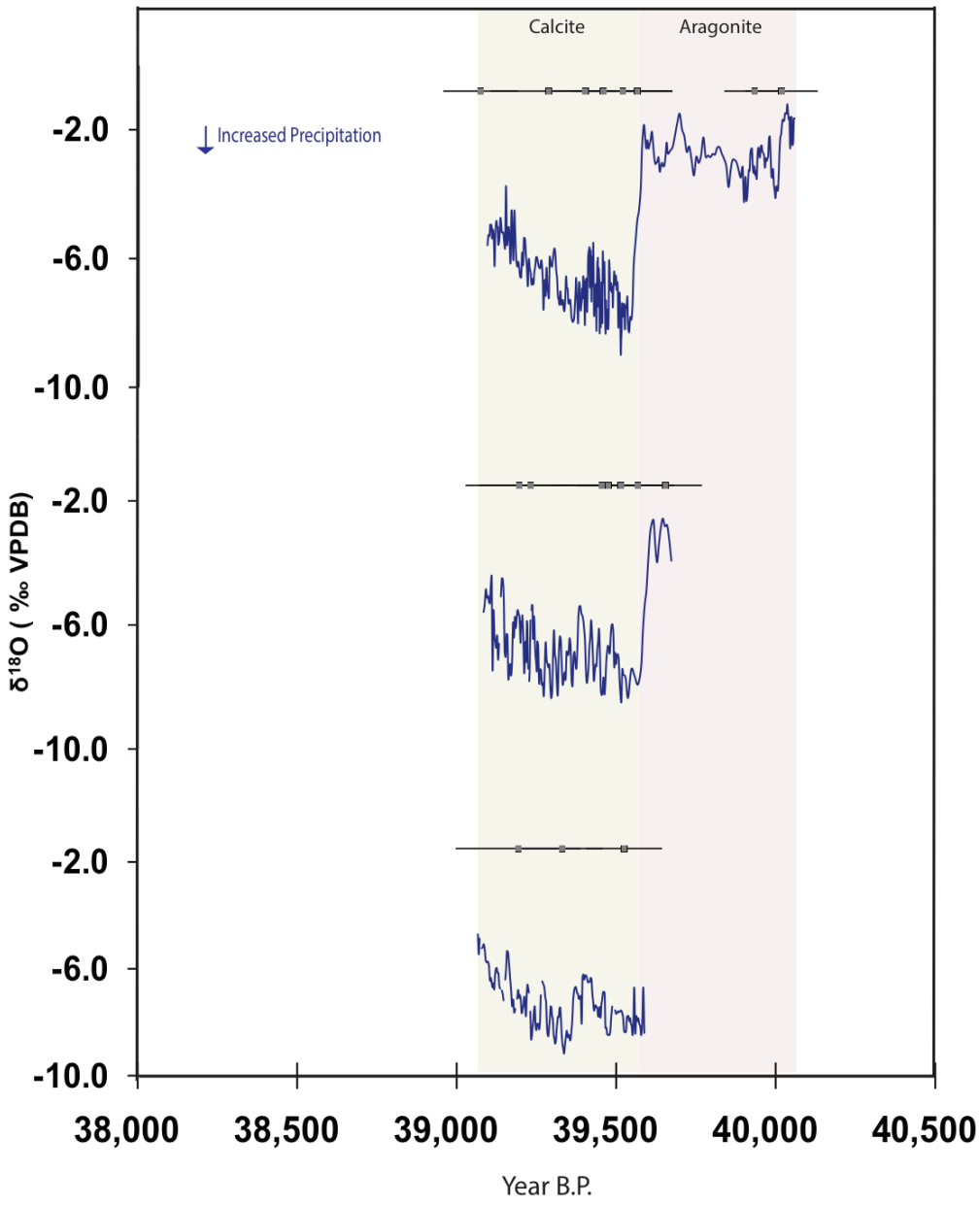

Figure 11: Pluvial period corresponding to HS-4, as recorded in NE Brazilian samples (from top) TBV40, TBV63, and TBR14. Black circles represent U/Th ages with respective errors. Brown shading signifies aragonite phase identified in TBV40 and TBV63, U/Th dated from 40.06 to 39.60 ka B.P within errors of 0.1 ka B.P.. Green shading represents subsequent calcite phase, U/Th dated from 39.60 to 39.06 ka B.P. (±0.1 ka). We interpret the shift from aragonite to calcite in NE Brazilian stalagmites to represent a shift in relative humidity due to increased rainfall.

2.5 Discussion

Speleothem growth in NE Brazil was highly episodic, suggesting that extended intervals of arid conditions across NE Brazil were punctuated with pluvial periods, each lasting approximately 1000 years (figure 8). Due to the high precision of ages, growth phases of TBV40 TBV63 and TBR14 can be correlated to HS1, HS4, HS5 and HS6. Growth phases are summarized in Table 4. By subtracting the maximum and minimum ages provided by the OxCal age model, we can calculate the duration of each NE Brazil pluvial period. The pluvial period corresponding to HS1 occurred over the longest period of time, approximately 1415±87 years.

Pluvial Period (PP)	Sample ID	Duration	B.P.		
PP1	TBR14	1420±90	17060±40	to	15640±50
PP4	TBV40	970±230	40060±60	to	39100±80
PP4	TBV63	580±290	39670 ±90	to	39080±110
PP4	TBR14	520±280	39590 ±120	to	39070±120
PP5	TBR14	1080±270	48880±100	to	47800±170
PP6	TBV40	1180±210	66740±100	to	65560±110

Table 4: summary of U/Th derived OxCal age model results. Pluvial periods represent periods of increased rainfall over NE Brazil that occurred during Heinrich Stadials.

Pluvial periods corresponding to HS1, HS4, HS5 and HS5 were discovered in samples TBV40, TBV63 and TBR14. To date, no NE Brazilian speleothem growth phases have been discovered that correlate with HS2 or HS3. This may be due to two reasons: (1) growth phases for HS2 and HS3 exist, but have not yet been sampled or (2) HS2 and HS3 did not trigger a large enough pluvial anomaly over NE Brazil to exceed the soil column and bedrock threshold, resulting in a lack of speleothem growth. The second argument is supported by calculated austral autumn insolation at 10ºS—both HS2 and HS3 occurred at a time of low austral autumn insolation. As discussed in Chapter 1, incoming equatorial insolation is a key component in

controlling the position of the ITCZ. The NE Brazil record suggests a strong dependency of the ITCZ position and associated tropical precipitation on precessional forcing (Wang 2004). This hypothesis is supported by the relatively weak HS2 and HS3 signals observed in the Cariaco Basin and NE Brazil margin marine core records (figure 18).

We interpret variations of $\delta^{18}O$ values in NE Brazil speleothem to represent variations in rainfall amount. Modern rainfall $\delta^{18}O$ values over NE Brazil averages -1.5‰ annually and are subject to the amount effect. Recorded pluvial periods in stalagmites range from -2‰ to -9‰, suggesting an increase in precipitation relative to modern conditions. The unusually large range in $\delta^{18}O$ values are also attributed to, in part, variations in stalagmite mineralogy: a transition from aragonite to calcite is estimated to induce a 0.6‰ increase in $\delta^{18}O$ values (Tarutani et al.., 1969). Observed 4‰ shifts at the aragonite-calcite boundaries of are therefore likely to represent a climatic forcings. The presence of cave aragonite is often used as an indicator of paleo-aridity (Railsback et al. 1994). Thus, we interpret the shift from aragonite to calcite in NE Brazilian stalagmites to represent a shift in relative humidity due to increased rainfall.

Due to the dry conditions of TBV and TBR caves, it was not possible to directly sample drip water. We are therefore unable to build a quantitative relationship between modern precipitation amounts and calcite $\delta^{18}O$ values. In lieu of direct evidence, the following three interpretation arguments are proposed:

I. Both TBV and TBR caves are relatively shallow, at approximately 10m below surface. Fast-draining caatinga soils and short groundwater residence times (<10 days) are likely to promote preservation of meteoric $\delta^{18}O$ signals (Auler, 1999).
II. The high correlation between U/Th dates and CFLM band counts suggests that fluorescent bands identified in TBV40 are annual. We can therefore assume that the width of a single annual growth band indicates the amount of precipitation during that year. In other words, an increasing thickness in annual bands

corresponds to increasing precipitation amount. Figure 12 suggest that increasing fluorescent band width (associated with precipitation amount) appears to correlate with decreasing $\delta^{18}O$ values—a pattern observed in modern day precipitation patterns (i.e. "amount effect").

III. $\delta^{18}O$ values for all three samples are similar in range, trend, and absolute values. A high degree of replication in $\delta^{18}O$ profiles between TBV and TBR caves argues against any substantial kinetic effect.

Pluvial periods recorded in NE Brazilian stalagmites correlate to with other climate events observed in high-resolution records worldwide. Pluvial periods are synchronous with periods of weak East Asian summer monsoons (Wang et al. 2001), cold periods in Greenland (Dansgaard et al. 1993; NGRIP et al. 2004), Heinrich Events in the North Atlantic (Heinrich 1988; Bond 1992), and periods of increased river runoff in the Cariaco basin (Peterson et al.l 2000, Deplazes et al. 2013). We highlight the striking anti-phase relationship between NE Brazil and Hulu records during HS events. The precision of the dates obtained for the Hulu records are comparable to that of the NE Brazil (0.1 kyr 2σ errors). Periods of low monsoon intensity appears to correspond to wet periods in NE Brazil. The synchronicity of these two distant records suggests a rapid transmission of atmospheric signals, likely through the global migration of the ITCZ during Heinrich Stadials.

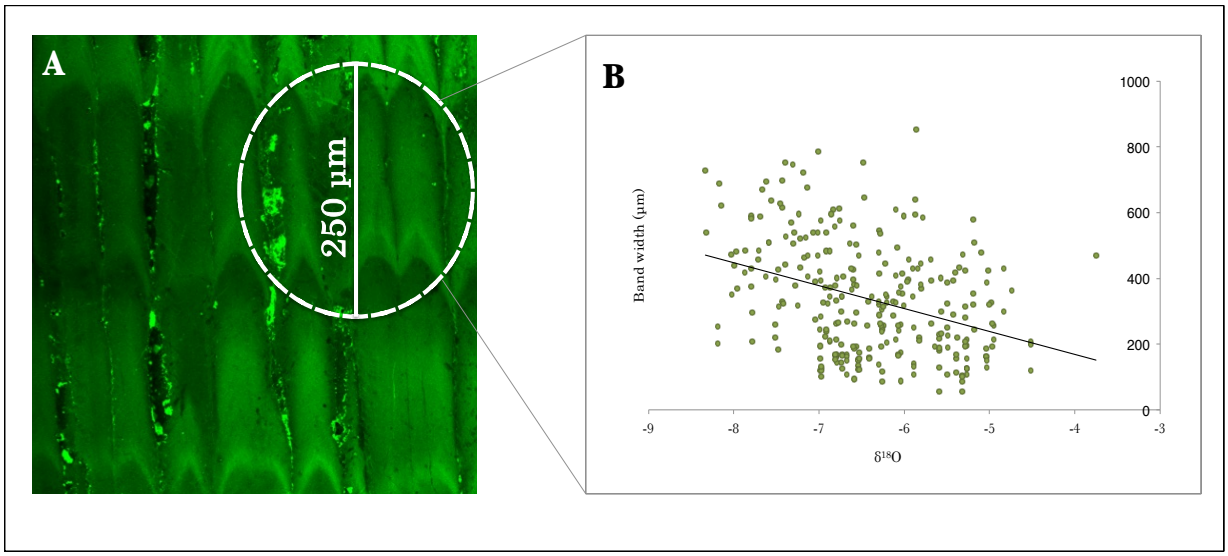

Figure 12: (A) Confocal laser fluorescent microscopy images of sample TBV40. Growth direction from bottom to top of image. Circle indicates approximate 0.25 mm diameter stable isotope subsample. (B) Measured widths of individual fluorescent band(s) paired with each associated oxygen isotope subsample along the growth axis of TBV40. Band widths were averaged across areas of TBV40 were multiple fluorescent bands encompassed the diameter of a single stable isotope subsample. $R^2 = 0.15$, although scatter is expected due to variable precision in assigning stable isotope subsamples to confocal band(s)—for example, difficulties associated with band overlap as demonstrated in figure 12a. trend of results suggests that increasing fluorescent band width (associated with precipitation amount) correlates with decreasing $\delta^{18}O$ values; a pattern observed in modern day precipitation patterns (i.e. "amount effect").

Also notable is the 2-phased structure of the NE Brazil pluvial periods associated with HS1 and HS4. The stalagmite record suggests that the first phases of both pluvial periods began with precipitation conditions slightly wetter than modern-day, as indicated relatively high $\delta^{18}O$ values during HS1 and aragonite growth during HS4. According to U/Th dating, the first phases occurred over a period of 820 years (±50) for HS1 and 500 years for HS4 (±100). The second phases are characterized by an abrupt increase in annual precipitation, as indicated by decreasing high $\delta^{18}O$ values during HS1 and calcite growth during HS4. U/Th dating results suggest that the second phases occurred over a period of 500 years (±50) for HS1 and 520 years for HS4 (±100).

The 2-phased pluvial periods may correspond to the 2-phased SST reconstructions observed in North and mid-Atlantic sediment cores. During HS1 and HS4, marine records suggest a period of precursor cooling that occurred a few centuries before each subsequent generation of icebergs (Bond et al. 1992, 1999; Bard 2000; Naughton et al. 2007; Martrat et al. 2007). For example, U^{k}_{37}-SST biomarkers found in marine sediments along the Iberian Margin suggest a SST cooling at 40.18 kyr B.P. (±200) that appears to have lasted 540-years before the maximum IRD deposition associated with Heinrich Event 4 (Martrat et al. 2007). The onset and duration of the SST precursor cooling agrees with the first phase of the HS4 pluvial phase recorded NE Brazil. Similar mid-Atlantic SST variations have been identified during HS1 (Naughton et al. 2007; Martrat et al. 2007). We suggest that the first phase of NE Brazil pluvial periods may correspond to the precursor SST coolings identified in mid-Atlantic Marine cores.

The following hypothesis is proposed: as discussed in Chapter 1, the Atlantic ITCZ is sensitive to mid-Atlantic SST changes. The Atlantic ITCZ may have migrated a few degrees south in response to the mid-Atlantic precursor cooling. A slight southern migration of the ITCZ may have provided NE Brazil with an initial increase in annual

precipitation observed in the first phase of HS1 and HS4. The discharge of icebergs (Heinrich Event) is thought to have triggered the slowdown of AMOC and additional SST cooling (Hemming 2004). During this time, the ITCZ may have migrated to its furthest southerly extent—providing NE Brazil with sufficient annual rainfall to prompt $\delta^{18}O$ minimums. The possible synchronicity of Heinrich Stadial structure highlights the teleconnection between Southern Hemisphere subtropical precipitation and mid-latitude Northern Hemisphere SST during the last glacial.

The 2-phased structure observed in NE Brazilian pluvial periods may also correspond to the "dry-to-drier" structure observed in the East Asian monsoon during HS4 and HS1 (Wang et al 2001). The first phase is identified as the initial period of decreased in monsoon intensity. The onset and duration of the second phased is identified as the period of subsequent yet weaker monsoon intensity (Wang et al. 2001). The synchronicity of these two distant records suggests that the 2-phased structure in HS4 and HS1 is not limited to the Atlantic ITCZ, but instead, may be global signal.

Curiously, there is the lack of 2-phases observed during Brazilian pluvial events associated with HS5 and HS6. This may be due to the quality of selected samples—a two-phased mineralogy structure (aragonite to calcite) is observed in the HS5 growth phase of TBV63, but could not be dated due to alteration. Additional high-resolution records are needed to fully piece together the unique global climate changes that occurred within the time period of a Heinrich Stadial.

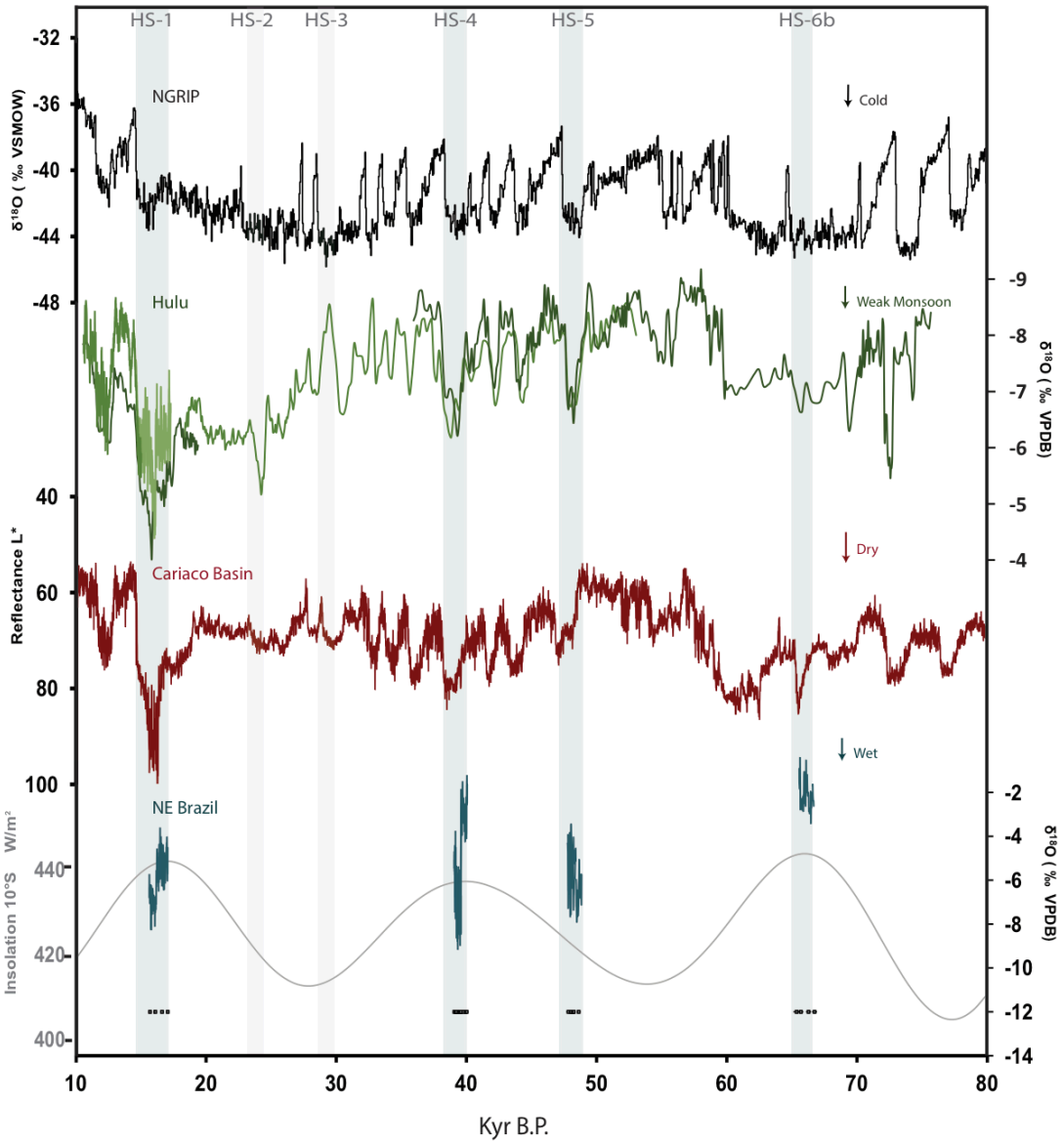

Figure 13: Comparison of NE Brazil record with several Northern Hemisphere paleoclimate records. (A) $\delta^{18}O$ ice core record from Northern Greenland (B) Hulu $\delta^{18}O$ speleothem record near Nanjung, China (C) Cariaco Basin L* reflectance (sm200) sediment record off the coast of North Central Venezuela (variations in reflectance due to relative contributions of terrigenous and biogenic components) and (D) NE Brazil $\delta^{18}O$ speleothem record form this study, including errors. Heinrich Stadials (HS) Events 1, 4, 5, and 6b are highlighted in grey. VSMOW, Vienna standard mean ocean water. VPDB, Vienna PeeBee Belemnite.

2.5.1 Discussion of HS4 growth phase

In total, the pluvial anomaly associated with HS-4 occurred over a maximum period of 995 ± 200 years. HS4 may be further divided into two growth stages, starting with an aragonitic phase lasting 495 years with $\delta^{18}O$ values averaging -2.6 ‰. A switch from aragonite to calcite between 39.59 to 39.54 ka B.P corresponds to a large (5.9 ‰) drop from -7.8 to -1.9 ‰ within the span of approximately 50 years. Under equilibrium conditions, a 0.6 ‰ difference in $\delta^{18}O$ values is expected between calcite and aragonite (Tarutani et al.., 1969). Thus, we argue that this sudden decrease in $\delta^{18}O$ values observed at the boundary of the aragonite to calcite switch is due to climatic forcing. The remaining calcitic portion lasted 500 years (±100), during which there is a gradual increase (drying) in $\delta^{18}O$ values from -7.8 to -5.6 ‰.

The calcitic portion of all three samples likely represents a period of maximum rainfall over NE Brazil during HS4, as indicated by low $\delta^{18}O$ values. The duration of this period is well constrained through both U/Th and band-counting techniques. However, one U/Th date located at 5mm on TBV40 (the end of HS4) was calculated to 38.38 ±0.1 ka B.P.. Under the confocal microscope, 3 distinct hiatuses were identified between 10mm and the top of TBV40. One hiatus located at 5.8 mm from the top is unusually large (130 microns across), which may represent a significant period of time without rainfall (see supplementary figure 5). It is likely that additional small hiatuses exist, but were unidentifiable due to thin banding (less than100 microns in width) above 10mm. Due to the presence of these hiatuses, whose durations are unknown, the U/Th age measured at 5mm was not included in the final age model. It is possible that sporadic rainfall occurred until 38.38 (±0.1), punctuated with small hiatuses. We propose that intermittent rainfall occurred between the end of maximum rainfall (39.0 ±0.1 ka B.P) and the onset of D/O event 8.

We argue that fluorescent banding discovered in the HS4 calcitic portion of NE Brazil samples is annual. NE Brazil is ideally situated to record annual fluorescent bands due to its distinct wet and dry seasons. Fast-draining caatinga soils and short groundwater residence times (<10 days) may aid in the preservation of seasonal signals (Auler, 1999). Band counts for calcitic portion of each stalagmite are well within error of U/Th dates, and are therefore likely annual (see table 3)

Annual bands within the calcitic portion provide detailed information on past precipitation patterns during this time. Measuring the width of annual bands provides a high-resolution growth rate. All three stalagmites exhibit the highest growth rates between 39.40 and 39.50 ka B.P. (±0.1). Unique "double bands" have been identified within these high growth-rate sections. Double bands may correspond to two or more distinct wet seasons within a single annual growth band (figure 14). We suggest that during this time the southernmost branch of the ITCZ was displaced south of our field site, more than several hundred kilometers south of its present southern-most limit. Due to seasonal fluctuations, a southerly displaced ITCZ would provide the region with two distinct wet periods per year—ultimately recorded in NE Brazil stalagmites as two bright bands at the beginning of each annual growth band couplet (i.e. "double banding" feature).

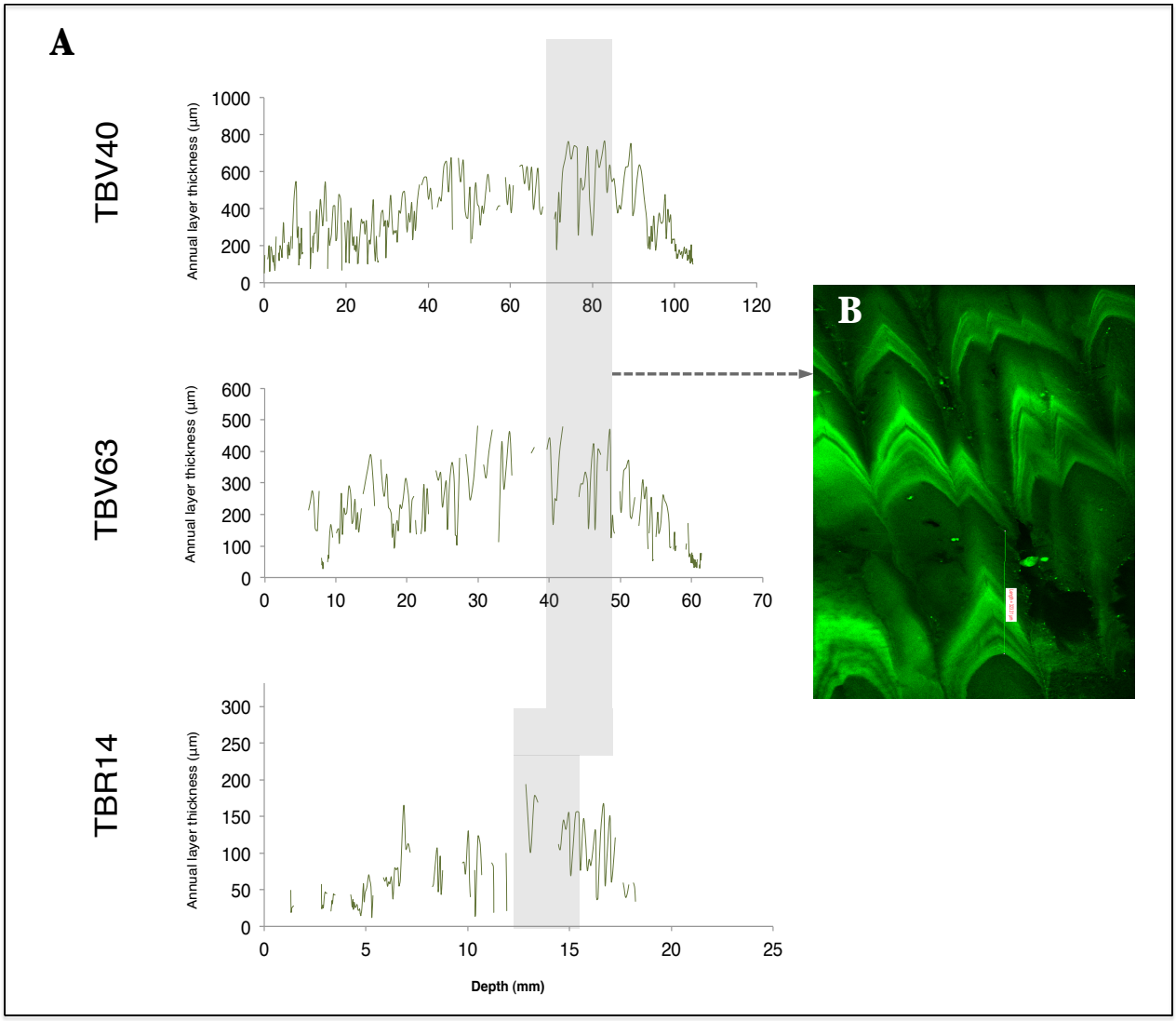

Figure 14: (A) Width measurements of individual bands reveal a high-resolution growth rate. All three stalagmites exhibit the highest growth rates between 39.40 and 39.50 ka B.P. (±0.1). (B) Unique "double bands" have been identified within these high growth-rate sections. We suggest that at this time, the ITCZ migrated south of our study site, thus providing the region with two distinct rainy seasons.

HS4 pluvial periods recorded in NE Brazilian stalagmites correlates with other climate events recorded worldwide. The pluvial period corresponding to HS4 is synchronous with periods of weak East Asian summer monsoons (Wang et al. 2001), cold period in Greenland (Dansgaard et al. 1993; Grootos et al. 1993; NGRIP 2004), Heinrich events in the North Atlantic (Bond 1993) and periods of creased river runoff in the Cariaco basin (Peterson et al.l 2000, Deplazes et al. 2013). The synchronicity of these events provides evidence of a global southerly-displaced ITCZ during HS4.

The start of HS4 (40.02 ±0.1 ka B.P.) as recorded in NE Brazil samples is within error of other high-resolution records worldwide, such as the East Asian summer monsoons (Wang et al. 2001), Greenland temperatures (Dansgaard et al. 1993; Grootos et al. 1993; NGRIP 2004), the Cariaco basin runoff (Peterson et al.l 2000, Deplazes et al. 2013). It is likely that the onset of HS4 occurred at this time.

HS4 NE Brazil record suggests a striking anti-phase relationship with the Chinese speleothem record from Hulu cave (figure 15). Periods of low monsoon intensity correspond to wet periods in NE Brazil—a relationship that is in agreement with a southern migration of the ITCZ. In both records, HS4 can be divided into a 2-phased structure. Phase 1 is characterized as the aragonitic portion of NE Brazil stalagmites, which correlates to the period of weak monsoon immediately following Chinese Interstadial 9. The switch from aragonite to calcite at 39.60 ka B.P. (±0.1) occurs simultaneously with the period of lowest monsoon intensity, within error. Phase 2 is characterized as the remaining calcitic portion of NE Brazil stalagmites, which correlates with the subsequent yet weaker monsoon. Throughout the calcitic portion, NE Brazil stalagmites exhibit a gradual increase (drying) in $\delta^{18}O$ values, corresponding to a gradual recovery of the East Asian monsoon.

As with HS4, a close anti-correlation is identified during HS1. A drop in monsoon intensity appears to occur simultaneously with an abrupt increase in NE Brazil

precipitation at 16.17 ka B.P. (±0.01). The drop is followed by an approximate 450-year period of gradual monsoon recovery and a parallel decrease in NE Brazil precipitation amount (figure 16). Variations of $\delta^{18}O$ values in Hulu speleothems are driven by changes in the Chinese monsoon intensity, which in turn is impacted by migrations of the ITCZ. Thus, the anti-phase relationship between Hulu and NE Brazil during HS4 and HS1 is concurrent with the hypothesis of a southward migrating ITCZ.

2.6 Conclusion

Constraining the chronology and duration of Heinrich Events and their subsequent stadials is critical to understanding their role in global climate change. Due to the high precision of ages, growth phases of TBV40 TBV63 and TBR14 have been successfully correlated to HS1, HS4, HS5 and HS6**.** Pluvial events recorded in NE Brazil stalagmites occurred over an approximate 1000-year time period. Collectively, the NE Brazil record suggest that HS1 occurred from 17055±35 to 15640±50, HS4 occurred from 40060±60 to 39065±120, HS5 occurred from 48880±100 to 47800±170, and HS6 occurred from 66737±102 to 65562±113 years B.P.. NE Brazil stalagmite $\delta^{18}O$ values during pluvial periods exhibit a strong anti-phase relationship with the high-resolution Northern Hemisphere subtropical Hulu cave record (Wang et al. 2001). Our data supports the hypothesis of a southern migration of the ITCZ during Heinrich Stadials.

Notable in the NE Brazil record is the 2-phased structure of the NE Brazil pluvial periods associated with HS1 and HS4. We hypothesize that this structure is facilitated by the ITCZ, whose position is sensitive to SSTs. A 2-stepped cooling of mid-Atlantic SSTs during HS4 and HS1 may have resulted in a 2-phased migration of the ITCZ, providing NE Brazil with a "wet-to-wetter" pluvial period observed in speleothems (Bard et al. 2000; Martrat et al. 2007; Naughton et al. 2007). The

synchronicity of these records highlights the relationship between the ITCZ position and mid-latitude Northern Hemisphere SSTs during the last glacial.

Samples TBV40, TBV63 and TBR14 have recorded a pluvial phase corresponding to HS4. Here, we provide high-resolution age constrains on HS4 as recorded in NE Brazilian stalagmites. This multi speleothem record provides evidence that increased precipitation associated with HS4 occurred over a period of 995 ± 200 years. The structure of HS4 may be further divided into two growth stages: an aragonitic phase lasting 460 years followed by a calcitic phase lasting 540 years (±100). It is likely that the calcitic portion of all three stalagmites corresponds to a period of maximum rainfall during HS4. Unique "double bands" during this time period may represent two distinct wet seasons within a single annual growth band. We suggest that during this time the southernmost branch of the ITCZ was displaced south of our field site, more than several hundred kilometers south of its present southern-most limit.

The NE Brazilian pluvial period corresponding to HS4 correlates with other climate events recorded worldwide—such as the East Asian Monsoon record in China (Wang et al. 2001). This Northern Hemisphere vs Southern Hemisphere anti-phase relationship in the subtropics supports an ITCZ migration in response to HS4.

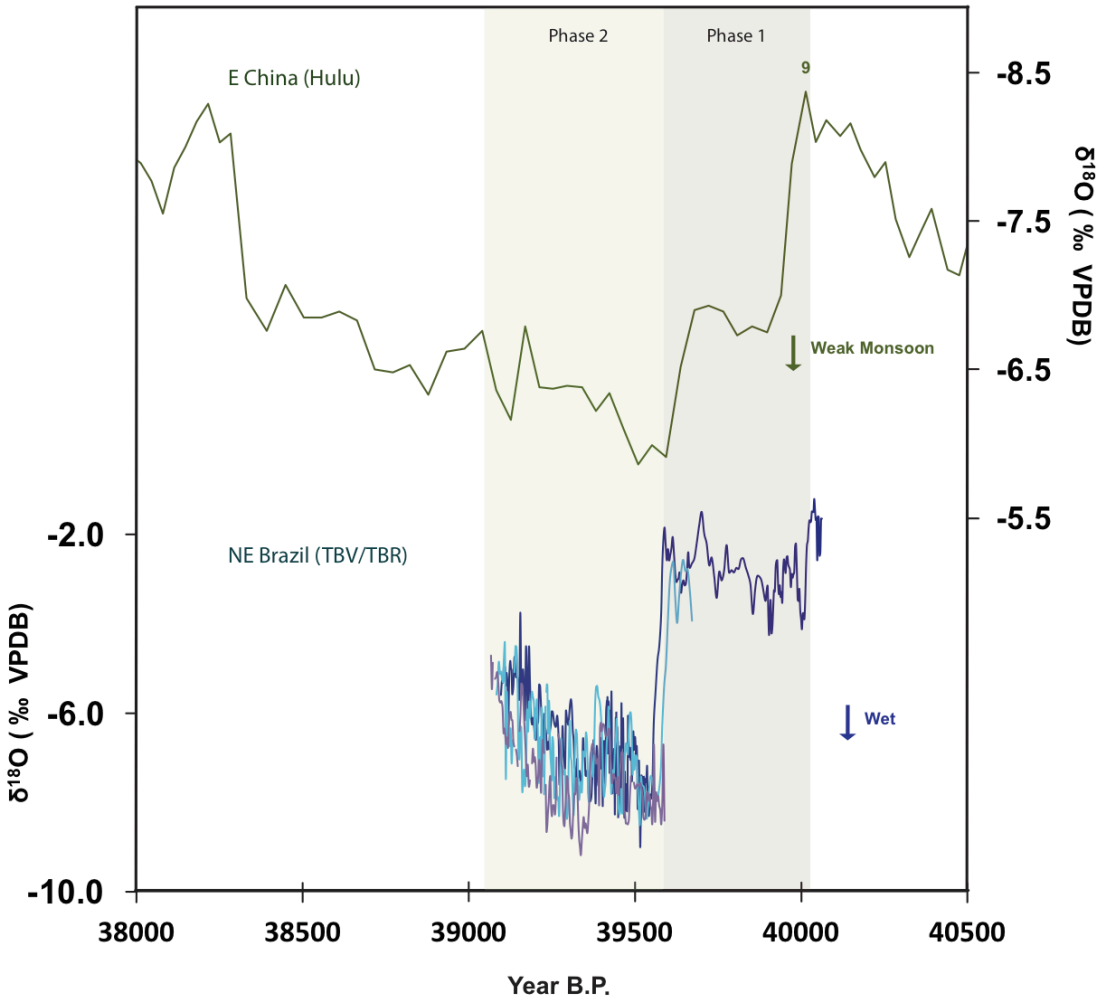

Figure 15: A comparison of the anti-phase relationship between NE Brazil and Hulu speleothem records during HS4. Black circles represent U/Th ages with respective errors. Brown rectangle highlights "phase 1" of HS4. Phase 1 is characterized as the aragonite portion of TBV40 and TBV63 and the period of weak monsoon immediately following Chinese Interstadial 9. Green rectangle highlights "phase 2" of HS4. Phase 2 characterized as the calcite portion of all three NE Brazil samples, and the period of subsequent yet weaker East Asian monsoon. The shift from aragonite to calcite in NE Brazil samples occurs at approximately 39.60 ka B.P. (±0.1).

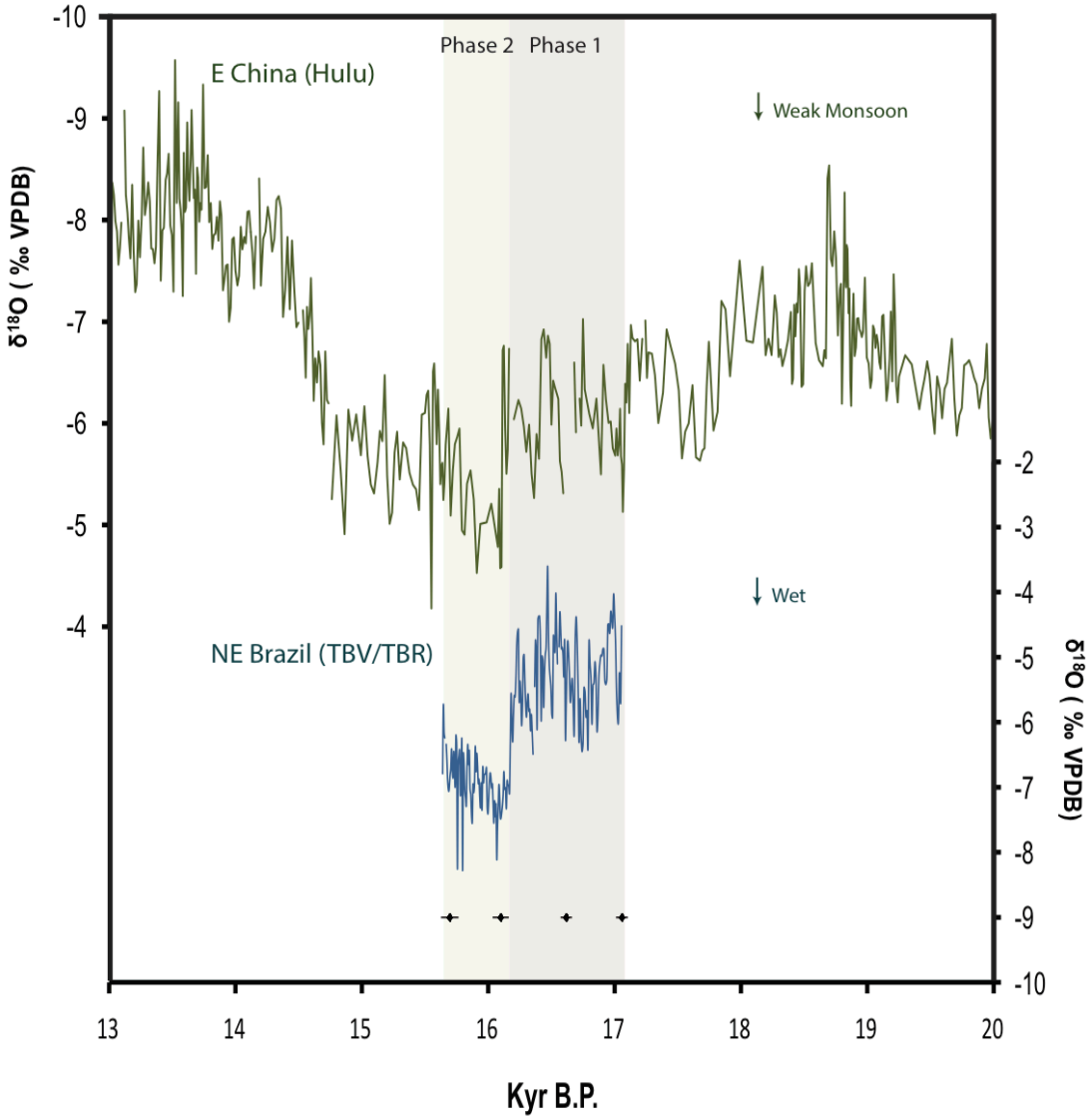

Figure 16: A comparison of the anti-phase relationship between NE Brazil and Hulu speleothem records during HS-Event 1. Black circles represent U/Th ages with respective errors. As in HS4, the colored rectangle highlight the 2-phased structure identified in HS1. A drop in monsoon intensity appears to occur simultaneously with an abrupt increase in NE Brazil precipitation at 16.17 ka B.P. (phase 1). The drop is followed by an approximate 450-year period of gradual monsoon recovery and a parallel decrease in NE Brazil precipitation amount (phase 2).

Chapter 3: Paleohydrological impacts on NE Brazil during Heinrich Stadial 1

3.1 Introduction

Arid NE Brazil is situated between the Amazon and the Atlantic rainforests. Evidence suggests that in the past, wetter periods in NE Brazil promoted an ecological "bridge" between both rainforests, as indicated in figure 17 (Costa 2003; De Oliveira 1999; Jennerjahn et al. 2004; Auler and Smart 2004, Wang et al. 2004). This bridge may have permitted the transfer of species between rainforests. In this Chapter, we discuss a 2-stepped environmental response recorded both in NE Brazil margin marine cores and NE Brazil speleothems during HS1. Characterizing these NE Brazil pluvial anomalies are critical in understanding the link between climate change and the response on environmental systems. In addition, providing high-resolution age constraints may provide further insight into the precise time span of ecological exchange.

3.2 Background

3.2.1 Ecological bridge

Botanical, genetic, and modeling studies suggest that high biodiversity resulted from periodic exchanges between the Amazonian and Atlantic rainforests (Por 1992; De Oliveira 1999; Auler et al. 2004; Carnaval and Moritz 2008; Costa et al. 2003). For example, Costa et al. (2003) suggest that the Amazon and the Atlantic forests are not exclusive in terms of their small mammal faunas. Instead, both overlap broadly with taxa occurring in gallery forests and dry forests in central Brazil.

The Amazon rainforest is believed to have had a long-term persistence of forest in the central and western portions of the biome (Cheng et al. 2013). Near Amazon boundaries, however, paleo-records show past fluctuations and replacement by semi-deciduous dry forest or savanna (De Oliveira 1999). Amazonian taxa data reinforce this view (Lessa et al. 2003).

The Caatinga biome lies long the eastern edge of the Amazon. Based on mammalian distributional patterns, the fossil record, and ecological physiology studies, its is hypothesized that the Caatinga was once replaced with a moist forest capable of supporting arboreal rainforest (Vivo 1997; Auler et al. 2004). During these wetter times, an ecological "bridge" may have connected the eastern Amazonian and the Atlantic forests (Costa et al. 2003). Preliminary work on NE Brazil speleothems by Wang et al. (2004) proposed that intermittent pluvial periods—corresponding to Heinrich Stadials—prompted the expansion and extension of gallery forest, resulting in faunal and flora exchange between the two forest areas.

3.2.2 Previous paleo-ecology studies of NE Brazil

Marine cores collected off the coast of NE Brazil have linked periods of excess runoff (high Ti/Ca ratios in sediments) to pluvial periods associated with Heinrich Stadials (Arz 1998). Palynological studies of NE Brazil marine cores GeoB 3910-2, GeoB3912-1 and GeoB3911-3 provide insight into the ecological changes that occurred during the time period of HS1 (Jennerjahn et al. 2004; Dupont et al. 2010; Arz 1998). Using both sedimentological and palynological techniques, Dupont et al. (2010) and Jennerjahn et al. (2004) have reconstructed the response of the NE Brazilian vegetation to changes in the precipitation regime during HS1. Their results suggest a two-step vegetation response in NE Brazil during HS1 (Dupont et al. 2010).

Marine records indicate an immediate response of the vegetation to an increase in precipitation at 18 (±0.1) ka B.P. over NE Brazil (Dupont et al. 2010). During this "first-step," pollen records suggest that herbal vegetation became denser and open woodland occurred (Dupont et al. 2010). Jennerjahn et al. (2004) report a rapid increase in moss fern spores (*Selaginella*) at the beginning of HS1. Moss ferns—a pioneer species—indicate a successional vegetation pattern (Jannerjahn et al. 2004). Also during this time, increased precipitation along the continental margin of NE Brazil led to an initial outwash of exposed shelf sediments and increased river inputs

of eroded top soil, represented by high Fe/Ca and Ti/Ca sediment ratios (Jannerjahn et al. 2004). Between 18 and 16.5 ka dry forest vegetation grew in formerly open caatinga grass and shrub-rich landscape (Dupont et al. 2010).

An increase of woody vegetation at 16.5 ka marks the beginning of the second phase (Dupont et al. 2010). A rapid reforestation in response to increased moisture appears to have occurred around 16 ka B.P., accounting for 100-year age errors (Ledru et al. 2002). During this time, the caatinga became wetter and gallery forest expanded (Dupont et al. 2010). The most humid period is recorded between 16.5 and 15 ka B.P., as evidenced by an increase in organic terrestrial material deposited on the continental slope of NE Brazil. An increase in organic carbon concentration and total nitrogen (C_{org}/TN) ratios suggests an increase in soil productivity (Dupont et al. 2010). During this time, Dupont et al. (2010) suggest that caatinga vegetation was replaced with a mosaic of closed an open canopy vegetation types, as well as an increase of organic material from forest soils. This so-called "second step" of the H1 stadial is therefore characterized by humid conditions probably persisted all year round. Evidence in sediment and pollen suggest that changes in sedimentology and vegetation were synchronous.

3.2.3 Study site

The interior of NE Brazil is a semiarid region located immediately south of the modern ITCZ. The position of the ITCZ determines the seasonality of rainfall over NE Brazil (Hastenrath, 1990). Precipitation (~ 500mm annually) is largely restricted to austral fall when the ITCZ reaches its southernmost position (Hastenrath, 1990; Hastenrath 2011). The aridity of NE Brazil is attributed to high evapotranspiration rates (>1,400 mm annually), resulting in frequent and extreme droughts. (Garreaud 2009; Moura and Shukla, 1988; Hastenrath and Heller, 1977).

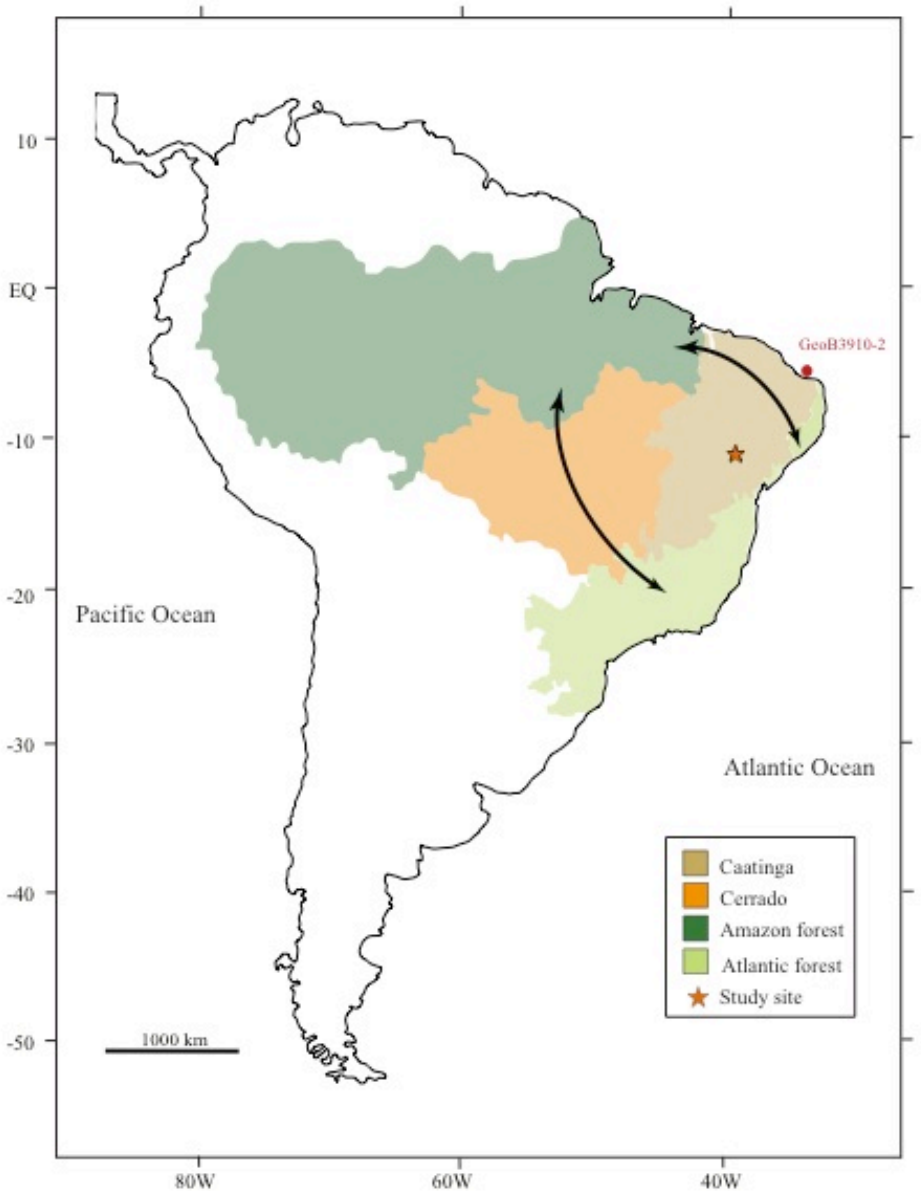

Figure 17: Modern day distribution of Amazon (dark green), Caatinga (brown), Cerrado/Savana (orange), and Atlantic Forest (light green). Orange star indicates location of study site. Red circle indicated location of marine core GeoB3910-2. Paleoecological studies suggest that humid forests could have developed in regions that today are covered by Caatinga or Cerrado vegetation (Jennerjahn et al. 2004; Dupont et al. 2012; Arz et al.. 1998; De Oliveira et al. 1999; Auler et al. 2004). Blank arrows represent possible formation of eastern corridors of humid forests, (ecological bridges) connecting eastern Amazon and northern Atlantic rainforest. Our records supporting this hypothesis by indicating increased rainfall during HS1.

NE Brazil vegetation primarily consists of low arboreal deciduous scrubland (xerophythic) known locally as caatinga (Auler 1999). The drought-resistant caatinga vegetation, such as spiny deciduous shrubs and cacti, lies dormant and leafless for much of the year. Soil profiles of NE Brazil are poorly developed (<1 m) and fast draining. The region has a well-developed underground karst system, with shallow cave passages developing in selected bedding horizons of dolomite. Modern surface streams are largely dry, with ephemeral flow only after high precipitation events (Auler 1999).

Paleobotantical remains embedded in travertine deposits located within a 100 km radius of our study site indicate that caatinga vegetation was replaced or mixed with semi-deciduous forest in the past (Auler et al. 2004). Casts of trunks, leaves, roots, and associated plant debris are commonly found embedded in travertine deposits. Duarte and Nogueira (1983) were the first to analyze the taxonomic and ecological relationships of travertine fossil leaves. They discovered a high diversity of plant species, a majority of which had fossil leaves that are membranous and coriaceous (Duarte and Nogueira 1983). Leaf sizes of fossil plants are overall larger than present vegetation, suggesting a past environment with a developed canopy with reduced luminosity. The specific leaf venation type and size identified is uniquely found in the Atlantic rainforest. Duarte and Nogueira (1983), followed by Auler (1999), interpreted the fossil flora as representing vegetation characteristic of riparian forest typical of more humid environments. Modern day riparian forests found at approximately 250 km to the south of central NE Brazil. Due to the abundance of travertine sites containing fossil botanical remains across NE Brazil, it is believed that forest expansion occurred over large areas of the now semi-arid zone (Auler et al. 2004).

A rich assemblage of vertebrate fossils has been identified within TBV, TBR and neighboring caves (Auler et al. 2004). Czaplewski and Cartelle (1998) preformed an extensive analysis of bat fossils within NE Brazil caves. Despite the lack of modern

day bat colonies in NE Brazil, the presence of fossilized guano and bone assemblages suggests that the caves were once home to a large bat population. The 20 species of bats identified by Czaplewski and Cartelle (1998) now only habitat rainforest ecosystems, suggesting a moister and semi-forested paleoenvironment in NE Brazil. U-series dating analysis of a calcite layer overlying fossil rich sediment yielded ages of 15, 865 ± 390 and 15,740 ± 425, both dates within the time period of HS1 (Auler et al. 2006).

3.3 Methods

Sample TBR14 was halved along the growth axis and polished. 1-2 mg of powder was hand drilled and adhered to an Eulerian Cradle sample holder micro X-diffraction (XRD) powder analysis. Samples were analyzed using a Bruker-AXS Microdiffractometer with a 2.2 kW sealed Cu X-ray source. Results were analyzed using Jade v7.0 Advanced Powder Data Processing Software (Materials Data, Inc). Diffractograms were identified using the Whole Pattern Fit function.

A total of 4 subsamples were drilled for U/Th dating techniques. An age model was developed using OxCal Program version 4.2 with a variable k value of 0.1 (Ramsey 2009a; Ramsey and Lee 2013; see supplementary figure 3).

A total of 213 stable isotope sub samples were drilled at 0.5mm intervals. $\delta^{18}O$ and $\delta^{13}C$ composition of samples were measured using a Finnigan Delta V Advantage mass spectrometer equipped with an automated carbonate preparation system (Gas Bench II) at the Institute of Geological Sciences, University of Bern, Switzerland. Results are reported relative to the Vienna Peedee Belemnite (VPDB) standard. Analytical errors for $\delta^{18}O$ and $\delta^{13}C$ are 0.07 ‰ VPDB (1σ) (Fleitmann et al. 2009). A Hendy Test (described in chapter 2) was preformed on each sample.

3.4 Results

XRD results show that TBR14 is made entirely of calcite and therefore did not undergo any digenesis. A Hendy test was preformed on TBR14. Results show that $\delta^{18}O$ varies no more than -0.5‰, without any overarching trends of increasing or decreasing values along a single growth layer. Relatively low correlations ($R^2 = 0.3$) between $\delta^{18}O$ and $\delta^{13}C$ suggests that kinetic fractionation has little effect (see supplementary figure 4). It is therefore likely that the isotopic signal is driven by climatic processes, rather than by kinetic processes.

U/Th dates are in stratigraphic order within measured uncertainties. High precision dating of TBR14 suggests that a pluvial period occurring from 17055 ±36 to 15640 ±51 B.P. corresponds to HS1, for a total duration of 1415 years. Throughout the pluvial period, there is a 2.39‰ range in $\delta^{18}O$ values. HS1 can be further separated into two stages. The first stage occurred between 17055 to 16181 (±50) B.P., during which $\delta^{18}O$ values fluctuated around -5‰. A sharp drop of -2‰ occurred over a time span of approximately 44 years from 16,181 to 16,137 B.P. (±50). The second stage $\delta^{18}O$ values gradually recover (-7 to -6‰) from 16.175 to 15.640 ka B.P. (±0.05). The NE Brazil pluvial period associated with HS1 terminates before the abrupt warming period commonly referred to as the Bolling-Allerod, which occurred at approximately 14,600 years B.P. (Wang et al. 2001).

3.5 Discussion

NE Brazil speleothem growth periods align with periods of increased runoff off the coast of NE Brazil (Arz 1998; Burckel et al. 2014) and decreased runoff into the Cariaco Basin (Peterson et al. 2000). These observations are in agreement with the hypothesis of a southern migration of the ITCZ (Figure 18).

Palynological studies of NE Brazil marine cores provide high-resolution insight into the ecological changes that occurred during the time period of HS1 (Jennerjahn et al. 2004; Dupont et al. 2010; Arz 1998). Using both sedimentological and palynological techniques, Dupont et al. (2010) and Jennerjahn et al. (2004) have reconstructed the response of the NE Brazilian vegetation to changes in the precipitation regime during HS1. Their results suggest a two-step vegetation response in NE Brazil during HS1, similar to the precipitation pattern recorded in NE Brazil stalagmite TBR14. Despite differences in dating techniques (carbon-12 versus U/Th), we note that variations in speleothem $\delta^{18}O$ values are within error of the first pollen phase, transition, and second pollen phase recorded in marine sediments during HS1. Thus, speleothem dates are likely to provide more precise age constraints on the two-step phase recorded in NE Brazil marine core GeoB 3910-2. We suggest that the "first phase" of HS1 corresponds to the period of relatively high $\delta^{18}O$ in TBR14 between 17.05-16.18 ±0.05 ka B.P.. The transition between phases occurs at 16.17 ± 0.05 ka B.P., during which there is a drop in $\delta^{18}O$ values. The "second phase" of HS1 corresponds to the period of relatively low $\delta^{18}O$ values between 16.17–15.64 ±0.05 ka B.P. (Figure 19).

Combined, the following series of events is proposed: a variety of different types of vegetation, such as Atlantic and gallery rainforest, existed alongside more open caatinga landscapes during the first phase of HS1. The onset of increased precipitation during the first phase of HS1 (17.01±0.05 ka B.P.) is indicated by the growth of speleothems in the NE Brazil caves. During the first phase of HS1, peaks in organic matter in recorded in marine cores suggest a development and stabilization of soils (Jennerjahn et al.., 2004). The second phase of HS1 is indicated by an abrupt decrease in speleothem $\delta^{18}O$ values at 16.2±0.05 ka B.P., suggesting an increase in precipitation. During this second phase of HS1, humid gallery forests may have received enough annual precipitation to have rapidly expanded, thus creating one or multiple "ecological bridges" between the Amazonian and the Atlantic Rainforest. An expansion of gallery forests is supported by an increase in arboreal pollen concentrations at this time (De Oliveira et al.., 1999; Behling et al.., 2000). By the

end of the H1 stadial (15 ka B.P.) forest declined (Dupont et al. 2010). The termination of speleothem growth at 15.64 ±0.05 ka B.P. suggests the second phase of HS1 ended at this time.

According to NE Brazil speleothems, HS1 occurred over 1415 years. Is this, theoretically, an appropriate period of time for such drastic ecological changes? Observational studies and paleo-records from the Caricao Basin suggests that tropical vegetation response to abrupt climate change is on the order of decades (Hughen et al. 2004; Walther et al. 2002). One hypothesis as to why vegetation response appears to have developed over a longer 1000-year time span was first proposed by Jannerjahn et al. (2004): the late Pleistocene NE Brazil was a semi-arid region with a dry period of approximately 8 months, thus preventing any development of rainforests. It is possible that at the beginning of HS events (phase 1), precipitation rapidly increased during the austral summer but not throughout the whole year. This first phase promoted soil erosion and increase of pioneer species, such as fern, grasses, and shrubs (Jannerjahn et al. 2004). A shift in seasonality rainfall during the second phase of HS1 may have stimulated a dry period shorter than 4 months, thus allowing a region-wide expansion of wet forests (Jannerjahn et al. 2004). We therefore suggest that the observed pluvial period lasting 1415 years is well within the timespan observed for modern day wet forest expansion.

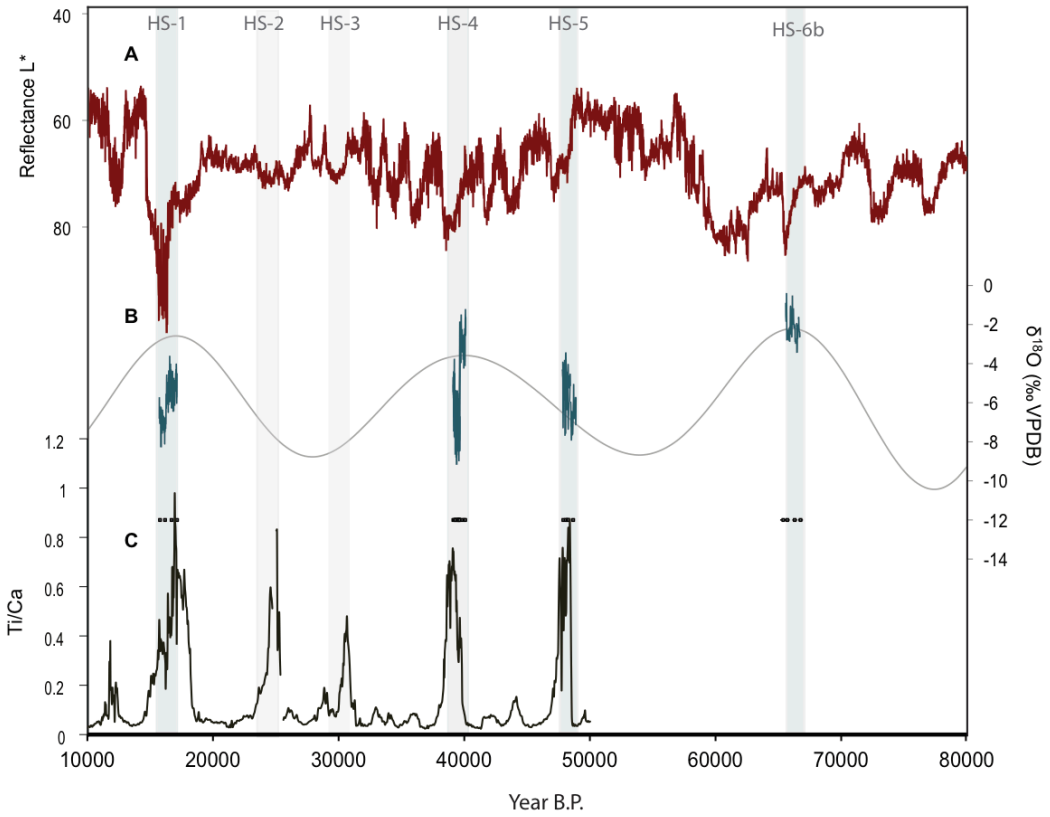

Figure 18: Comparison of NE Brazil record with several South American paleoclimate records. (A) L* reflectance (sm200) of Cariaco Basin sediment record (Deplazes et al. 2014) off the coast of North Central Venezuela. A higher reflectance of sediments indicate increased aridity, as explained in section 1.3 (B) NE Brazil $\delta^{18}O$ speleothem record form this study, including errors. Grey line indicates calculated austral summer insolation at 15°S and (C) Ti/Ca ratios—higher Ti/Ca ratios indicating increased runoff—of marine core MD09-3257 (Burckel et al. 2014), located off the coast of northern NE Brazil. Heinrich Stadials (HS) Events 1, 4, 5, and 6b are highlighted in grey. HS Events 2 and 3, highlighted in light grey, were not recorded in the three samples selected for this study.

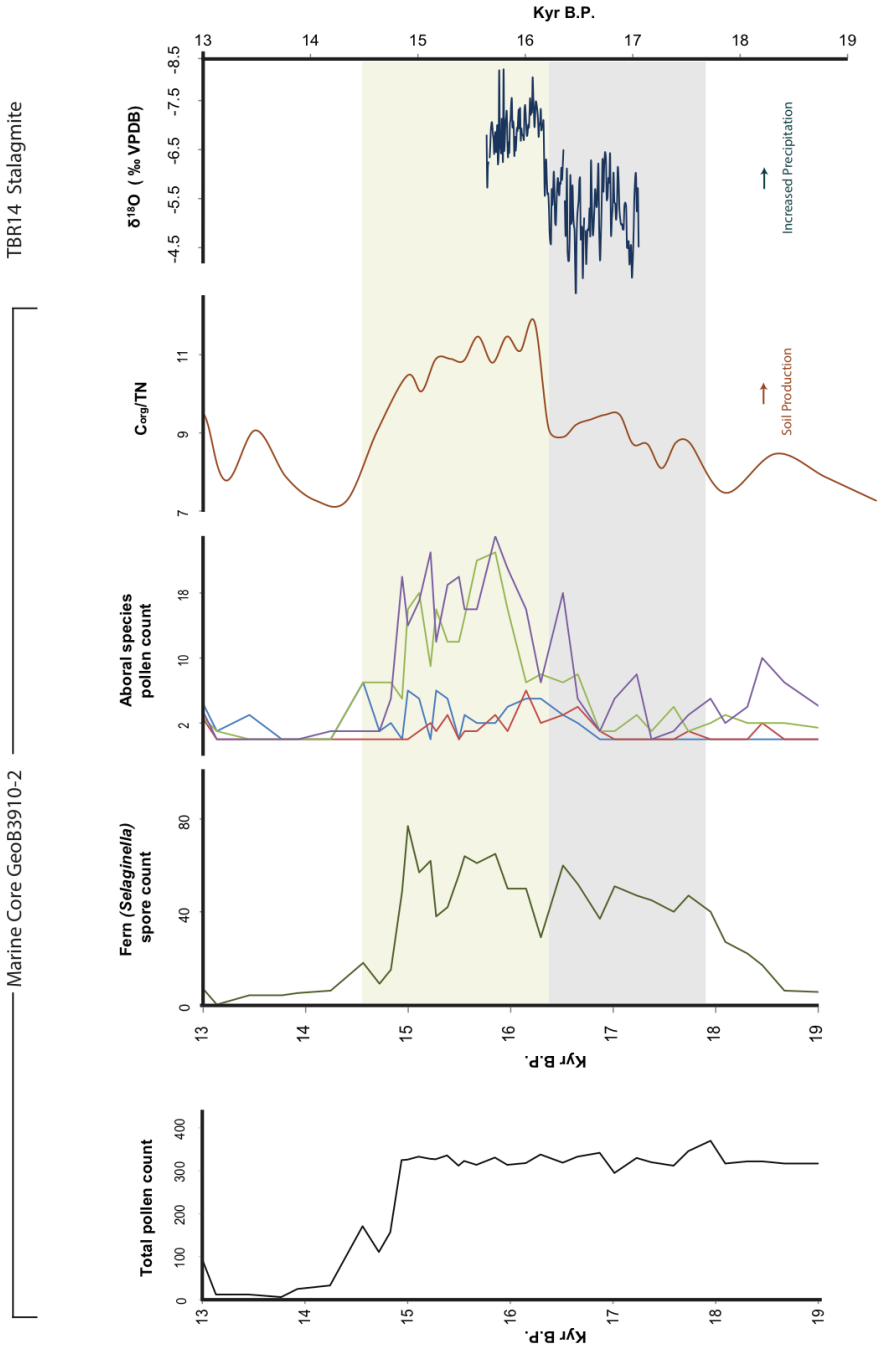

Figure 19: Comparison of HS1 recorded in NE Brazil speleothems to HS1 recorded in NE Brazil marine core GeoB3910-2 (Dupont et al. 2010). Marine core data argues a "2-stepped environmental response" to HS1, as indicated by the jump in arboreal pollen. The same 2-stepped precipitation pattern appears to be recorded in NE speleothem TBR-14.

3.6 Conclusion

High-resolution precipitations proxies, such as NE Brazil speleothems, provide insight into the exact timing and duration of possible ecological exchange. Stalagmite TBR14 suggests that a pluvial period occurring from 17055 ±36 to 15640 ±51 B.P. corresponds to HS1. Pluvial periods recorded in NE Brazilian speleothems appear to have similar structure to neighboring marine cores. Supported by both proxies, we suggest that NE Brazil experienced a 2-stepped environmental response to the pluvial period associated with HS1. During the first step (17,055 to 16,181 B.P ±50), proxies suggest increased rainfall, soil erosion, and the expansion of pioneer species. The second step (16,181 to 15,137 B.P. ±50) is characterized by a greater increase in rainfall followed by the development of soil and expansion of wet forests. We therefore concluded that forest expansion occurred between 16,181 to 15,137 B.P. ±50. This duration is well within the timespan observed for modern day wet forest expansion.

Chapter 4: Conclusion

Low latitude paleo-precipitation records play a key role in understanding how North Atlantic climate anomalies may affect tropical hydroclimate change. NE Brazil speleothems provide valuable insight into how the Atlantic ITCZ migrated in response to Heinrich Stadials.

In chapter 2, we present high-resolution, absolute dated, multi-stalagmite record of HS1, HS4, HS5 and HS6 as recorded in NE Brazilian stalagmites. We conclude that the maximum pluvial period associated with HS4 occurred from 40062±62 to 39066±117, totaling 995 ± 200 years. The structure of HS4 may be further divided into two growth stages: an aragonitic phase lasting 460 years followed by a calcitic phase lasting 540 years (±100). We suggest that the growth of calcite, accompanied by a decrease in $\delta^{18}O$ values, indicates the period of maximum rainfall over NE Brazil. Unique "double bands" within calcitic portion of HS4 may indicate a period when the southernmost branch of the Atlantic ITCZ was displaced south of our field site, more than several hundred kilometers south of its present southern-most limit.

In chapter 2, we discuss some possible interpretations regarding the behavior of the ITCZ during Heinrich Stadials. Results show an anti-correlation in precipitation amount between Southern Hemisphere NE Brazil stalagmite record and distant high-resolution Northern Hemisphere subtropical records. We emphasize the striking anti-correlation relationship with Chinese cave records, whose precipitation amount is indirectly affected by the position of the ITCZ. The synchronicity of these distant records suggests a rapid transmission of atmospheric signals, likely through the southern migration of the global ITCZ system.

In addition, the NE Brazil record may provide preliminary insight into the sensitivities of the ITCZ to past incoming solar radiation and interhemispheric SST variations. The lack of NE Brazil pluvial periods associated with HS2 and HS3

correspond to periods of low autumn insolation at 10ºS. Relatively weak signals during HS2 and HS3 are record in Cariaco Basin and NE Brazil margin marine cores. Combined evidence suggests a dependency of the ITCZ position on precessional forcing during the last glaciation. During HS4 and HS1, the NE Brazil record suggests a 2-phased pluvial period. This structure may be the result of a 2-phased ITCZ migration in response to the "cool to cooler" mid-Atlantic SSTs decrease, as recorded in North and mid-Atlantic sediments. The synchronicity of these records highlights the sensitivity of the ITCZ position to mid-latitude Northern Hemisphere SSTs during the last glacial. We note, however, the lack of a 2-phased signal in HS5 and HS6. This may be due to the quality of selected samples—a two-phased mineralogy structure (aragonite to calcite) is observed in the HS5 growth phase of TBV63, but could not be dated due to calcite alteration. Analysis of additional NE Brazil growth phases is critical to clarifying the true structure of HS5 and HS6.

In chapter 3, we discuss the NE Brazil pluvial period associated with HS1. Our record supports the 2-stepped environmental response to the pluvial period recorded in NE Brazil margin marine cores. During the first step (17,055 to 16,181 years B.P ±50), proxies suggest increased rainfall, soil erosion, and growth of pioneer species. The second step (16,181 to 15,137 years B.P. ±50) is characterized by a greater increase in rainfall, paralleled by the development of soil and expansion of wet forests. We concluded that forest expansion likely occurred between 16,181 to 15,137 years B.P. ±50. The total HS1 duration of 1415 years is well within the timespan observed for modern-day wet forest expansion.

Future work on the NE Brazil speleothem project would benefit from additional focus on HS5 and HS6 in order to clarify discrepancies between recorded pluvial periods. In addition, climate modeling could be used as a tool to test the sensitivity of the Atlantic ITCZ position to past variations in solar radiation and mid-Atlantic SSTs in association with Heinrich Stadials, as suggested by this study.

References

Adler, R.F., G.J. Huffman, A. Chang, R. Ferraro, P. Xie, J. Janowiak, B. Rudolf, U. Schneider, S. Curtis, D. Bolvin, A. Gruber, J. Susskind, and P. Arkin, 2003: The Version 2 Global Precipitation Climatology Project (GPCP) Monthly Precipitation Analysis (1979-Present). J. Hydrometeor., 4,1147-1167

Ahn J and Brook E (2014) Siple Dome ice reveals two modes of millennial Co2 change during the last ice age *Nature Communications* **5** 3723

Alley R, Shuman C, Meese D, Gow A, Taylor K, Cuffey K, Fitzpatrick J, Brootes P, Zielinski G, Ram M, Spinelli G, Elder B (1997) Visual-stratigraphic dating of the GISP2 ice core: Basis, reproducibility, and application *Journal of Geophysical Research* **102** (C12) 26367-26381

Alley R, Dupont T, Parizek B, Anandakrishnan S, Lawson D, Larson G, Evenson E (2006) Outburst flooding and the initiation of ice-stream surges in response to climatic cooling: a hypothesis *Geomorphology* **75** (1-2) 76-89

Anderson R, Ali S, Bradtmiller L, Nielsen S, Fleisher M, Anderson B, Burckle L (2009) Wind-driven Upwelling in the Southern Ocean and the Deglacial Rise in Atmospheric CO_2 *Science* **323** (5920) 1443-1448

Arz W, Paetzold J, Wefer G (1998) Correlated millennial-scale changes in surface hydrography and terrigenous yield inferred from last glacial marine deposits off northeastern Brazil *Quarternary Research* **50** 157-166

Auler A (1999) Karst Evolution and Paleoclimate of Eastern Brazil. Ph.D. dissertation, University of Bristol.

Auler A and Smart P (2001)Late Quaternary Paleoclimate in Semiarid Northeastern Brazil from U-series Dating of Travertine and Water-Table Speleothems *Quaternary Research* **55** (2) 159-167

Auler A and Smart P (2004) Rates of condensation corrosion in speleothems of semi-arid northeastern Brazil *Speleogenesis and Evolution of Karst Aquifers* **2** (2)

Baker A, Proctor C, and Barnes W (2002) Stalagmite lamina doublets: a 1000 year record of extreme winters in NW Scotland. *International Journal of Climatology* **22** 1339-1345

Baker P, Rigsby C, Seltzer G, Fritz S, Lowenstein T, Bacher N, Veliz (2001) Tropical climate changes at millennial and orbital timescales on the Bolivian Antiplano *Nature* **409** 698-701

Bar-Matthews M, Ayalon A, Kaufman A (2000) Timing and hydrological conditions of Sapropel events in the Eastern Mediterranean, as evident from speleothems, Sorreq Cave, Israel Chemical Geology 169 145-156

Bar-Matthews M, Ayalon A, Kaufman A, Wasserburg G (1999)The Eastern Mediterranean paleoclimate as a reflection of regional events: Soreq cave, Israel *Earth and Planetary Science Letters* **166** (1-2) 85-95

Barnes J, Lang E, Potrazt H (1956) Ratio of ionium to uranium in coral limestone *Science* **124** (3213) 175-176

Bard E, Rostek F, Turon J-L, Gendreau S (2000) Hydrological Impact of Heinrich Events in the Subtropical Atlantic *Science* **289** (5483) 1321-1324

Bard E, Delaygue G, Rostek F, Antonioli F, Silenzi, Schrag D (2002) Hydrological conditions over the western Mediterranean basin during the deposition of the cold Sapropel 6 (ca. 175 kyr BP) **202** (2) 481-494

Behling H, Arz H, Paetzold J, Wefer G (2000) Late Quaternary vegetation climate dynamics in northeastern Brazil, inferences from marine core GeoB 3104-1 *Quaternary Science Reviews* **19** (10) 981-994

Bischoff T and Schneider T (2014) Energetic constraints on the position of the Intertropical Convergence Zone *Journal of Climate* **27** 4937-4951

Blunier T and Brook EJ (2001) Timing of millennial-scale climate change in Antarctica and Greenland during the last glacial period. *Science* **291** 109-112

Bond G and Lotti R (1995)Iceberg Discharges into the North Atlantic on Millennial Time Scales during the Last Glaciation *Science* **267** (5200) 1005-1010

Bond G, Broecker W, Johnsen S, McManus J, Labeyrie L, Jouzel J (1993) Correlations between climate records from North Atlantic seidments and Greeland ice *Nature* **365** 143-147

Bond G, Heinrich H, Broecker W, Labeyrie L, McManus J, Andrews J, Huon S, Jantschik R, Clasen S, Simet C, Tedesco K, Klas M, Bonani G, Ivy S (1992) Evidence for massive discharges of icebergs into the North Atlantic during the last glacial period *Nature* **360** 245-249

Bond G, Showers W, Elliot M, Evans M, Lotti R, Hajdas I, Bonani G, Johnson S (1999) The North Atlantic's 1-2 Kyr climate rhythm: relation to Heinrich Events, Dansgaard/Oeschger Cycles and the Little Ice Age, in Mechanisms of Global Climate Change at Millennial Time Scales (eds P.U. Clark, R.S. Webb and L.D. Keigwin) American Geophysical Union, Washington D.C.

Broecker W and Thurber D (1965) Uranium-series dating of corals and oolites from Bahaman and Flordia Key limestones *Science* **149** (3679) 58-60

Broecker W, Bond G, Klas M, Clark E, McManus J (1992) Origin of the northern Atlantic's Heinrich events *ClimateDynamics* (6) 265-273

Broecker WS (2000) Abrupt climate change: causal constraints provided by the paleoclimate record *Earth-Science Reviews* **51** (1-4) 137-154

Burkel P, Waelbroeck C, Gherardi JM, Pichat S, Arz H, Lippold J, Dokken T, Thil F (2015) Atlantic Ocean circulation changes preceded millennial tropical South America rainfall events during the last glacial *Geophysical Research Letters* **28** (2) 411-418

Cabrol P, Coudray J, Dandurand J, Schott J (1978) Possible Transpormation of Calcite to Aragonite at Ordinary Conditions of Temperatures and CO2 Pressure Observation on Carbonate Deposits from Caves and Experimentally Reproduction in Solution *Comptes Rendus Hebdomadaires des Seances De L'Academie Des Sciences Serie D* **287** (5) 411

Carnaval AC and Moritz C (2008) Historical climate modeling predicts patterns of current biodiversity in the Brazilian Atlantic forest *Journal of Biogeography* **35** (7) 1187-1201

Chappell J (2002) Sea level changes forced ice breakouts in the last glacial cycle: new results from coral terraces *Quart Sci Rev* **21** 1229-1240

Cheng H, Edwards RL, Shen C-C, Polyak V, Asmerom Y, Woodhead J, Hellstrom J, Wang Y, Kong X, Spotl C, Wang X, Alexander EC Jr. (2013) Improvements in 230Th dating, 230Th and 234U half-life values, and U-Th isotopic measurements by multi-collector inductively coupled plasma mass spectrometry *Earth and Planetary Science Letters* **371-371** 82-91

Cheng H, Sinha A, Cruz F, Wang X, Edwards RL, d'Horta F, Ribas C, Vuille M, Stott L, Auler A (2013) Climate change patterns in Amazonia and biodiversity *Nature Communications* **4**:1411

Chiang J and Friedman A (2012) Extra tropical cooling interhemispheric thermal gradients, and tropical climate change *Annual Re Earth Planetary Science* **40** 383-412

Cobb K, Adkins J, Partin J, Clark B (2007) Regional-scale climate influences on temporal variations of rainwater and cave dripwater oxygen isotopes in northern Borneo *Earth and Planetary Science Letters* **263** (3-4) 207-220

Cortijo E, Labeyrie L, Vidal L, Vautravers M, Chapman M, Duplessy J-C, Elliot M, Arnold M, Turon J-L, Auffret G (1997) Changes in sea surface hydrology associated with Heinrich event 4 in the North Atlantic Ocean between 40 and 60 N *Earth and Planetary Science Letters* **146** (1-2) 29-45

Costa L (2003) The historical bridge between the Amazon and the Atlantic Forest of Brazil: a study of molecular phylogeography with small mammals *Journal of Biogeography* **30** (1) 71-86

Czaplewski N and Cartelle C (1998) Pleistocene Bats from Cave Deposits in Bahia, Brazil *Journal of Mammalogy* **79** (3) 784-803

Dahl K, and Broccoli A, (2005) Assessing the role of North Atlantic freshwater forcing in millennial scale climate variability; a tropical Atlantic perspective *Climate Dynamics* **24** (4) 325-346

Dansgaard W (1964) Stable Isotopes in Precipitation *Tellus* **16** (4) 436-468

Dansgaard W, Johnsen S, Clausen H, Dahl-Jensen D, Gundestrup N, Hammer C, Hvidberg C, Steffensen J, Sveinbjoernsdottir A, Jouzel J, Bond G (1993) Evidence for general instability of past climate from a 250-kyr ice-core record *Nature* **365** 218-220

De Oliveira P, Magnolia A, Barreto F, Sugio Kl (1999) Late Pleistocene/Holocene climatic and vegetational history of the Brazilian caatinga: The fossil dunes og the middle Sao Francisco River *Paleogeographical Paleoclimatologyical Paleoecology* **152** 319-117

DeMenocal et al. (2000) Abrupt onset and termination of the African Humid Period: rapid climate response to gradual insolation forcing *Quat Sci Rev* **19** 346-361

Denton G, Anderson R, Toggweiler, Edwards R L, Schaefer J, Putnam A (2010) The last Glacial Termination *Science* **328** (5986) 1652-1656

Deplazes G, Lueckge A, Peterson L, Timmermann A, Hamann Y, Hughen K, Roehl U, Laj C, Cane M, Sigman D, Haug G (2013) Links between tropical rainfall and North Atlantic climate during the last glacial period. *Nature Geo Sciences* **6** 213-217

Dorale J and Liu Z (2009) Limitations of Hendy Test Criteria in judging the Paleoclimatic suitability of speleothems and the need for replication *Journal of Cave and Karst Studies* **71** (1) 73-80

Dorale J, Edwards R L, Alexander Jr. C, Shen C-C, Richards D, Cheng H (2004) Uranium-series Dating of Speleothems: Current Techniques, Limitations, and Applications *Studies of Cave Sediments* 177-197

Dorale J, Gonzalez L, Reagen M, Pickett, Murrel M, Baker R (1992) A High-resolution Record of Holocene Climate Change in Speleothem Calcite from Cold Water Cave, Northeast Iowa *Science* **258** (5088) 1626-1630

Duarte L and Nogueira M (1983) Vegetais do Quaternario do Brasil III. Flórula do Morro do Chapéu-BA. In *Coletânea de Trabalhos Paleontológicos do 8° Congresso Brasileiro de Paleontologia*. DNPM Brasília.

Dupont L, Schluetz F, Ewah C, Jennerjahn T, Paul A, Behling H (2010) Two-step vegetation response to enhanced precipitation in Northeast Brazil during Heinrich event 1 *Global Change Biology* **16** 1647-1660

Edwards R L, Chen J, Wasserburg G (1987) 238U-234U-230Th-232Th systematics and the precise measurements of time over the past 500,000 years. Earth And Planetary Science Lettes **81** 175-192

Fasullo J.T. and Trenberth, K.E. (2008) The annual cycle of the energy budget. Part 11: Meridional structures and poleward transports. *Journal of Climate* **21** 2313-2325

Fleitmann D and Metter A (2009) The speleothem record of climate variability in Southern Arabia *Comptes Rendus Geoscience* **341** (8-9) 633-645

Fleitmann D, Burns S, Mudelsee M, Neff U, Kramers J, Mangini A, Matter A (2003) Holocene forcing of the Indian monsoon recorded in a stalagmite from Southern Ocean Science 300 1737-1739

Frisia A, Borsato A, Fairchild I, McDermott, and Selmo E (2002) Aragonite-calcite relationships in speleothems, 'Grotte de Clamouse', France: environment, fabrics, and carbonate geochemistry

Garreaud R (2009) The Andes climate and weather *Advances in Geosciences* **22** 3-11

Grimm E, Jacobson G Jr., Watts A, Hansen B, Maasch K (1993) A 50,000 year record of climate oscillations from Florida and its temporal correlation with the Heinrich Events. *Science* **261** 198-2000

Grootes P, Stulver M, White J, Johnsen S, Jouzel J (1993) Comparison of oxygen isotope records from the GISP2 and GRIP Greenland ice cores *Nature* **366** 552-554

Grousset F (2001) Abrupt climatic changes over the last 60,000 years *Quaternaire* **12** (4) 203-211

Grousset F, Labeyrie L, Sinko A, Cremer M, Bond G, Duprat J, Cortijo E, Huon S (1993) Patterns of Ice-Rafted Detritus in the Glacial North Atlantic (40-55°N) *Paleoceanography* **8** (2) 175-192

Hastenrath and Heller (1977) Dynamics of Climatic Hazards in Northeast Brazil *Quarterly Journal of the Royal Meteorological Society* **103** (435) 77-92

Hastenrath S (1990) The Relationship of Highly Reflective Clouds to Tropical Climate Anomalies *American Meteorological Society* **3** (3) 353-365

Hastenrath S and Polzin D (2011) Long-term variations of Circulation in the Tropical Atlantic Sector and Sahel rainfall *International Journal of Climatology* **31** (5) 649-655

Heinrich H (1998) Origin and consequences of cyclic ice rafting in the northeast Atlantic Ocean during the past 130,000 years *Quart Res* **29** 142-152

Heiri O, Koinig K, Spoetl C, Barrett S, Brauer A, Drescher-Schneider R, Gaar D, Ivy-Ochs S, Kerschner H, Luetscher M, Moran A, Nicolussi K, Preusser F, Schmidt R, Schoeneich P, Schwoerer C, Sprafke T, Terhorst G, Tinner W (2014) Paleoclimate records 60-8ka in the Austrian and Swiss Alps and their forelands *Quaternary Sci Rev* **106** 186-205

Helgeson H, Delany H, Nesbitt J, Byrd D (1978) Summary and critique of the thermodynamic properties of rock-forming minerals *American Journal of Science* **278** 1-229

Hemming S, Broecker W, Sharp W, Bond G, Gwiazda R, McManus J, Klas M, Hajdas I (1998) Provenance of Heinrich layers in core V28-82, northeastern Atlantic: 40Ar/39Ar ages of ice-rafted hornblende, Pb isotopes in feldspar grains, and Nd–Sr–Pb isotopes in the fine sediment fraction *Earth and Planetary Science Letters* **164** (1-2) 317-333

Hemming S. (2004) Heinrich Events: massive late Pleistocene detritus layer of the north Atlantic and their global climate imprint. *American Geophysical Union* **42** RG1005

Hendy C.H. (1971) The isotopic geochemistry of speleothem –I. The calculation of effects of different modes of formation on the isotopic composition of speleothem and their applicability as Paleoclimatic indicators Geochimica et Cosmochimica Acta 35 801-824

Houghton R W (1996) Subsurface quasi-decadal Fluctutations in the North Atlantic *American Meteorological Society* **9** (6) 1363-1373

Huffman G, Bolvin D, Nelkin E, Wolff D (2007) The TRMM Multisatellite Precipitation Analysis (TMPA): Quasi-Global, Multiyear, Combined-Sensor Precipitation Estimates at Fine Scales *American Meteorological Society* **8** (1) 38-55

Hughen K, Eglinton T, Xu Li, Makou M (2004) Abrupt Tropical Vegetation Response to Rapid Climate Changes *Science* **304** (5679) 1955-1959

Hulbe C (1997) An ice shelf mechanism for Heinrich layer production *Paleoceanography* **12** (5)

Hulbe C, MacAyeal D, Denton G, Kleman J, Lowell T (2004) Catastrophic ice shelf breakup as the source of Heinrich event icebergs *Paleoceanography* **19** (1)

IAEA/WMO (2015). Global Network of Isotopes in Precipitation. The GNIP Database. Accessible at: http://www.iaea.org/water

INMET (2015) Instituto Nacional de Meteorologia Rainfall Database. Accessible at: http://www.inmet.gov.br/portal/

Jennerjahn T, Ittekkot V, Arz H, Behling H, Paetzold J, Wefer G (2004) Asynchronous Terrestrial and Marine signals of climate change during Heinrich Events *Nature* **306** 2236-2239

Jullien E, Grousset F, Hemming S, Peck V, Hall I, Jeantet C, Billy I (2006) Contrasting conditions preceding MIS3 and MIS2 Heinrich events Global and Plantary Change **54** (3-4) 225-238

Kageyama M, Paul A, Roche D, Van Meerbeeck C (2010) Modelling Glacial Climatic Millennial-scale Variability related to changes in the Atlantic Meridional Overturning Circultation: a review *Quaternary Science Reviews* **29** (21-22) 2931-2956

Kang S, Deser C, Polvani L (2013) Uncertainty in Climate Change Projections of the Hadley Circulation: The Role of Tinernal Variability *Journal of Climate***26** (19)7541-7554

Kanner L, Burns S, Cheng H, Edwards R L (2012) High latitude forcing of the South American Summer Monsoon during the Last Glacial *Science* **335** 570-573

Lessa E, Cook J, Patton J (2003) Genetic footprints of demographic expansion in North America, but not Amazonia, during the Late Quaternary P*NAS* **100** (18) 10331-10334

Linge, Lauritzen, Baker, Proctor (2001) Luminescent growth banding and stable isotope stratigraphy in a stalagmite from Northern Norway: preliminary results for the period AD1734 to 995 BC. *Proceedings of the 13th International Congress of Speleology*

Lowell T, Heusser C, Andersen B, Moreno P, Hauser A, Heusser L, Schluechter C, Marchant D, Denton G (1995) Interhemispheric Correlation of Late Pleistocene Glacial Events *Science***269** (5230) 1541-1549

MacAyeal D (1993) Binge/purge oscillations of the Laurentide Ice Sheet as a cause of the North Atlantic's Heinrich events *Paleoceanography* **8** (6) 775-784

Martrat B, Grimalt J, Shackleton N, Abreu L, Hutterli M, Stocker T (2007) Four Climate Cycles of Recurring Deep and Surface Water Destabilizations on the Iberian Margin *Science* **317** 502-207

McCabe A and Clark P (1998) Ice-sheet variability around the North Atlantic Ocean during the last deglaciation *Nature* **392** 373-377

McDermott F. (2004) Paleo-climate reconstructions from stable isotope variations in speleothems: a review. Quarternary Science Reviews 23 901-918

McGarry S and Baker A (2000) Organic acid fluorescence: applications to speleothem palaeoenvironmental reconstruction *Quaternary Science Reviews* **19** (11) 1087-1101

Mosblech N, Bush A, Gosling W, Hodell D, Thomas L, van Calsteren P, Correa-Metrio A, Valencia B, Curtis J, van Woesik R (2012) North Atlantic forcing of Amazonian precipitation during the last ice age *Nature Geoscience* **5** 817-820

Moura A and Shukla J (1981) On the Dynamics of Droughts in Northeastern Brazil: Observations, Theory, and Numerical Experiments with a General Circulation Model *American Meteorological Society* **38** (12) 2653-2675

Muller J, Kylander M, Wuest R, Weiss D, Martines-Cortizas A, LeGrande A, Jennerjahn T, Behling H, Anderson W, Jacobson G (2008) Possible evidence for wet Heinrich phases in tropical NE Australia: the Lynch's Crater deposit. *Quarternary Science Review* **27** 465-475

Naughton F, Sanchez Goni A, Desprat S, Turon J-L, Duprat J, Malaize B, Joli C, Cortijo E, Drago T, Freitas M (2007) Present-day and past (last 25 00 years) marine pollen signal off western Iberia *Marine Micropaleontology* **62** (2) 91-114

Neelin J and Held I (1987) Modeling tropical convergence based on the moist static energy budget. *Monthly Weather Review* **115** 3-12

NGRIP (2004) High-resolution record of Northern Hemisphere climate extending into the last interglacial period *Nature* **431** 147-151

Oppo D and Curry W (2012) Deep Atlantic Circulation During the Last Glacial Maximum and Deglaciation *Nature Education Knowledge* **3** (10)

Orland I, Bar-Matthews M, Aalon A, Matthews A, Kozdon R, Ushikubo T, Valley J (2012) Seasonal resolution of Eastern Mediterranean climate change since 34 ka from a Soreq Cave speleothem *Geochimica et Cosmochimica Acta* **89** 240-255

Orland I, Bar-Matthews M, Kita N, Ayalon A, Matthews A, Valley J (2009) Climate deterioration in the Eastern Mediterranean as revealed by ion microprobe analysis of a speleothem that grew from 2.2 to 0.9 ka in Soreq Cave, Israel *Quaternary Research* **71** (1) 27-35

Peck V, Hall I, Zahn R, Grousset F, Hemming S, Scourse J (2007) The relationship of Heinrich events and their European precursors over the past 60 ka BP: a multi-proxy ice-rafted debris provenance study in the North East Atlantic *Quaternary Science Reviews* **26** (7-8) 862-875

Peterson L, Haug G, Hughen K, Roehl U (2000) Rapid changes in the hydrologic cycle of tropical Atlantic during the last glacial *Science* **290** 1947-1951

Por F (1992) *Sooretama: The Atlantic Rain Forest of Brazil* 130 (SPB Academic, The Hague)

Proctor C, Baker A, Barnes W, Gilmour A (2000) A thousand year speleothem proxy record of north Atlantic climate from Scotland *Climate Dynamics* **16** 815-820

Railsback B, Brook G, Chen J, Lakin R, Fleisher C (1994) Environmental Controls on the Petrology of a LateHolocene Speleothem Botswana with Annual Layers of Aragonite and Calcite *Journal of Sedimentary Research* **64** (1) 147-155

Ramsey C (2009a) Bayesian Analysis of Radiocarbon dates *Radiocarbon* **51** (1) 337-360

Ramsey C and Lee S (2013) Recent and Planned Developments of the Program OxCal *Radiocarbon* **55** (2-3)

Robert W, Valdes P, Payne A (2014) A new constraint on the size of Heinrich Events from an iceberg/sediment model *Earth and Planetary Science Letters* **386** 1-9

Roche D, Paillard D, Caley T, Waelbroeck C (2014) LGM hosing approach to Heinrich Event 1: results and perspectives from data–model integration using water isotopes *Quaternary Science. Rev*iew **106** 247–261

Ruddiman W (1977) North Atlantic Ice-Rafting: A Major Change at 75,000 Years before the Present *Science* **196** (4285) 1208-1211

Salgueiro E, Naughton F, Voelker A, de Abreu L, Alberto A, Rossignol L, Dupart J, Magalhaes V, Vaqueiro S, Turon J-L, Abrantes F (2014) Past circulation along the Western Iberian Margin: a time slice vision from the Last Glacial to the Holocene *Quaternary Science Reviews* **106** 316-329

Schneider T, Bischoff T, Haug G (2014) Migrations and dynamics of the Intertropical convergence zone. *Nature* **513** 45-53

Scourse J, Haapaniem A, Colmenero-Hidalgo E, Peck V, Hall I, Austin W, Knutz P, Zahn R (2009) Growth, dynamics and deglaciation of the last British-Irish ice sheet: the deep-sea ice-rafted detritus record *Quaternary Science Review* **28** (27-28) 3066-3084

Stager, Ryves, Chase, Pausata (2011) Catastrophic Drought in the Afro-Asian monsoon region during Heinrich event 1 *Science* **331** 1299-1302

Tan M, Liu T, Hou J, Qin X, Zhang H, Li T (2003) Cyclic rapid warming on centennial-scale revealed by a 2650-year stalagmite record of warm season temperature *Geophysical Research Letters* **30** (12) 1617

Tan L., Orland I.J., and H. Cheng (2014) Annually laminated speleothems in paleoclimate studies *PAGES Magazine* **22** (1) 22-23

Tan M, Baker A, Genty D, Smith C, Esper J, Cai B (2006) Applications of stalagmite laminae to paleoclimate reconstructions: comparison with dendrochronology/climatology *Quaternary Sci Rev* **25**2103-2117

Tarutani T, Clayton R, Mayeda T (1969) The effect of polmorphism and magnesium substitution on exygen isotope fractionation between calcium carbonate and water *Geochimica et Cosmochimica Acta* **33** (8) 987-996

Thomson J, Higgs N, Clayton T (1995) A geochemical criterion for the recognition of Heinrich events and estimation of their depositional fluxes by the 230Th-excess profiling method *Earth and Planetary Science Letters* **135** (1-4) 41-56

Tjallingi R, Claussen M, Stuut, J-B, Fohlmeister J, Jahn A, Bickert T, Lamy F, Roehl U (2008) Coherent high- and low-latitude control of the northwest African hydrological balance *Nature Geoscience* **1** 670-675

Trenberth K and Solomon A (1994) The global heat balance: heat transports in the atmosphere and ocean *Climate Dynamics* **10** 107-134

van Beynen P, Bourbonniere R, Ford D, Schwarcz H (2001) Causes of colur and fluorescence in speleothems *Chemical Geology* **175** (3-4) 319-341

Vinther B, Clausen H, Johnsen S, Rasmussen S, Andersen K, Buchardt S, Dahl-Jensen D, Seierstad I, Siggaard-Andersen M-L, Steffensen J, Svensson A, Olsen J, Heinemeier J (2006) A synchronized dating of three Greenland ice cores throught the Holocene *Journal of Geophysical Research* **111** (13)

Vivo A (1997) Mammalian evidence of historical ecological change in the Caatinga semiarid vegetation of northeastern Brazil *Journal of Comparative Biology* **2** (1) 65-7

Walther G-R, Post E, Convey P, Menzel Am Parmesan C, Beebee T, Fromentin J-M, Hoegh-Guldberg O, Bairlein (2002) Ecological Responses to Recent Climate Change *Nature* **416** 389

Wang Y, Cheng H, Edwards R L, An Z, Wu J, Shen C-C, Dorale J (2001) A high-resolution absolute dated late Pleistocene monsoon record from Hulu Cave, China *Science* **294** 2354-2348

Wang X, Auler A, Edwards R L, Cheng H, Cristalli P, Smart P, Richards D, Shen C-C (2004) Wet periods in northeastern Brazil over the past 210 kyr linked to distant climate anomalies *Nature* **432** 740-743

Wang X, Auler A, Edwwards L R, Cheng H, Ito E, Solheid M (2006) Interhemispheric anti-phasing of rainfall during the last glacial period *Quarternary Science Reviews* **25** 3391-3403

Yokoyama Y, Esat T, Lambeck K (2001) Coupled climate and sea-level changes deduced from Huon Peninsula coral terraces off the last ice age. *Earth and Planetary Science Letters* **193** 579-587

Zhang X, Lohmann G, Knoor G, Purcell C (2014) Abrupt glacial climate shifts controlled by ice sheet changes *Nature* **512** 290-294

Supplementary data

Supplementary table 1: full list of U/Th dates separated by sample. Analytical errors are 2σ of the mean. $\delta^{234}U = ([^{234}U/^{238}U]_{activity} - 1) \times 1000$. $\delta^{234}U_{initial}$ corrected was calculated based on ^{230}Th age (T), i.e., $\delta^{234}U_{initial} = \delta^{234}U_{measured} \times e^{\lambda_{234}*T}$, where T is corrected age. $[^{230}Th/^{238}U]_{activity} = 1 - e^{-\lambda_{230}T} + (\delta^{234}U_{measured}/1000)[\lambda_{230}/(\lambda_{230} - \lambda_{234})](1 - e^{-(\lambda_{230} - \lambda_{234})T})$, where T is the age and λ is decay constant of respective isotope. Half-life values determined by Cheng et al. (2013). An asterisk (*) indicates the location of replicate sub-samples, results of which are listed below sample dates.

TBR 14

Sample Number	^{238}U (ppb)	^{232}Th (ppt)	$^{230}Th / ^{232}Th$ (atomic x10^{-6})	$\delta^{234}U$* (measured)	$^{230}Th / ^{238}U$ (activity)	^{230}Th Age (yr) (uncorrected)	^{230}Th Age (yr) (corrected)	$\delta^{234}U_{...}$** (corrected)	Age ka B.P.
5mm	30 ±0	6 ±1	29879.1 ±2917.2	1516.2 ±3.5	0.3512 ±0.0017	16158 ±87	16156 ±87	1587 ±4	**15696 ±70**
40mm	57 ±0	1 ±1	254830.8 ±103170.6	1718.1 ±4.3	0.3798 ±0.0013	16164 ±64	16164 ±64	1798 ±4	**16099 ±64**
80mm	82.5 ±0.1	3 ±1	235029 ±48847	2121.5 ±3.1	0.4499 ±0.0011	16684 ±45	16683 ±45	2224 ±3	**16618 ±45**
105 mm	171.1 ±0.2	9 ±1	149725 ±12201	2175.8 ±3.0	0.4691 ±0.0011	17123 ±47	17123 ±47	2283 ±3	**17058 ±47**
hiatus									
113mm	30.2 ±0.0	19 ±1	22266 ±1350	1734.1 ±3.1	0.8550 ±0.0035	39264 ±196	39257 ±196	1937 ±4	**39192 ±196**
120mm*	67.4 ±0.1	3 ±1	329076 ±116949	1857.0 ±2.8	0.8968 ±0.0023	39397 ±127	39396 ±127	2075 ±3	**39331 ±127**
125mm	111.4 ±0.1	46 ±1	35926 ±1108	1881.5 ±3.2	0.9085 ±0.0021	39594 ±119	39590 ±119	2104 ±4	**39525 ±119**
hiatus									
130mm	70.6 ±0.1	124 ±3	9069 ±199	1602.3 ±2.7	0.9627 ±0.0022	47917 ±147	47899 ±147	1834 ±3	**47834 ±147**
140mm	83.0 ±0.1	68 ±2	19472 ±511	1602.2 ±3.5	0.9672 ±0.0027	48191 ±179	48182 ±179	1836 ±4	**48117 ±179**
160mm	172.5 ±0.2	116 ±3	25983 ±578	1828.8 ±3.2	1.0627 ±0.0021	48695 ±133	48688 ±133	2098 ±4	**48623 ±133**

TBV40

Sample Location	^{238}U (ppb)	^{232}Th (ppt)	$^{230}Th / ^{232}Th$ (atomic x10^{-6})	$\delta^{234}U$* (measured)	$^{230}Th / ^{238}U$ (activity)	^{230}Th Age (yr) (uncorrected)	^{230}Th Age (yr) (corrected)	$\delta^{234}U_{...}$** (corrected)	Age ka B.P.
5 mm	*67.0 ±0.1*	*25 ±1*	*39752 ±925*	*1887.1 ±3.4*	*0.8876 ±0*	*38449 ±95*	*38446 ±95*	*2103 ±4*	***38382 ±95***
10 mm	67.3 ±0.1	8 ±1	135550 ±22148	1967.3 ±2.8	0.9268 ±0	39141 ±118	39139 ±118	2197 ±3	**39074 ±118**
30 mm	68.7 ±0.1	15 ±1	68291 ±4188	1931.3 ±3.7	0.9197 ±0.0035	39355 ±183	39353 ±183	2158 ±4	**39288 ±183**
50 mm*	63.5 ±0.1	14 ±1	71440 ±2951	1940.7 ±2.8	0.9251 ±0.0018	39471 ±101	39469 ±101	2169 ±3	**39404 ±101**
70 mm	66.4 ±0.1	48 ±1	21144 ±458	1920.7 ±5.2	0.9211 ±0.0027	39593 ±157	39586 ±157	2148 ±6	**39521 ±157**
105 mm*	62.4 ±0.1	13 ±1	73181 ±3859	1992.5 ±2.5	0.9428 ±0.0018	39527 ±96	39525 ±96	2228 ±3	**39460 ±96**
hiatus									
108 mm	4745.9 ±6.7	43 ±8	1881694 ±346750	2253.7 ±3.4	1.0289 ±0.0022	39632 ±108	39632 ±108	2520 ±4	**39567 ±108**
130 mm	4720.7 ±5.5	1247 ±26	63788 ±1320	2207.6 ±3.2	1.0223 ±0.0018	40002 ±94	40000 ±94	2471 ±4	**39935 ±94**
161 mm*	5202 ±7	649 ±14	127188.4 ±2822.5	2019.3 ±3.2	0.9630 ±0.0021	40087 ±115	40086 ±115	2261 ±4	**40021 ±115**
hiatus									
164 mm	1918.0 ±3.3	4441 ±94	9631 ±206	1834.7 ±3.5	1.3524 ±0.0037	65452 ±251	65431 ±252	2207 ±4	**65366 ±252**
hiatus									
167 mm	3901.3 ±4.9	305 ±10	281792 ±9573	1787.5 ±3.3	1.3340 ±0.0025	65755 ±188	65754 ±188	2152 ±4	**65689 ±188**
190 mm	6883.4 ±9.3	87 ±4	1726946 ±77005	1762.3 ±3.1	1.3308 ±0.0026	66343 ±191	66343 ±191	2125 ±4	**66278 ±191**
205 mm	7894.3 ±10.2	767 ±17	230230 ±5256	1798.5 ±2.8	1.3560 ±0.0027	66805 ±191	66804 ±191	2172 ±4	**66739 ±191**

TBV63

Sample Location	^{238}U (ppb)	^{232}Th (ppt)	$^{230}Th / ^{232}Th$ (atomic x10^{-6})	$\delta^{234}U$* (measured)	$^{230}Th / ^{238}U$ (activity)	^{230}Th Age (yr) (uncorrected)	^{230}Th Age (yr) (corrected)	$\delta^{234}U_{...}$** (corrected)	Age ka B.P.
10 mm	42.2 ±0.0	21 ±2	16843 ±1467	650.0 ±1.9	0.5093 ±0.0045	39243 ±413	39234 ±413	726 ±2	**39169 ±413**
20 mm*	57 ±0	209 ±4	2328.3 ±47.9	661.3 ±2.5	0.5138 ±0.0016	39320 ±162	39259 ±168	739 ±3	**39194 ±168**
30 mm	77.7 ±0.1	71 ±2	9410 ±261	682.4 ±1.8	0.5204 ±0.0017	39310 ±159	39295 ±160	762 ±2	**39230 ±160**
40 mm	78.3 ±0.1	137 ±3	4950 ±103	694.3 ±2.0	0.5271 ±0.0014	39567 ±134	39538 ±136	776 ±2	**39473 ±136**
50 mm	98.1 ±0.1	148 ±3	5823 ±122	712.2 ±2.3	0.5325 ±0.0014	39542 ±138	39518 ±139	796 ±3	**39453 ±139**
58 mm	138.9 ±0.2	167 ±4	7504 ±159	755.1 ±2.0	0.5469 ±0.0012	39596 ±117	39577 ±117	844 ±2	**39512 ±117**
hiatus									
62mm*	5369.5 ±10.1	1365 ±44	37206 ±1191	836.3 ±2.3	0.5735 ±0.0017	39635 ±149	39631 ±149	935 ±3	**39566 ±149**
64mm	5867.3 ±11.2	718 ±37	78583 ±4087	864.5 ±2.4	0.5836 ±0.0019	39719 ±160	39717 ±160	967 ±3	**39652 ±160**
hiatus									
69mm	68 ±0	124 ±3	5464.5 ±120.9	728.9 ±2.3	0.6043 ±0.0018	45409 ±181	45380 ±182	829 ±3	**45315 ±182**
74mm	624 ±1	1644 ±33	4524.6 ±92.2	740.1 ±2.4	0.7235 ±0.0024	56202 ±258	56160 ±260	867 ±3	**56095 ±260**
hiatus									
77mm	6345.2 ±8.1	3542 ±72	18906 ±387	745.8 ±2.2	0.6401 ±0.0021	48098 ±210	48090 ±210	854 ±3	**48025 ±210**
80mm	3065.4 ±3.5	65 ±6	508507 ±48670	781.9 ±2.1	0.6555 ±0.0012	48245 ±126	48245 ±126	896 ±2	**48180 ±126**
85mm	3105.5 ±4.1	515 ±13	68155 ±1725	857.5 ±2.3	0.6852 ±0.0014	48316 ±140	48313 ±140	983 ±3	**48248 ±140**

* = includes a replicate

Replicate data									
TBR14 120mm	67.4 ±0.1	3 ±1	329076 ±116949	1861.2 ±2.8	0.8968 ±0.0023	39328 ±126	**39328 ±126**	2080 ±3	**39266 ±126**
TBV40 50mm	64 ±0	89 ±2	11002.7 ±224.8	1933.1 ±3.1	0.9231 ±0.0018	39495 ±103	**39483 ±103**	2161 ±4	**39418 ±103**
TBV40 105mm	117.9 ±0.2	24 ±1	75852 ±1903	2000.7 ±3.7	0.9472 ±0.0018	39612 ±105	**39610 ±105**	2237 ±4	**39545 ±105**
TBV40 161mm	5138.1 ±6.5	32 ±15	2601776 ±1240171	2042.5 ±2.7	0.9727 ±0.0018	40191 ±96	**40191 ±96**	2288 ±3	**40126 ±96**
TBV63 20mm	405.0 ±0.5	675 ±14	5211 ±105	701.5 ±2.1	0.5268 ±0.0011	39343 ±112	**39316 ±113**	784 ±2	**39251 ±113**
TBV63 64 mm	5856.8 ±8.5	1356 ±36	41599 ±1114	870.1 ±1.9	0.5843 ±0.0013	39633 ±115	**39629 ±115**	973 ±2	**39564 ±115**

Supplementary table 2: Mean and standard deviation (SD) of contamination concentrations from 5 chemistry blanks. Chemistry blanks were measured with each round of chemistry. Calculated contamination levels were subtracted from final age results. Average measurement error of chemistry blanks is approximately 50%. Ag= attograms, pg=picograms, and fg=femtograms.

	230 Th (ag)	**232 Th (pg)**	**234 U (ag)**	**235 U (fg)**	**238 U (pg)**
Mean	45	0.15	185	27	1
SD	35	0.01	50	20	0.5

Supplementary table 6: Chemistry iron solutions were measured for total iron concentration in order to calculate the exact dilution factors for a stock iron solution. The University of Minnesota Analytical Geochemistry Laboratory measured iron concentrations of the lab standard and stock solution, results shown below. By calibrating to a lab standard iron solution, the author calculated that 0.1 mg of iron is added to each sample. One drop of iron solution is equivalent to 0.03g. Thus, our laboratory's stock iron solution must be diluted roughly 10 times by super-clean hydrochloric acid to obtain the desired concentration of iron per drop.

Stock and standard iron solution we measured for ^{230}Th and ^{2234}U contamination. Fe iron solution were spiked with approximately 0.01 g of ^{235}U-^{233}U-^{229}Th spike. Solution was fumed with 14N HNO_3 and dried completely. Iron was separated from sample using an anion exchange column. Resulting solution was measured on the Neptune ICP-MS under normal chemistry blank procedures. Results are listed below. Average measurement error of chemistry blanks is approximately 50%.

Solution ID	Concentration (ppm)	^{230}Th Contamination (*ag per 100 µg Fe)*	^{234}U Contamination (*ag per 100 µg Fe)*
Standard	4430.0 ±0.7	3.0	14.0
Stock Solution	42575.0 ±0.3	4.0	2.5

Supplementary figure 1: Results of two powder micro-XRD samples from stalagmite TBV40, as analyzed by Jade mineralogy identification software.

TBV40 Calcite

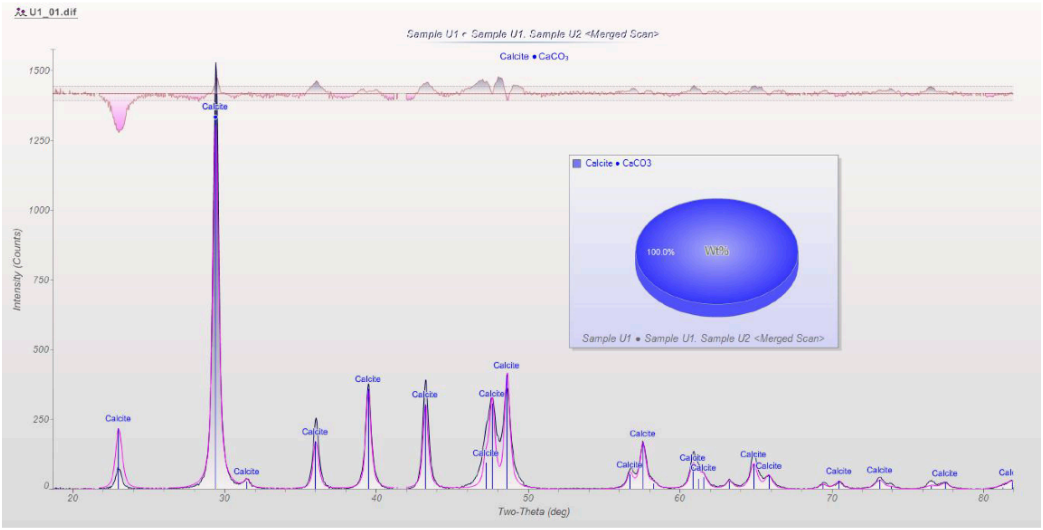

TBV40 Aragonite

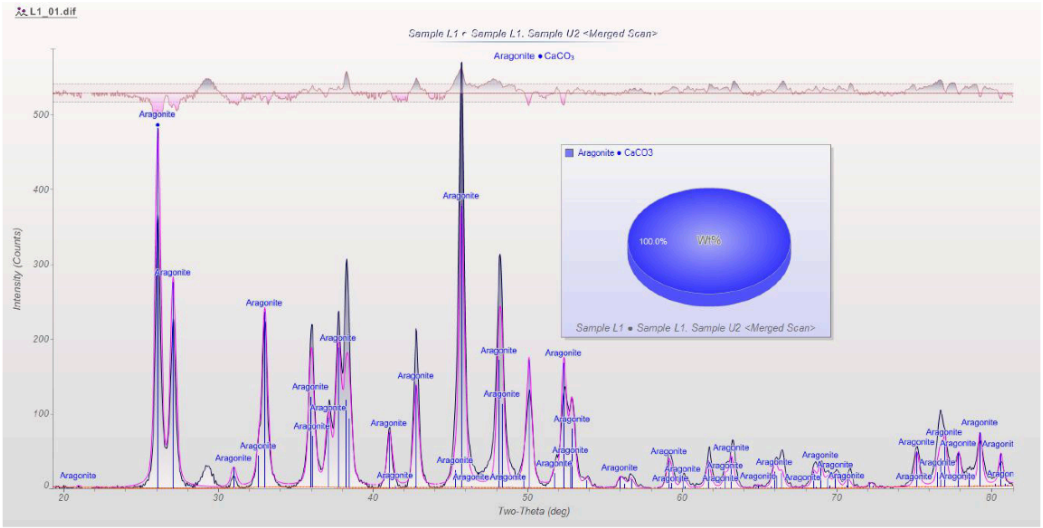

Supplementary figure 2: example age versus depth (position) plot from the HS1 section of stalagmite TBR14, derived form OxCal age model. U/Th age locations are listed such that the bottom of stalagmite is z=0. Results reported in Gregorian years.

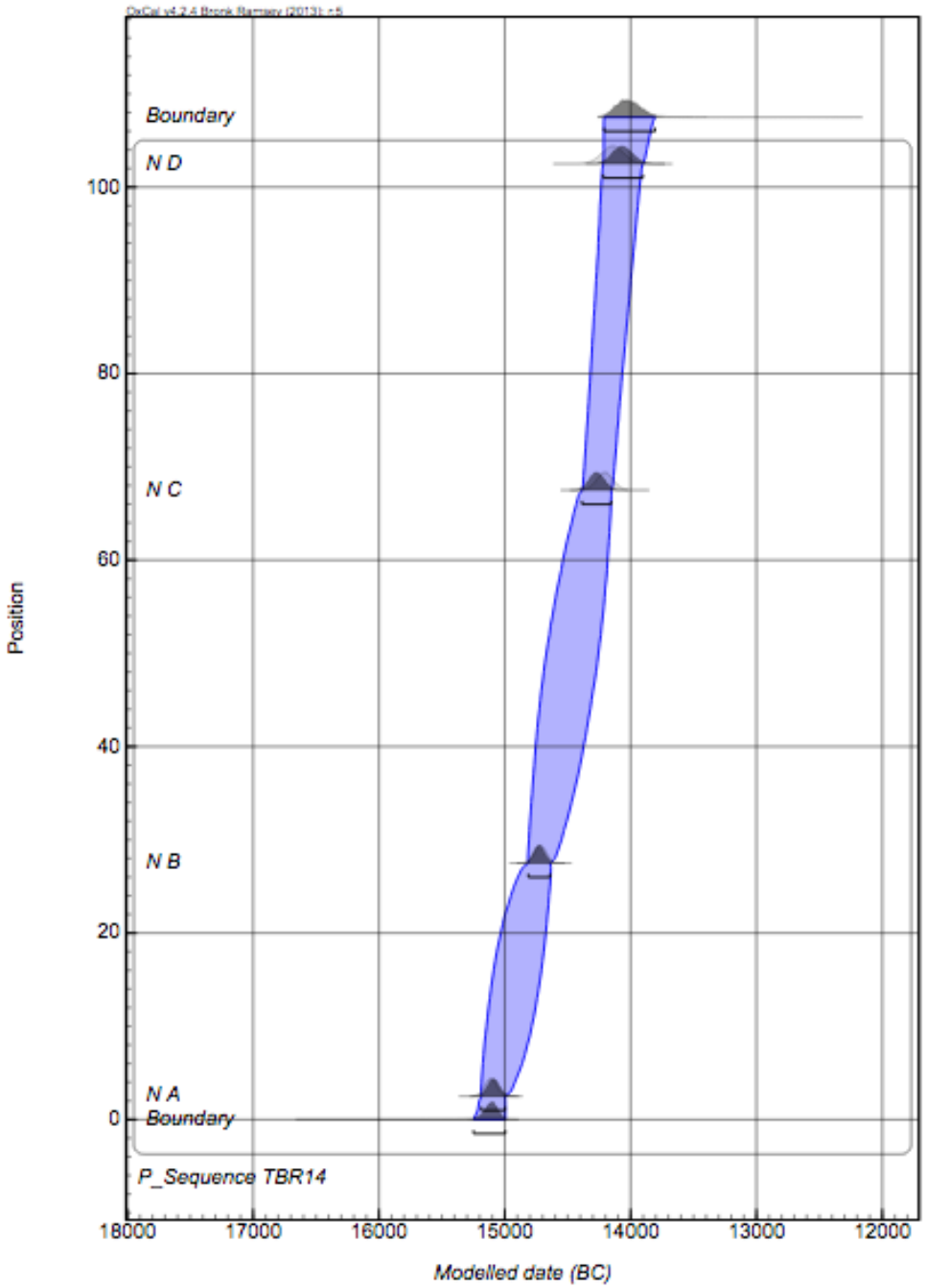

Supplementary figure 3: example P sequence code used to calculate TBV40 HS4 age model using OxCal Program version 4.2 with a variable k value of 0.1. U/Th age locations are listed such that the bottom of stalagmite is z=0. “Boundary” represents the boundary between aragonite and calcite growth phases. (Ramsey 2009a; Ramsey and Lee 2013).

```
TBV40 HS4
Plot()
 {
  P_Sequence("TBV40",0.1,1,U(-2,2))
  {
   Boundary()
   {
    z=0;
   };
   Date("A",N(calBP(40022),57))
   {
    z=1;
   };
   Date("B",N(calBP(39937),47))
   {
    z=32;
   };
   Date("C",N(calBP(39567),54))
   {
    z=54;
   };
   Boundary()
   {
    z=55;
   };
   Date("D",N(calBP(39545),52))
   {
    z=57;
   };
   Date("E",N(calBP(39521),78.5))
   {
    z=92;
   };
   Date("F",N(calBP(39404),48))
   {
    z=112;
   };
   Date("G",N(calBP(39288),91))
   {
    z=132;
   };
Date("H",N(calBP(39074),59))
   {
    z=152;
   };
   Boundary()
   {
    z=162;
   };
  };
 };
```

Supplementary figure 4: Results of Hendy test from sample TBR14. Hendy tests includes total of 5 subsamples along a single growth layer. Reported $R^2 = 0.3$

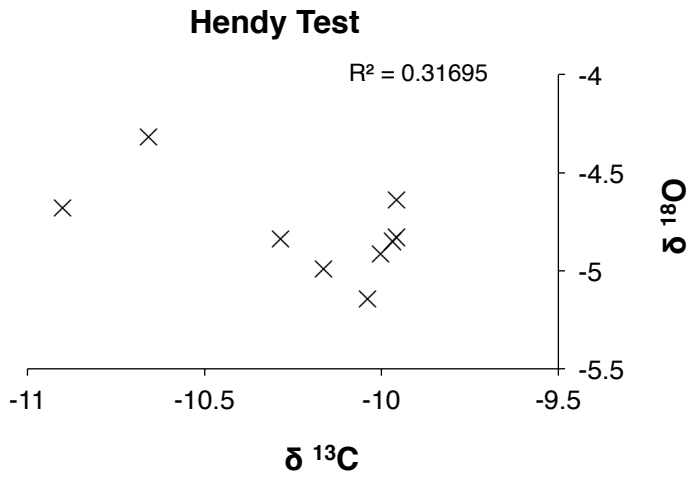

Supplementary figure 5: A) example of identified hiatus in sample TBV40. White bar represents 130 micrometers in distance. B) Counting confocal bands adjacent to a drilled U/Th sub-sample seen along lower edge of photo. C) Example of counting confocal bands using *Nikon Elements Viewer* software